LOWER METABOLIC CAPACITY IN SKELETAL MUSCLE MITOCHONDRIA FROM INTRAUTERINE GROWTH RESTRICTED SHEEP FETUSES

by

Alexander Lindblom Pendleton

Copyright © Alexander Lindblom Pendleton 2020

A Dissertation Submitted to the Faculty of the

GRADUATE INTERDISCIPLINARY PROGRAM IN PHYSIOLOGICAL SCIENCES

In Partial Fulfillment of the Requirements

For the Degree of

DOCTOR OF PHILOSOPHY

In the Graduate College

THE UNIVERSITY OF ARIZONA

2020

THE UNIVERSITY OF ARIZONA
GRADUATE COLLEGE

As members of the Dissertation Committee, we certify that we have read the dissertation prepared by: Alexander Pendleton, titled: *Lower Metabolic Capacity in Skeletal Muscle Mitochondria from Intrauterine Growth Restricted Sheep Fetuses* and recommend that it be accepted as fulfilling the dissertation requirement for the Degree of Doctor of Philosophy.

Sean W Limesand
Sean W. Limesand, Ph.D. Date: 12-28-2020

Ronald M Lynch
Ronald M. Lynch, Ph.D. Date: 12-28-2020

Dawn K. Coletta, Ph.D. Date: 12-28-2020

Benjamin J. Renquist, Ph.D. Date: 12-28-2020

Paul R Langlais
Paul R. Langlais, Ph.D. Date: 12-28-2020

Final approval and acceptance of this dissertation is contingent upon the candidate's submission of the final copies of the dissertation to the Graduate College.

I hereby certify that I have read this dissertation prepared under my direction and recommend that it be accepted as fulfilling the dissertation requirement.

Sean W Limesand
Sean W. Limesand, Ph.D. Date: 12-28-2020
Dissertation Committee Chair
Physiological Science GIDP

Acknowledgements

I would like to acknowledge the members of my dissertation committee, including Dr. Sean W. Limesand, Dr. Ronald M. Lynch, Dr. Benjamin J. Renquist, Dr. Dawn K. Coletta, and Dr. Paul R. Langlais and the members of their laboratories for their time, mentorship, guidance, and technical assistance in conducting the work presented in this thesis. I would especially like to thank Horst Christian Simco for his continual support and help throughout my PhD experience.

I would also like to acknowledge the Physiological Sciences program and faculty for their support over the past five years. I am thankful to have had such wonderful educators and peers. Finally, I would like to thank our collaborators and funding, especially the Cardiovascular Training Grant and the ARCS Foundation Phoenix Chapter.

Dedication

I would like to dedicate this work to my parents, Katie, all my wonderful friends, and all the haters that told me that I could not make it. I am so grateful for your love, support, and encouragement.

Table of Contents

List of Figures

List of Tables

Abstract

Placental insufficiency (PI) induced intrauterine growth restriction (IUGR) increases the risk of mortality and morbidity in both newborns and adults. PI causes a progressive, chronic, and severe decline in the maternal-fetal nutrient transport starting in mid-gestation, which results in fetal hypoxemia and hypoglycemia. Unfortunately, the decline in nutrient availability occurs concurrently with critical myogenic windows in fetal development establishing the proper complement of skeletal muscle mass *in utero*. Thus, IUGR fetuses are also afflicted with sarcopenia that persists into adulthood and predisposes offspring to metabolic diseases. Recent evidence indicates that the metabolic capacity of the skeletal muscle of IUGR fetuses is lowered in response to low nutrient availability. IUGR skeletal muscle adaptations to low nutrient availability includes lower protein synthesis rates as well as lower fractional glucose oxidation and amino acid oxidation rates.

In the current studies, we test the hypothesis that mitochondria isolated from IUGR fetal sheep skeletal muscle have defects in both nutrient oxidation and energy production. Previous findings have linked hypoglycemia and hypoxemia to lower glucose oxidation rates in the IUGR fetus. It was postulated that pyruvate oxidation was hindered in IUGR skeletal muscle mitochondria due to the inhibition pyruvate dehydrogenase (PDH), the first step in pyruvate metabolism. However, we show PDH activity is 67% higher in IUGR skeletal muscle. Moreover, the abundance of Mitochondrial Pyruvate Carrier 2 (MPC2), the primary mitochondrial pyruvate transporter, as well as the abundances of rate-limiting Tricarboxylic Acid Cycle (TCA) enzymes, isocitrate dehydrogenase and oxoglutarate dehydrogenase, are lower in IUGR mitochondria

compared to controls ($P<0.05$). The lower abundances of enzymes involved in substrate oxidation in IUGR fetuses are accompanied by a 47% lower complex-I mediated oxygen consumption rate (OCR) and 18% lower Complex I activity, both of which indicate impaired electron transport chain (ETC) function. Reduced pyruvate oxidation in IUGR fetal skeletal muscle is the result of concomitant decreases in pyruvate transport, TCA cycle function, and ETC function.

Fetal adaptations to nutrient restriction program metabolic dysfunction in postnatal skeletal muscle in IUGR individuals. We hypothesized that mitochondria isolated from myotubes which are differentiated from 30-day old IUGR lamb satellite cells have a 44% lower complex-I mediated OCR compared to controls. The lower OCR in IUGR myotube mitochondria is associated with lower abundances of ETC Complex III and IV subunit abundances. Although the mitochondrial metabolic changes observed in IUGR myotubes differ from the metabolic changes observed in IUGR fetal skeletal muscle mitochondria, these results show the persistence of skeletal muscle mitochondrial dysfunction in IUGR individuals from birth into postnatal life.

Chapter 1

Introduction

1.1 Intrauterine Growth Restriction in Humans

Birthweight is an indicator of long-term future health (1,2). Epidemiological studies have demonstrated that perturbations to the *in-utero* environment, leading to lower birth weight, increases an individual's risk of developing metabolic diseases later in life such as type 2 diabetes, cardiovascular disease, obesity, and glucose intolerance (3–6). In humans, small for gestation age (SGA) is defined as a birth weight of less than 2 standard deviations of the mean (1). A more refined approach to fetal growth restriction has identified intrauterine growth restriction (IUGR) as a contributor to SGA (7). However, in contrast to SGA, IUGR specifically a reduces growth trajectory, and the fetus fails to reach their genetic size potential (8).

IUGR is a continual public health issue, especially in developing countries. World-wide estimates of IUGR prevalence in 1998 estimated ~24% newborns born in developing countries are born IUGR (9). Additionally, this study showed Africa and Asia bear the highest burden of IUGR, accounting for ~75% of all IUGR pregnancies which occurred worldwide (9). Within the realm of IUGR, there are two classifications of fetal growth restriction: symmetrical and asymmetrical. Symmetrical IUGR comprises ~25% of all occurrences of IUGR, and it is characterized by growth restriction occurring early in gestation leading to proportionately reduced organ size in relation to body size. Alternatively, asymmetric IUGR, encompassing ~75% of all IUGR pregnancies, is characterized by growth restriction later in gestation resulting in thin fetuses with greater head circumference to abdominal circumference ratio (10,11). The latter, and more prevalent form, demonstrates fetal adaptation during IUGR to spare the brain at the expense of other organs.

A multitude of factors can attribute to the development of IUGR including medical complications (e.g. maternal hypertension or infection), environmental factors (e.g. smoking or alcohol), or other conditions such as genetics(7). Commonly, many cases of asymmetric IUGR are caused by placental insufficiency (PI), and it is distinguished as a smaller than normal placenta which limits blood flow and the maternal-fetal transfer of oxygen and nutrients (12,13). For the IUGR fetus, PI is postulated to cause preferential redistribution of nutrients/oxygen from peripheral tissues to metabolically inflexible organs, such as the brain (10). As a result, skeletal muscle growth in these fetuses is preferentially restricted through metabolic adaptations (14,15).

1.2 Skeletal Muscle: A Primary Metabolic Organ

The metabolic rate in organs such as the kidney or brain experience little fluctuation. Alternatively, adult skeletal muscle metabolism can drastically vary from 20-30% of whole-body oxygen consumption during rest, to ~90% of whole-body oxygen consumption during exercise (16). Skeletal muscle comprises ~40% of body mass (in non-obese adults) and has a major impact on whole-body energy homeostasis (17).

Skeletal muscle is responsible for a majority of an adult's energy expenditure through thermogenesis, nutrient uptake, muscle contraction, and protein synthesis. Adult skeletal muscle also regulates nutrient concentrations in the blood (18–20). Studies in healthy adults demonstrate that skeletal muscle is responsible for ~80% of post-prandial glucose uptake, ~20% of post-prandial amino acid uptake, and ~4% of triacylglyceride uptake (21–24). However, during the fasting state, plasma glucose concentrations are lower, and free fatty acid concentrations are elevated. As a result, skeletal muscle

primarily uses lipids in the fasting state, deriving ~85% of its energy needs from lipid oxidation (25). The metabolic flexibility of skeletal muscle between feeding periods allows substrate inflexible tissues, like the brain, to utilize glucose.

Numerous studies have shown resting energy expenditure is highly correlated with the lean mass percentage of the individual (26). Moreover, because protein turnover is a major contributor to resting energy expenditure in adults, increased lean mass to fat mass ratio may prevent the development of metabolic disorders such as obesity and type 2 diabetes (27,28). Finally, substantial cross-talk occurs between the skeletal muscle, brain, and other organs, including adipose tissue. Myokines and metabolites released from the skeletal muscle have been shown to modulate a variety of non-muscle events including increasing hippocampal neurogenesis, positively regulating sleep and sleep recovery, modulating hepatic gluconeogenesis, and increasing adipose energy consumption (29). Thus, an inadequate amount of lean mass in adults has important implications for adverse health outcomes including metabolic dysfunction seen in obesity, dyslipidemia, and type 2 diabetes.

1.3 Skeletal Muscle Development in Humans

1.3.1 Normal Development. Skeletal myofiber number is set by birth, making the *in-utero* generation of myofibers critical to long-term health outcomes (30,31). The generation of skeletal muscle during fetal development occurs in two myogenic phases. Multipotent skeletal muscle progenitors, satellite cells, are first derived from mesodermal precursor cells originating from the somite-derived myotome during embryogenesis (32). As development progresses, the self-renewing proliferation of satellite cells gives rise to

a unipotent population of myoblasts as well as maintains a stable population of satellite cells. At ~0.2 of gestation in humans, temporal and spatial signaling gives rise to primary myogenesis: the first wave of myoblast differentiation and fusion into multinucleated myofibers (33). This population of myofibers subsequently forms the basic scaffold on which succeeding generations of myoblasts—still derived from satellite cells—proliferate, differentiate, and fuse to form secondary myotubes (secondary myogenesis) at ~0.35 of gestation (33,34). At the end of secondary myogenesis, nearly all of the postnatal skeletal myofiber number is established along with a compliment of quiescent satellite cells (30,31,35). Thus, primary myogenesis early in gestation establishes the basic muscle pattern, secondary myogenesis later in gestation is critical for the growth, development, and maturation of skeletal muscle (36,37). Postnatal muscle growth is defined by myofiber hypertrophy from the fusion of active satellite cells (30,31,35).

1.3.2 The Potential Impact of PI-IUGR on Muscle Development. Lower skeletal muscle mass to bodyweight ratio is a defining characteristic of human PI-IUGR, putting these individuals at greater risk of developing insulin resistance, type 2 diabetes, and cardiovascular disease later in life (14,15,38–41). Myofiber number is established *in-utero*, and perturbations to fetal myogenesis may have lasting results as this loss of lean mass is not postnatally recovered (42–44). If nutrient/oxygen restriction occurs in early pregnancy, both primary and secondary myogenesis are at risk of disruption. Alternatively, asymmetric IUGR results from PI that begins in early pregnancy but results in progressive, chronic, and severe reductions in maternal-fetal nutrient flux with late-gestation fetal nutrient restriction resulting in skeletal muscle growth restriction (Figure 1). Therefore, PI disproportionately impacts secondary myogenesis, growth

potential of fetal skeletal muscle, and the potential metabolic homeostasis of fetal skeletal muscle (45–51).

1.4 Skeletal Muscle Metabolism

1.4.1 Overview. Skeletal muscle produces energy from nutritive sources in the form of adenosine triphosphate (ATP). Sustained metabolism of any tissue, including skeletal muscle, is dependent on its ability to balance ATP demand with ATP supply. ATP demand in the skeletal muscle consists of the sum of energy consuming activities which are central to all cellular processes including ion transport, biochemical synthesis, cellular trafficking, and protein turnover. As ATP is used in the skeletal muscle for these processes, its stores must be replenished in parallel to its utilization in order to maintain homeostasis. ATP resynthesis from ADP can be accomplished through 3 main mechanisms: creatine phosphate (short-term supply), glycolysis (intermediate-term supply), and oxidative phosphorylation (long-term supply). During periods of immediate energy need, such as muscle contraction, creatine phosphate acts as a nearly instantaneous phosphate donor which can quickly regenerate ATP without consuming oxygen. However, the concentration of creatine phosphate in the skeletal muscle is limited. Moreover, cellular processes in the developing fetus, such as protein synthesis, require a constant, enduring supply of ATP which cannot be matched by creatine phosphate alone (52). Therefore, long-duration, but higher yield, metabolic systems, such oxidative phosphorylation, are needed for ATP synthesis.

Adult and fetal skeletal muscle utilize different fuel substrates and require different metabolic pathways. Adult skeletal muscle preferentially uses fatty acids as a

fuel source in the fasting state, and glucose in the post-prandial state, due to the natural changes in feeding behavior. Alternatively, the placental unit provides the fetus with an uninterrupted nutrient and oxygen supply. The developing fetus is colloquially referred to as a "glucose-dependent parasite". As the name implies, carbohydrates are the primary fuel source for the fetus, with glucose and lactate accounting for ~80% of fetal energy consumption (53,54). Secondary to carbohydrate metabolism, the remaining 20% of fetal energy consumption is provided by amino acids, ketones, some fatty acids, and others (55). Therefore, fetal metabolism relies heavily on glucose oxidation pathways, with some supplementation from amino acid oxidation, for growth and development.

1.4.2 Glucose. Glycolysis is the catabolic glucose pathway occurring in the cytoplasm (Figure 2). The rate and conversion of glucose into pyruvate (the end product of glycolysis) is determined by two main cellular needs: ATP demand and carbon substrates for synthetic reactions (such as glycogenesis or fatty acid synthesis). Although it is not strictly an oxygen-dependent process, cellular oxygen levels dictate the glycolytic end products in the skeletal muscle.

During glycolysis, each glucose results in a net production of 2 ATP molecules and 2 NADH, which can be transported into the mitochondrion via the malate-aspartate shuttle, as well as 2 pyruvate molecules. Under adequate oxygen tension, each pyruvate molecule is then transported into the mitochondrion and further catabolized into acetyl-CoA and 1 NADH via pyruvate dehydrogenase (PDH)(56). Each NADH molecule is then oxidized in the mitochondrion, via oxidative phosphorylation, to produce additional 2.5 ATP molecules per NADH. Thus, complete oxidation of glucose via glycolysis produces

~ 12 ATP molecules (4NADH + 2ATP molecules produced per pyruvate) along with carbon skeletons (acetyl-CoA) needed for oxidative phosphorylation.

Glycolysis under anaerobic conditions results in the same production of 2 pyruvate molecules per glucose, but pyruvate is converted to lactate, via lactate dehydrogenase (LDH). The conversion of pyruvate to lactate comes at the cost of 1 NADH molecule per pyruvate. While the conversion of pyruvate to lactate is important as it replenishes NAD+ needed to sustain glycolysis, low-oxygen-glycolysis only nets 2 ATP per glucose molecule. The primary benefit of using anaerobic glycolysis opposed to aerobic glycolysis is that it provides a convenient source of ATP production when oxygen availability is low

1.4.3 Regulation of Pyruvate Conversion. Cellular energetics, along with substrate availability, dictate the metabolic endpoint of pyruvate and its conversion into either lactate, acetyl-CoA, or oxaloacetate (Figure 2). The conversion of pyruvate to acetyl-CoA leads to pyruvate (glucose) oxidation. PDH is a trimeric protein complex comprised of E1 (pyruvate dehydrogenase), E2(dihydrolipoyl transacetylase), and E3 (dihydrolipoyl dehydrogenase) subunits that are dependent upon vitamin B1 as a cofactor. PDH decarboxylates pyruvate, using NAD+ and CoA as cofactors, thereby producing NADH, acetyl-CoA, and CO_2. Because this step is central to the aerobic metabolism of glucose, its activity is tightly regulated by phosphorylation and dephosphorylation of the E1 subunit in concert with energy demand. The phosphorylation sites that regulate PDH activity are Ser293 (site 1), Ser300 (site 2), or Ser232 (site3) of the E1α, and phosphorylation of any one of these sites by pyruvate dehydrogenase kinase (PDK) 1-4 inactivates the PDH complex. Alternatively, PDH is active when all 3 sites are not

phosphorylated, and the dephosphorylation of PDH is controlled by pyruvate dehydrogenase phosphatase (PDP) 1 and 2.

Products of the PDH reaction (acetyl-CoA and NADH), along with low oxygen tension, inhibit PDH because they activate PDKs (56). Alternatively, substrates (pyruvate and NAD+) inhibit PDKs (56). During starvation, tissues, such as the skeletal muscle, increase PDK transcription and decrease PDP transcription (57). This prevents the skeletal muscle from oxidizing glycolytic end products. Moreover, it promotes a shift to fatty acid and amino acid oxidation, thereby sparing glucose. In summary, PDH is regulated at multiple points, including expression and enzyme activity, to regulate pyruvate oxidation rate.

Pyruvate can be converted into oxaloacetate, a necessary TCA cycle intermediate. The ATP and biotin-dependent carboxylation of pyruvate into oxaloacetate is performed by pyruvate carboxylase (PC), and the function of PC in non-gluconeogenic cells, such as skeletal muscle, is to promote pyruvate transfer into the TCA cycle intermediates for the maintenance of oxaloacetate-acetyl CoA condensation (58–60). PC is allosterically activated by high acetyl-CoA and ATP concentrations. Interestingly, high acetyl-CoA and ATP concentrations also act as indirect inhibitors of PDH. Thus, increased acetyl-CoA and ATP concentrations act as a signal to the cell that energy needs are met, and pyruvate flux into the TCA cycle is adjusted accordingly.

1.4.4 Regulation of Lactate Conversion. LDH is regulated by substrate equilibrium opposed to post-translational modification like PDH. Human LDH is a tetrameric enzyme complex formed by the combination of two subunits “M”, known as the muscle isoform, and “H”, known as the heart isoform. The M and H isoforms are

encoded by the *LDHA* and *LDHB* genes, respectively, and differ in their affinities to catalyze the pyruvate:lactate interconversion. LDHA has a higher affinity for converting pyruvate to lactate, while LDHB has a higher affinity for converting lactate to pyruvate. These two subunits can form five possible tetramers: 4H, 4M, 3H:1M, 2H:2M, and 1H:3M. Each isomer has a different *overall* affinity for the direction of performing pyruvate:lactate interconversion based upon the ratio of M:H isoforms. In skeletal muscle, the 4M isozyme predominates, and it facilitates the conversion of pyruvate to lactate. Under times of PDH inactivation in the skeletal muscle, pyruvate is preferentially shuttled down its concentration gradient towards lactate, which can then be released into circulation. Accordingly, skeletal muscle shunts pyruvate towards lactate production to sustain glycolytic capacity.

1.4.5 Amino Acids. The average 70kg adult man contains ~12kg of protein and ~200g of free amino acids (61,62). Skeletal muscle comprises ~40% of total mass, comprises ~60% of protein stored in the body, and ~50% of free amino acids are found in the intracellular space of skeletal muscle (61). Although skeletal muscle sequesters a about half of all free amino acids in the body, the fractional protein synthesis rate of adult human and pig skeletal muscle is relatively low, ~1% per day(63–65).

Studies on diurnal cycling of protein turnover in adults shows overnight fasting produces a moderate net protein breakdown in muscle (synthesis < degradation) (65–67). In contrast to the liver, where most of the twenty amino acids that are present in human proteins are readily oxidizable, rat and human skeletal muscle can only oxidize six of the twenty: asparagine, aspartate and glutamate, and the branched-chain amino acids (BCAA: leucine, isoleucine, valine (68–72). Therefore, it can be assumed that amino acids that are

released from the fasting skeletal muscle are released in proportion to their occurrence in skeletal muscle protein. Human skeletal muscle does not exhibit a net release aspartate, asparagine, glutamate, or BCAAs (61). Instead, the skeletal muscle releases much more glutamine (48% of total release), alanine (32% of total release) than is expected from their occurrences in muscle alone (each comprise ~8% of skeletal muscle). This process is beneficial as these amino acids are gluconeogenic and can, therefore, supplement hepatic gluconeogenesis during fasting. Moreover, the preferential release of glutamine/alanine, compared to the normal composition of the skeletal muscle, implies amino acid interconversion exists within the muscle for the *de novo* synthesis of glutamine and alanine(73).

Under protein-balance, hyperinsulinemic conditions, adult rat skeletal muscle perfused with [U-^{14}C]valine produced no radiolabeled lactate, pyruvate, glutamine, or alanine (74). Because valine can only enter the TCA cycle as succinyl-CoA, this shows TCA cycle intermediates are not converted into pyruvate. More importantly, this also implies that the other oxidizable amino acids that do not enter the TCA cycle as acetyl-CoA (e.g. asparagine, aspartate, glutamate, leucine, and isoleucine) cannot be used for complete oxidation, as complete oxidation can only occur if a substrate enters as acetyl-CoA (73).

The fetal skeletal muscle primarily uses amino acids in the circulation for protein synthesis and accretion (75,76). Therefore, combined with negligible rate of hepatic glucose production in normal fetuses, it is not thought that fetal skeletal muscle produces substantial quantities of glutamine or alanine (77). It is also unknown at what capacity amino acids serve as TCA cycle intermediates in fetal skeletal muscle, although amino

acids may be used in fetal skeletal muscle as they serve as precursors for other biosynthetic reactions such as purine (α-ketoglutarate) or pyrimidine (oxaloacetate) production.

1.4.6 Energy Needs in the Fetal Skeletal Muscle. Glycolysis is useful in anaerobic situations where aerobic oxidation may be unable to provide energy to the muscle due to limited oxygen availability. Pyruvate generated in aerobic glycolysis must be transported across the mitochondrial membrane and then subsequently oxidized. However, in most tissues, the energy produced from anaerobic glycolysis is too low to sustain resting metabolic homeostasis. Unsurprisingly, glycolytic flux in resting adult skeletal muscle is low, and studies performed in anoxic skeletal muscle shows glycolytic flux alone is insufficient to generate enough ATP to meet ATP demand (78,79). This rate has not been measured in fetal skeletal muscle; however, it is assumed that glycolysis cannot sustain fetal skeletal muscle metabolism as it is an actively developing and growing tissue. Therefore, in the growing skeletal muscle of the fetus, ATP demand must be met through aerobic metabolism (oxidative phosphorylation).

1.4.7 Oxygen, Oxidative Phosphorylation, and the Powerhouse of the Cell. Aerobic respiration in the mitochondrion (oxidative phosphorylation) is the principle method for ATP synthesis. Oxidative phosphorylation yields ~30 ATP molecules per glucose (80). As is implied by the name, aerobic metabolism relies on the presence of oxygen to function. However, unlike nutritive substrates (glucose, amino acids, lipids) which are transported in the blood plasma or bound to carrier proteins, oxygen is transported in mammalian circulation bound to hemoglobin found in erythrocytes. The

supply of oxygen must also be constant as there are minimal oxygen stores in the tissues of most mammalian species.

But, why is oxygen critical to oxidative phosphorylation? The answer to this question lies in the electron transport chain (ETC). Within the mitochondrion, on the inner mitochondrial membrane, sits the electron transport chain which is comprised of Complex I-IV and ATP synthase. As nutrients (e.g. glucose or amino acids) are oxidized in their respective pathways, reducing equivalents (NADH or $FADH_2$) are produced. These reducing equivalents are oxidized at the electron transport chain at Complexes I and II, respectively. As the reducing equivalents are oxidized, two events occur: electrons are donated to the electron transport chain, and protons are released into the mitochondrial matrix. The electrons donated to Complex I/II, from the oxidation of $NADH/FADH_2$, flow down the ETC according to increasing redox potential. First, they are transferred to Complex III, then Complex IV, then donated onto singular, relatively more electropositive, oxygen (Complexes I/II → Complex III → Complex IV → $O^{\bullet}$). The protons released by $NADH/FADH_2$ oxidation flow from the matrix into the intermembrane space, building a proton gradient (proton motive force) that ATP synthase uses to drive ATP production from ADP and P_i. Thus, the energy generated by the proton motive force is captured as a high energy phosphate bond in ATP. Importantly, because oxygen is the terminal electron donor in the ETC, this process can only occur in the presence of oxygen.

In cells with a normal partial pressure of oxygen (1-10mmHg at the mitochondrial surface), mitochondrial respiration rate is determined by ATP utilization (81,82). Thus, to maintain ATP homeostasis, the rate of ATP synthesis is synchronized with the rate of

ATP utilization. A majority of ATP consumption can be accounted for by 3 processes: Na+/K+ ATPases (up to 30% of O_2 consumption), protein synthesis (up to 28% of O_2 consumption), and Ca^{2+} ATPases (~8% of O_2 consumption) (83). ATP synthesis for these processes is primarily handled by oxidative phosphorylation, but, how are these processes regulated under times of energy stress caused by hypoxia or low nutrient conditions as is seen in IUGR fetuses?

1.4.8 Energy Regulation Under Energy Stress. Intuitively, reducing the demand for ATP-dependent processes during stress (e.g. malnutrition) would reduce the demand for ATP and therefore maintain cellular energy balance. Cellular processes that demand ATP differentially regulated. This is exemplified in studies that partially inhibit cellular oxygen consumption through sub-inhibitory doses of ETC inhibitors. When using sub-inhibitory doses of ETC inhibitors, partial inhibition of ATP synthesis occurs, and DNA/RNA/protein synthesis rates are drastically lowered; however, ion transport rates are only slightly impacted (84–86). Importantly, it is not until the severe inhibition of ATP synthesis that transport capacities of Na+/K+ ATPases and Ca^{2+} ATPases (the processes governing the ion-motive forces) are significantly affected (84,85). It is from these two observations that a biological hierarchy emerges for ATP demand in descending order: protein synthesis > RNA/DNA synthesis and substrate oxidation > Na^+ cycling and Ca^{2+} cycling > other ATP consumers and mitochondrial proton leak (85). This pattern implies that those processes most important to cell survival, such as maintaining the ion-motive force, will continue to function at low [ATP], while other processes, such a protein synthesis, are, at least acutely, expendable.

Although lowering ATP utilization is beneficial to survival under energy stress conditions, energy supply must be similarly coordinated to maintain cellular homeostasis. This has been substantially studied in hypometabolic animals that undergo conditions such as torpor or hibernation. In hibernating ground squirrels, skeletal muscle [ATP] decreases by ~40%, and both protein synthesis and proteolysis are lowered to conserve energy (87–89). The reductions in energy demanding pathways in these animals are also matched by lower activity rates of glycolytic enzymes, including phosphofructokinase and pyruvate kinase (90–92). Reductions in both energy supplying and energy demanding pathways are also observed in the skeletal muscle of the African lungfish during aestivation (summer hibernation), where glycolytic enzyme and mitochondrial state 3 and state 4 respiration rates are both lowered relative to non-aestivation periods (93). Changes in energy demand and supply are also observed in hepatopancreas cells isolated from aestivating snails where mitochondrial oxygen consumption rates decrease ~60% relative to non-aestivation (94). Bioenergetic analysis of the hypometabolic state in these snails shows ~ 75% of the total mitochondrial respiration was due to changes in the kinetics of substrate oxidation (glycolysis, TCA cycle, ETC), and the remaining ~25% was related to changes in ADP phosphorylation and utilization (94). The hypometabolic state represents a concomitant lowering of energy supply and demand. As the mitochondria are central to the production of ATP, the modulation of energy homeostasis during mal-nutritive states involves modulating substrate oxidation, lowering mitochondrial ATP synthesis, and lowering ATP demand. IUGR fetuses exist in an environment of chronically lower nutrient and oxygen supplies, not unlike hibernation. Thus, reducing mitochondrial

bioenergetics and substrate kinetics to induce a hypometabolic state may be a central adaptation needed for adaptation to low substrate conditions.

1.5 Global Metabolic Adaptation in IUGR Fetuses

The IUGR fetus must develop metabolic adaptations in response to placental restriction. Although glucose is the primary fuel for the fetus, the flux of glucose, oxygen, and amino acids, is reduced with PI in IUGR pregnancies (95–97). Moreover, and likely due to hypoxia associated with low oxygen flux across the placenta, human IUGR fetuses exhibit hypercatecholinemia (98,99). IUGR fetuses also exhibit smaller pancreatic beta cell masses resulting in hypoinsulinemia (100–103). Insulin functions to promote tissue growth by increasing glucose oxidation in peripheral tissues such as skeletal muscle (16). However, IUGR fetuses have increased peripheral insulin sensitivity (104–106). Thus, the lower insulin concentrations, but increased insulin sensitivity, leads to normal glucose clearance in IUGR fetuses (76). Understanding how IUGR skeletal muscle adapts to low nutrient and oxygen availability may be key to understanding why these individuals are predisposed to metabolic syndromes later in life.

The abnormal metabolic and physiologic factors that cause IUGR confer a predisposition to metabolic pathologies later in life because, in part, IUGR fetuses have lower lean masses (107–112). The reduction in lean mass at birth is retained into adulthood, despite adequate nutrition, and adipose tissue in these individuals is preferentially deposited opposed to skeletal muscle accretion (107,109,110,113–115). Human IUGR neonates have higher respiratory rates and greater energy expenditure,

indicative of a thrifty metabolic phenotype in response to relative nutrient overabundance (116–118).

Considering growth is dictated by the balance between energy production and energy utilization, and this relationship is governed by ATP, these observations imply defects in the prenatal environment lays the molecular foundation for postnatal growth; failure to increase adequate muscle mass in adulthood potentiates adiposity through a disjointed metabolic phenotype (119–124). Additionally, the greater adiposity may serve as a comorbidity that exacerbates or causes additional strain throughout the life-course (125). These observations imply mitochondrial metabolism is altered in the skeletal muscle of IUGR individuals, and exposure to low nutrient and oxygen availability *in utero* may disrupt skeletal muscle mitochondrial function. However, to clearly parse the mechanisms of IUGR skeletal muscle mitochondrial metabolism and function, animal models that recapitulate the human IUGR phenotype are needed.

1.6 Animal Models of IUGR

1.6.1 Overview. Animal models are critical to understanding the pathophysiological mechanisms of skeletal muscle adaptation in IUGR fetuses. Using animal models of IUGR allows investigators to study the acute and chronic effects of nutrient restriction on metabolism while simultaneously avoiding ethical issues involved in human IUGR studies. Human IUGR fetuses are afflicted with hypercatecholinemia, hypoinsulinemia, hypoglycemia, hypoxia, and sarcopenia (126,127). Thus, it is critical to select an animal model that recapitulates most, if not all, of these pathophysiological conditions. Common animal models of IUGR include rats, pigs, and sheep; importantly,

the maternal or placental nutrient supply in each model system can be manipulated differently to produce IUGR. While each animal can produce fetal growth restriction, the resulting physiology of that fetus is not equal across species or methods used to induce growth restriction. The common IUGR animal model systems are discussed below.

1.6.2 Rats. The short lifespans and generation lengths of the rats make it beneficial for exploring relationships between fetal growth restriction and persistent metabolic complications from an IUGR pathology. Three well-defined rat models of IUGR show lasting metabolic consequences in skeletal muscle due to reduced nutrient availability during gestation. Maternal dietary restriction is used in a variety of animal models, and IUGR can be produced through either global caloric restriction or singular nutrient (e.g. protein) restriction. A 50% caloric restriction (CR) of dams during mid to late gestation results in a ~10% reduction in bodyweight at or near the time of birth, as well as lower β cell mass and insulin content (121,128–130). Feeding dams an isocaloric, low protein (LP) diet starting from mid-gestation results in a 40-50% reduction in pup bodyweight, highlighting the importance protein availability for fetal tissue accretion (131,132). Both CR and LP diet lead to IUGR by restricting the maternal supply of nutrients; however, in these models, fetal oxygen availability is unaffected. Alternatively, uterine artery ligation (UAL) at embryonic day 19 (E19) causes acute decreases in both oxygen and nutrient availability to the fetus by E20-21 resulting in a 10-20% reduction in pup bodyweight (113,133). These studies demonstrate the connection between low nutrient availability and restricted fetal mass that may affect fetal metabolism.

Although the exact mechanisms are unclear, the progression of metabolic dysfunction from fetal life into adulthood is portrayed in rat models of IUGR. Here, rat

pups afflicted with IUGR due to CR, UAL, or LP diet possess defects in metabolic profiles, such as oxidative phosphorylation or nutrient signaling, in the skeletal muscle likely due to *in utero* adaptations to a nutrient restricted environment (114,115,139,121,128,133–138). The persistent disparity in lean mass may serve as an IUGR trait that underscores defects in skeletal muscle metabolic function leading to glucose intolerance, fatty liver disease, and altered amino acid metabolism in juveniles with IUGR (115,129,136,140–144).

1.6.3 Piglets. The relative metabolic and functional similarities of pig and human physiology is advantageous for studying the postnatal consequences of perinatal complications such as IUGR (145–147). Natural runting of piglets (IUGR) arises from a disproportionate supply of nutrients along the uterine horn causing growth restriction of 15-20% of piglets from each litter (148). As a result of in utero nutrient restriction, runt piglets exhibit metabolic perturbances which lasts into adulthood (149). Moreover, the runt piglet possesses pathologies similar to common occurrences of human IUGR: asymmetric growth restriction, an increased brain:liver ratio, and reduced bodyweight at birth (150–152).

Similar to other animal models of IUGR, IUGR piglets are born with less lean mass than their normally grown counterparts, which limits the extent of postnatal lean mass (153,154). Consistent with this observation, IUGR piglets also have a lower capacity for skeletal muscle protein accretion and protein synthesis evidenced by a greater abundance of proteasomes, and a lower abundance of translation-initiating enzymes (155,156). The impact of IUGR not only skeletal muscle growth, but also the abundances of proteins involved in energy production in the skeletal muscle, potentially

altering cellular redox state in the skeletal muscle of IUGR piglets (155). As adults, energy production, amino acid catabolism, and glucose metabolism remain dysregulated in both the skeletal muscle (149,157). Although it is unclear how IUGR broadly affects metabolic homeostasis, clues to metabolic adaptation of IUGR piglets may be found in supplementation studies. Specifically, while mid-gestation arginine/glutamine supplementation of gilts reduces the number of IUGR piglets per litter, neonatal supplementation of amino acids to IUGR piglets results in hyperammonemia, elevated blood urea concentrations, and death (156,158). Alternatively, during the first 21 days post-parturition, postnatal glucose injections increased IUGR piglet bodyweight compared to non-supplemented IUGR piglets (159). Based on these observations, IUGR piglets may have predetermined fuel preferences that is programmed in utero. Thus, in IUGR piglets the asymmetric growth restriction coupled with metabolic dysfunction, indicates underlying defects in mitochondrial function that continues postnatally (160–165).

1.6.4 Sheep. Experiments in fetal sheep are advantageous for studying placental-fetal metabolism during normal pregnancy and in pregnancies with complications that represent human pathologies. Sheep have the propensity to have singleton or twin pregnancies, eliminating the confounding factor(s) of large litters found in other models such as rats and pigs. Moreover, a variety of experimental models are available to induce asymmetric IUGR in sheep, and generally these models are created by one of two methods: reducing placental structure/function or preventing normal placental development. Reducing placental structure/function can be accomplished through either surgical removal of uterine caruncles (carunclectomy) or mechanical manipulation of

placental blood flow (placental embolization and single umbilical artery ligation). These methods mimic placental insufficiency and yield fetuses with 15-66% growth restriction compared to matched controls (166–168). Alternatively, methods that inhibit placental development (such as maternal hyperthermia) lead to IUGR of the fetus. Subsequently, fetal weights in these sheep models of IUGR are reduced by 30-60% (169–172). However, slight differences between sheep models in relation to human IUGR exists.

In the ovine carunclectomy model, the number of placentomes is limited through surgical removal of endometrial caruncles from the uterus of non-pregnant ewes prior to mating. Thus, the number of placentomes that form during pregnancy are limited, thereby limiting placental, fetal growth, and lean mass (173).The carunclectomy model induces both fetal hypoglycemia and hypoxia (~23% decrease in glycaemia, and ~40% decrease in oxygen tension vs control (174–176). Moreover, umbilical blood flow in the carunclectomy model is reduced ~40% compared to controls, and circulating norepinephrine concentrations are nearly doubled (175,177). This model produces growth restricted fetuses with similar nutrient supply and blood gas profiles of human infants that are born SGA (173).

The placental embolization model mimics the onset of IUGR in late gestation through repeated injections of microspheres into the placenta via the umbilical artery at ~0.7 of gestation (178,179). As a result, the microspheres physically block the maternal-fetal transfer of nutrients resulting in a progressive onset of chronic hypoxia (~40% decrease over 20 days), hypoglycemia (~50% decrease over 20 days), as well as 3-4 fold increase of fetal plasma norepinephrine over 20 days, resulting in IUGR (179–182).

The single uterine artery ligation (SUAL) model involves ligating an umbilical artery in close proximity to the fetal abdomen at approximately 0.75 of gestation (183). SUAL mechanically inhibits blood flow of the placenta, reducing umbilical flood blow by ~30%, and resulting in a reduced capacity of the placenta to transfer nutrients to the fetus (183,184). The resulting fetus is growth restricted, as lower lean mass, and exhibits hypoxemia.

The hyperthermia-induced model of placental insufficiency reduced fetal growth by exposing pregnant ewes to elevated ambient temperatures in a diurnal cycle (40 °C for 12 h and 35 °C for 12 h) during mid-gestation (~40 days gestation to ~90 days gestation) (185). Ewes placed in ambient hyperthermic environments redistribute blood flow to the periphery, leading to ~50% reduction in umbilical blood flow and lower placental mass (185). As a result of mid-gestation insult to placental growth, the IUGR fetus must cope with a progressive decline in placental transport of nutrients, which is progressively worsened by increasing fetal weight, and results in metabolic adaptations that aim to conserve energy expenditure *in utero*. As such, placental insufficiency-induced IUGR sheep fetuses are afflicted with severe nutrient restriction in late gestation that results in severe hypoxemia (~50% lower compared to controls) , hypoglycemia (~50% lower compared to controls), hypercatecholinemia(4-5 fold increase compared to controls), hypoinsulinema (~75% lower compared to controls), and reduced transport of amino acids (185–189).

1.6.5 Sheep: Models of IUGR. Due to their aptitude to *in utero* surgical manipulation, potential for chronic catheterization of the fetus, and capability of serial blood sampling from both mother and fetus, sheep models of IUGR provide important

insights into the maladaptive metabolic developments of IUGR. Compared to rodent models, gestation is longer in sheep, which affords experiments on the progression of IUGR pathologies during gestation (190–192). Sheep also have a propensity for precocial, singleton pregnancies, unlike pigs and rats, which have litters. Importantly, in sheep, primary myogenesis begins at ~0.2 of gestation and secondary myogenesis begins at ~0.27 of gestation (33,34,193). Both of these events parallel human myogenesis (0.2 and 0.35 for primary and secondary myogenesis, respectively (33,34,193).

The mid-gestation maternal hyperthermia model best mimics the gradual onset of placental insufficiency found in human cases of IUGR. As a result, the slowing of fetal growth in this model results from fetal adaptations which match progressive, chronic decreases in placental function and subsequent lower nutrient supply. Alternatively, the sheep carunclectomy model restricts blood and nutrient flow to the fetus throughout gestation, the SUAL and embolization models only restrict blood and nutrient flow starting later in gestation (~0.75 of gestation). The SUAL, embolization, and carunclectomy models do not capture the progressive pathology of IUGR. Therefore, the mid-gestation maternal hyperthermia sheep model most accurately recapitulates the human pathophysiology of PI-IUGR.

1.6.6 Metabolic Consequences of IUGR Using the Maternal Hyperthermia Sheep Model. In the maternal hyperthermia sheep model of IUGR, the conservation and scavenging of oxygen and nutrients from expendable metabolic processes, such as systemic growth, is a necessary adaptation to meet basal metabolic demands. Accordingly, because protein synthesis during the latter half of gestation accounts for ~18% of fetal oxidative metabolism, and protein synthesis is an ATP consuming process,

slowing protein accretion may be a primary mechanism of conserving energy, oxygen, and nutrients in PI-IUGR fetuses (194,195). This is evidenced by lower skeletal muscle accretion and fractional synthetic rates, but normal amino acid oxidation rates in ovine IUGR fetuses (76). Furthermore, in an attempt to redirect energy requirements to vital organs, ovine IUGR fetuses have greater peripheral insulin sensitivity, but lower fractional glucose oxidation rates relative to glucose utilization (76,104,196–199). Strikingly, hepatic glucose production also develops to fulfill the placental deficiencies in glucose uptake and is resistant to insulin (200).The *in-utero* adaptations lead to postnatal metabolic dysfunction where young lambs afflicted with IUGR continue to have lower lean masses and skeletal muscle protein contents, altered glucose metabolism, and greater adiposity (106,201–204). These observations show that metabolic adaptations that impact growth and energy balance of the fetus persist postnatally. Considering many of these catabolic processes occur in the mitochondria, where a majority of ATP production and oxygen consumption takes place, these adaptations imply IUGR fetuses have altered skeletal muscle mitochondrial function.

1.7 Overview of Specific Aims

The pathophysiology of human IUGR results from a progressive decrease in placental function and nutrient transport, and animal models that mimic the human condition must also possess similar progressive declinations leading to adaptation. Within the realm of IUGR animal models, the hyperthermic sheep model represents a unique model for studying IUGR physiology that cannot be accomplished by any other species.

The hypoglycemia and hypoxemia present in IUGR sheep fetuses due to placental insufficiency leads to unique fetal adaptations of the skeletal muscle such as sarcopenia and lower fractional glucose oxidation rates relative to glucose utilization. Moreover, the upregulation of glucose transporters in the brain and the heart of these fetuses indicates mechanisms exist to increase glucose extraction in non-peripheral tissues (196,205). However, because glucose transporters are not upregulated in skeletal muscle, the redistribution of glucose may also depend on alterations in glucose metabolism (43,206).

Glucose is the primary fuel for the developing fetus and altering skeletal muscle glucose metabolism can have profound consequences on fetal development. However, because IUGR skeletal muscle is growth restricted, and has lower fractional glucose oxidation rates, the IUGR fetus may be restricting skeletal muscle glucose oxidation in an attempt to conserve glucose and oxygen for vital tissues. These adaptations to glucose homeostasis may also cause reductions in energy production in the IUGR skeletal muscle. Mitochondria are the central organelle for glucose oxidation, and the first step of non-glycolytic (post-glycolysis) glucose oxidation begins with the conversion of pyruvate to acetyl-CoA via PDH. As such, we test the hypothesis that pyruvate metabolism skeletal muscle mitochondria is inhibited in IUGR fetuses as an adaption to low glucose and oxygen availability. Therefore, in **AIM 1**: The activity and expression of PDH, and the expressions of the positive and negative regulators of PDH, were determined in order to define the extent of inhibition of pyruvate oxidation in IUGR skeletal muscle.

Next, to fully understand the bioenergetic landscape of IUGR mitochondria, it will be important to understand how overall energy production may be impacted by low substrate and low oxygen conditions. As reviewed above, glucose oxidation, while the

primary fuel of the fetus, does not exclusively fulfill fetal energy needs. Alternatively, fetuses derive ~20% of their energy from amino acid oxidation (55,207). Growth restricted ovine fetuses lower the rates of protein synthesis, protein accretion, and growth in response to low nutrient and oxygen availability (76). Thus, IUGR fetuses may adapt to low nutrient availability in a similar manner as hibernating animals in that skeletal muscle ATP utilization and ATP synthesis are concomitantly lowered in order to permit survival. However, this places the fetal skeletal muscle in an overall "lower energy state". Substrate oxidation, TCA cycle, and electron transport chain enzyme abundances are all postulated to be lower in IUGR skeletal muscle mitochondria. Therefore, in **AIM 2**: the oxygen consumption rates, and ETC subunit activities were measured in isolated skeletal muscle mitochondria as a means to quantitatively measure ETC function. Additionally, whole-mitochondrial bioenergetics will be evaluated by measuring differences in protein abundances within the mitochondria-proteome between IUGR and control fetuses.

Although the sheep model is a well-established animal model for the study of IUGR, both pig and rat models of IUGR are used for fetal and neonatal research. However, comparisons of fetal skeletal muscle mitochondrial metabolism between animal models of IUGR has not been established and gaps in our knowledge remain. Therefore, in **AIM 3**: comparisons were drawn between the animal models of IUGR (rats, sheep, humans) in an attempt to accurately describe mitochondrial metabolism in skeletal muscle and liver of IUGR fetuses.

IUGR results in severe growth restriction of the skeletal muscle. This reduced lean mass persists even after compensatory postnatal catch up growth, ands skeletal

muscle hypertrophy can only partially compensate for reductions in fiber number. Low lean mass at birth is compelling linked to the risk of developing metabolic discordance later in life. In IUGR fetuses, the fetal environment is known to influence postnatal quality of life. PI disproportionately impacts fetal skeletal muscle growth and, in combination with the low nutrient/substrate environment of IUGR fetal development, leads to changes in global fetal substrate metabolism in the skeletal muscle such as lower fractional glucose oxidation rates and lower protein synthesis rates. Alterations to global metabolism persist into the postnatal environment where neonates have lower adiposity, lower lean mass, but enhanced skeletal muscle glucose disposal. These observations imply that alterations to substrate availability *in utero* may program alterations to postnatal metabolism. Substrate utilization is intrinsically tied to the mitochondria, IUGR environment in which fetal skeletal muscle develops *in utero* may negatively impact postnatal skeletal muscle mitochondrial metabolism. Therefore, in **AIM 4**: oxygen consumption rates were measured in mitochondria isolated from differentiated myotubes of 30- day old lambs to quantitatively measure ETC function in postnatal skeletal muscle. Additionally, whole-mitochondrial bioenergetics were evaluated by measuring differences in protein abundances within the mitochondria-proteome between IUGR and control lambs.

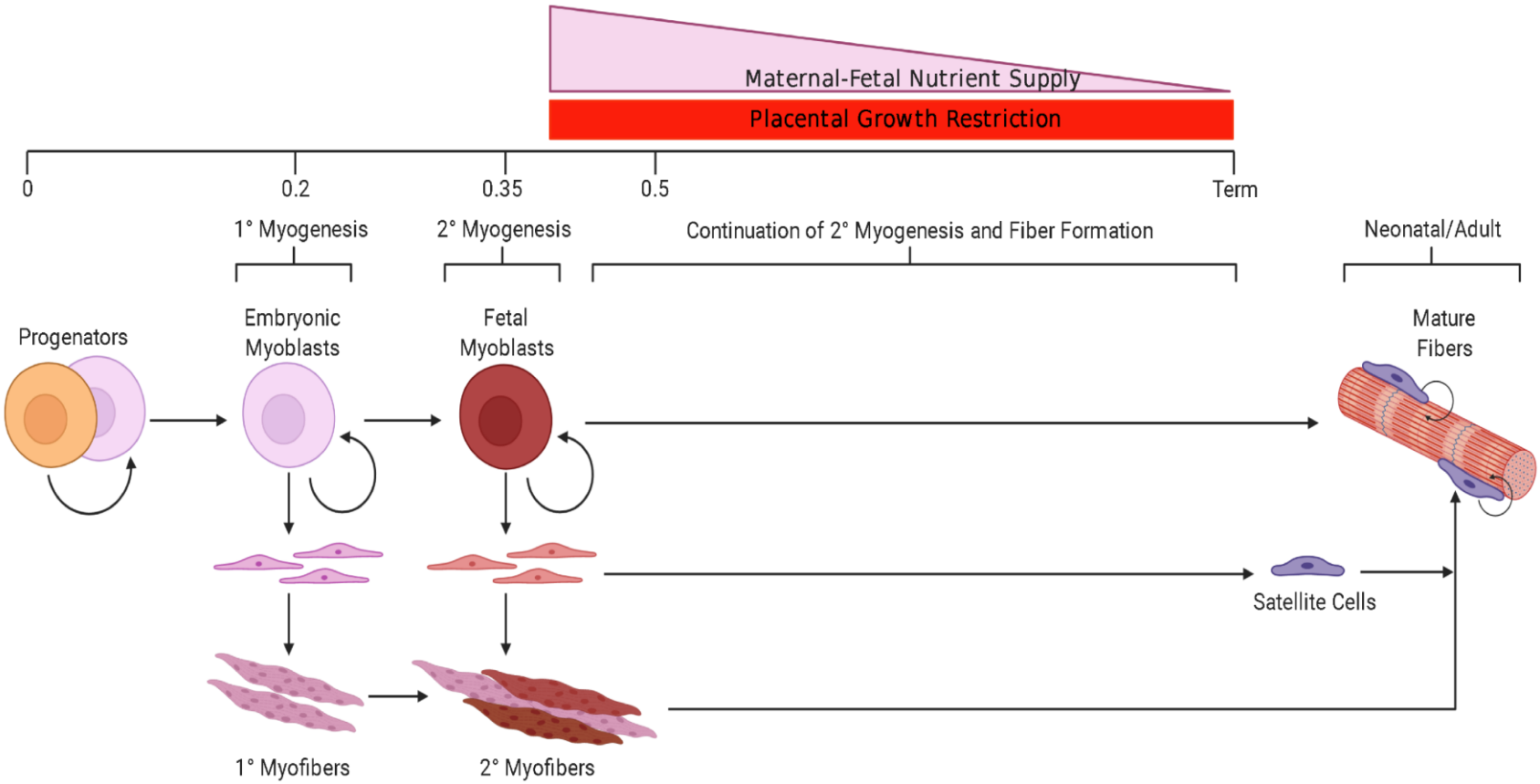

Figure 1. Impact of nutrient Restriction on human skeletal muscle development. During embryonic development, self-renewing progenitors give rise to embryonic myoblasts. At ~.2 of gestation, primary myogenesis occurs when self-renewing embryonic myoblasts proliferate yielding 1º myotubes and a pool of embryonic myoblasts. The 1º myotubes act as the scaffolding on which 2º myotubes will form. During secondary myogenesis, fetal myoblasts that arose from embryonic myoblasts proliferate. Fetal myoblast proliferation yields a pool of fetal myoblasts, and 2 º myotubes which use 1º myotube as a scaffold to promote skeletal muscle growth. Close to term, and later in secondary myogenesis, satellite cell precursors are produced and localize within mature fibers. Figure created using Biorender.com

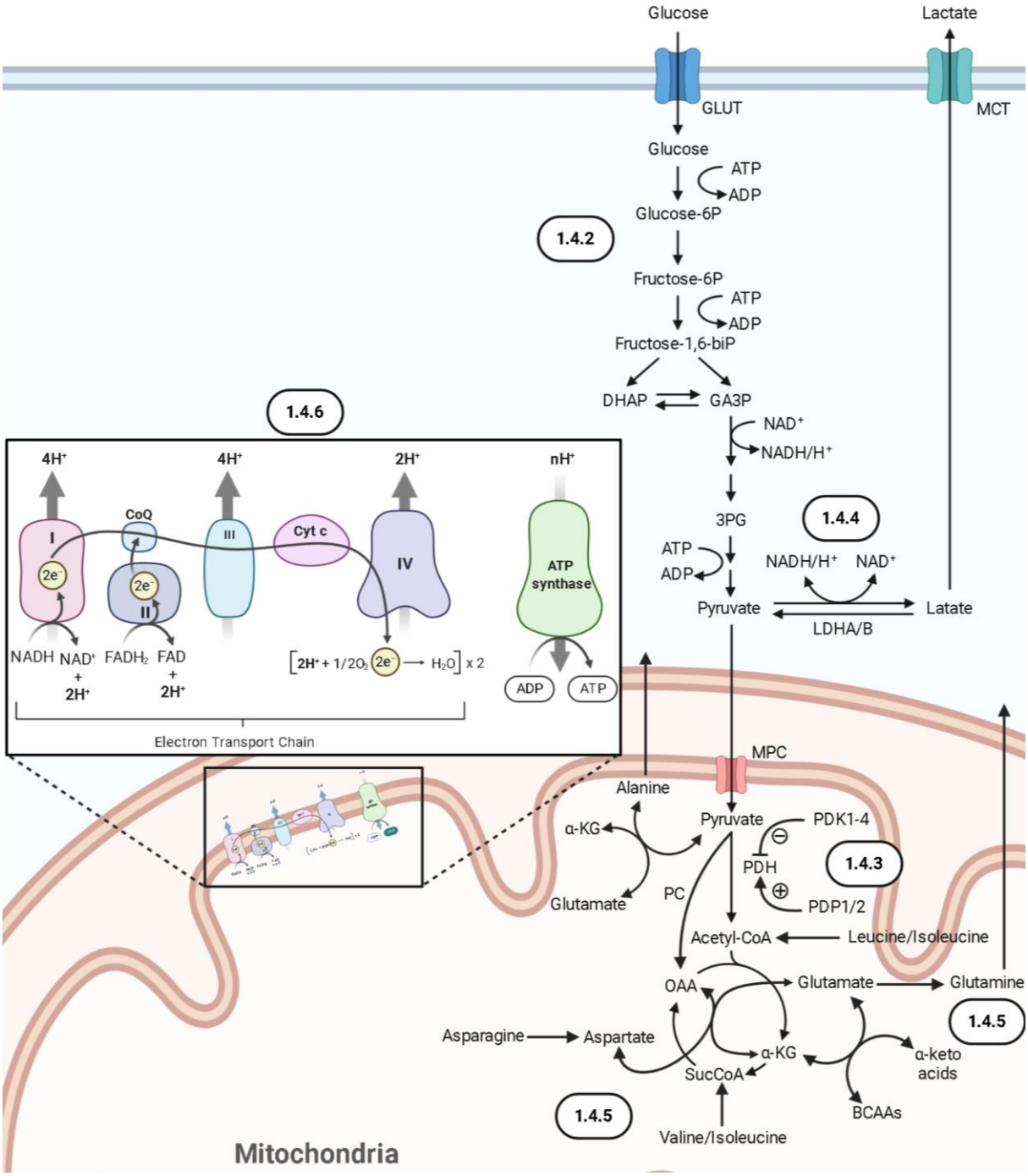

Figure 2. Summary figure of skeletal muscle metabolism. An outline of skeletal muscle metabolism is presented for glucose metabolism and glycolysis (1.4.2), regulation of pyruvate metabolism (1.4.3), regulation of lactate metabolism (1.4.4), amino acid metabolism (1.4.5), and oxidative phosphorylation (1.4.6). Figure created using Biorender.com.

Chapter 2

Increased Pyruvate Dehydrogenase Activity in Skeletal Muscle of Growth-Restricted Ovine Fetuses.

The contents of this chapter have been accepted for publication in the American Journal of Physiology-Regulatory, Integrative, and Comparative Physiology.

The full citation is given below.

Pendleton AL, et al. Increased pyruvate dehydrogenase activity in skeletal muscle of growth-restricted ovine fetuses. Accepted for publication in Physiology-Regulatory, Integrative, and Comparative Physiology (2019).

2.1 Abstract

Fetal sheep with placental insufficiency-induced intrauterine growth restriction (IUGR) have lower fractional rates of glucose oxidation and greater gluconeogenesis, indicating lactate shuttling between skeletal muscle and liver. Suppression of pyruvate dehydrogenase (*PDH*) activity was proposed because of greater pyruvate dehydrogenase kinase (PDK) 4 and PDK1 mRNA concentrations in IUGR muscle. Although PDK1 and PDK4 inhibit PDH activity to reduce pyruvate metabolism, PDH protein concentrations and activity have not been examined in skeletal muscle from IUGR fetuses. Therefore, we evaluated the protein concentrations and activity of PDH and the kinases and phosphatases that regulate PDH phosphorylation status in the semitendinosus muscle from placenta insufficiency-induced IUGR sheep fetuses and control fetuses. Immunoblots were performed for PDH, phosphorylated PDH (E1α), PDK1, PDK4, and pyruvate dehydrogenase phosphatase 1 and 2 (PDP1 and PDP2, respectively). Additionally, the PDH, lactate dehydrogenase (LDH), and citrate synthase (CS) enzymatic activities were measured. Phosphorylated PDH concentrations were 28% lower ($P < 0.01$) and PDH activity was 67% greater ($P < 0.01$) in IUGR fetal muscle compared with control. PDK1, PDK4, PDP1, PDP2, and PDH concentrations were not different between groups. CS and LDH activities were also unaffected. Contrary to the previous speculation, PDH activity was greater in skeletal muscle from IUGR fetuses, which parallels lower phosphorylated PDH. Therefore, greater expression of PDK1 and PDK4 mRNA did not translate to greater PDK1 or PDK4 protein concentrations or inhibition of PDH as proposed. Instead, these findings show greater PDH activity in

IUGR fetal muscle, which indicates that alternative regulatory mechanisms are responsible for lower pyruvate catabolism.

2.2 Introduction

Placental insufficiency-induced intrauterine growth restriction (IUGR) causes deficits in oxidative glucose metabolism and a reduction in the lean mass (189,208). The deterioration of placental function leading to fetal growth restriction is a leading cause of perinatal death, and those surviving the perinatal period are at greater risk of developing metabolic syndromes (189,209–211). Our ovine model of hyperthermia-induced placental insufficiency successfully recapitulates several aspects of the human IUGR phenotype (185). The IUGR fetus has reductions in skeletal muscle mass and other peripheral tissues relative to neural tissues, as a result of lower plasma glucose and insulin concentrations and lower blood oxygen content (212–217)

Glucose and lactate are the primary fuels in the fetus and their oxidation accounts for ~50% of the fetal oxygen consumption in normally grown fetuses (218). Although IUGR fetuses are hypoxemic compared to control fetuses, IUGR fetuses have normal or near normal rates of weight-specific oxygen consumption (185,219,220). Though IUGR fetal oxygen uptake rates are normal or near-normal, weight-specific rates of fetal glucose uptake are depressed in IUGR fetuses with placental insufficiency resulting in measurable rates of endogenous glucose production to maintain normal rates of glucose utilization (76,104,196,221). Upregulation of glucose transporters in the brain and heart indicate mechanisms are enhanced to improve glucose extraction (196,205,222). However, alterations in glucose transporters are not evident in all tissues, which indicates

that redistribution of glucose may also depend on changes in glucose metabolism (43,206,223). IUGR fetuses oxidize a smaller fraction of glucose and have lower glucose oxidation rates, even though glucose utilization rates are normal, compared to control fetuses (196,197,200). These findings have led to the hypothesis that IUGR fetuses have higher expression of enzymes that hinder pyruvate oxidative metabolism in skeletal muscle to promote lactate transfer to the liver to support glucose production (196,197,200).

The findings to date indicate a central role for inhibition of pyruvate oxidation after glycolysis in skeletal muscle, which is regulated by the phosphorylation status of the pyruvate dehydrogenase (PDH) complex. PDH complex converts pyruvate into acetyl-CoA, which is an obligatory process for pyruvate catabolism in the Tricarboxylic Acid (TCA) cycle. PDH complex activity is regulated by phosphorylation, and pyruvate dehydrogenase kinases (PDK 1-4) and pyruvate dehydrogenase phosphatases (PDP 1-2) modulate pyruvate catabolism in response to nutrient and endocrine stimuli (224). Phosphorylation of the PDH complex at any of the three serine residues: Ser293 (site 1), Ser300 (site 2), or Ser232 (site3) of the E1α subunit lowers the activity of the PDH complex, and dephosphorylation of these sites by PDP1 or PDP2 rescues function (224). PDK1-4 are capable of phosphorylating site 1 (Ser293) of the PDH complex, and this site serves as a primary regulatory site of the PDH complex in skeletal muscle (225–227).

Due to the importance of PDH complex activity for glucose homeostasis, it is not surprising that previous IUGR studies show greater PDK4 mRNA expression in fetal skeletal muscle as either a metabolic consequence of, or fetal adaptation to, low glucose and insulin concentrations (197,200). Although not previously studied in IUGR fetal

skeletal muscle, PDK1 may also play a role in pyruvate metabolism. Therefore, our objective was to measure protein and mRNA concentrations of PDH, PDP1, PDP2, PDK1, and PDK4 to determine the regulation of PDH complex activity in skeletal muscle of IUGR fetuses. Based on normal glucose utilization and higher glucose production rates in IUGR fetuses, we hypothesize that IUGR fetal skeletal muscle will have greater PDK1,4 and lower PDP1,2 protein and mRNA concentrations to lower PDH complex activity and promote lactate production.

2.3 Materials and Methods

2.3.1 Fetal Sheep Model of IUGR. Studies on pregnant Columbia-Rambouillet ewes were approved by the University of Arizona Institutional Animal Care and Use Committee and performed at the Agricultural Research Complex, which is accredited by the American Association for Accreditation of Laboratory Animal Care International. Ewes (n=16) carrying singleton pregnancies were determined with ultrasonography prior to randomly assigning pregnant ewes to an experimental group, either control (n=8) or IUGR (n=8). IUGR fetuses were created by exposing pregnant ewes to elevated ambient temperatures (40°C for 12 h; 35°C for 12 h; dew point maintained at 22°C) from 40 ± 1 to 91 ± 1 days gestational age as described previously (172). Control fetuses were from ewes maintained 22 ± 1°C that were fed alfalfa pellets to the average *ad libitum* feed intake of ewes in the IUGR group. Water and salt were available to ewes ad libitum. After the hyperthermic exposure, all ewes were maintained in a thermoneutral environment alongside ewes in the control group.

2.3.2 Surgical Preparation and Fetal Physiological Studies. At day 123±1, each fetus underwent a surgical procedure to place indwelling, polyvinyl arterial and venous catheters for blood sampling and infusion as described previously (196). Animals were allowed to recover for at least 5 days prior to in vivo physiological experiment to determine rates of fetal glucose, oxygen, and lactate umbilical uptakes. Fetal catheters for blood sampling were placed in the abdominal aorta via hindlimb pedal arteries and the umbilical vein. Infusion catheters were placed in the femoral veins via the saphenous veins. Maternal catheters were placed in the femoral artery and vein for arterial sampling and venous infusions. All catheters were tunneled subcutaneously to the ewe's flank, exteriorized through a skin incision, and kept in a plastic mesh pouch sutured to the ewe's skin. Catheters were flushed daily with heparinized saline solution (100 U/mL heparin in 0.9% NaCl solution, Vedco, Inc, St. Joseph, MO, USA).

Rates of umbilical uptakes for O_2, glucose, and lactate were measured at 130 ± 1 days gestational age. Umbilical blood flows were measured by steady state tritiated water diffusion methods (New England Nucleotides; PerkinElmer Life Sciences, Boston, MA). After a priming bolus of 50 μCi ^3H_2O, the intravenous ^3H_2O infusion (0.83 μCi/min) began 60 minutes before sampling commenced. Six sets of blood samples were collected at 10-min intervals to determine blood flow, blood gasses, blood oximetry, plasma metabolites, and hormone concentration. At the start of tracer infusion, an infusion of maternal blood (8-10mL/h) was given to the fetus to avoid fetal anemia from sampling.

2.3.3 Biochemical Analysis. Arterial blood gases and oximetry were measured with an ABL 825 (Radiometer, Copenhagen, Denmark), and values were temperature-corrected to 39.1°C. Plasma glucose and lactate concentrations were measured with the

YSI model 2700 SELECT Biochemistry Analyzer (Yellow Springs Instruments, Yellow Springs, OH, USA). Additionally, plasma concentrations of insulin (ovine insulin ELISA; ALPCO Diagnostics, Windham, NH; intra- and inter-assay coefficients of variation <6%; sensitivity 0.14 ng/mL) and norepinephrine (noradrenaline ELISA; Labor Diagnostika Nord GmbH & Co., KG, Germany; intra- and inter-assay coefficients of variation <14%; sensitivity 35 pg/mL) were quantified.

2.3.4 Tissue Collection. At day 134±1, the ewe and the fetus were euthanized with an intravenous administration of sodium pentobarbital (86 mg/kg) and phenytoin sodium (11 mg/kg; Euthasol; Virbac Animal Health). Organs and skeletal muscles (biceps femoris and semitendinosus) from control and IUGR fetuses were dissected and weighed. These tissues were then snap frozen in liquid nitrogen and stored at -80°C for *in vitro* experiments.

2.3.5 Quantitative PCR. PDK1, PDK4, PDH, PDP1, and PDP2 mRNA concentrations were measured with qPCR on IUGR (n = 8) and control (n = 8) fetuses on semitendinosus muscle. Total cellular RNA was extracted from semitendinosus muscle as described previously(228). RNA concentration and purity were determined from absorbance measurements with a NanoDrop ND-1000 Spectrophotometer (NanoDrop, Wilmington, DE), and RNA quality (RNA integrity number >9.5) was measured with an Experion Automated Electrophoresis Station (Bio-Rad). Messenger RNA (1 μg total cellular RNA per reaction) was reverse transcribed, in triplicate, into cDNA with Superscript III reverse transcription (Invitrogen, Carlsbad, CA). cDNA was amplified using a QuantiTect SYBR® Green PCR Kit (Qiagen, Venlo, Netherlands) and a CFX Connect Real-Time PCR Detection System (Bio-Rad). Optimal annealing temperatures

for primer pairs were determined. Primer specificity was confirmed with nucleotide sequencing of the cloned PCR products (pCR 2.1-TOPO vector; catalog no. K4510oo20; Thermo Fisher Scientific). Primer efficiencies and sensitivities were measured with serial cDNA dilutions. All primers had efficiency ≥85%, and threshold cycles were linear over six orders of magnitude. After an initial 15-minute denaturation incubation at 96°C, all reactions went through 40 cycles at 96°C (30 seconds), annealing temperature (30 seconds), and 72°C (10 seconds) extension and read. Primers synthesized for qPCR are as follows: *PDK1 (F, 5'- TGGAGCATCACGCTGACAAA -3', R, 5'- CTCAGAGGAACACCACCTCC -3'), PDK4 (F, 5'- CCCAGAGGACCAAAAGGCAT -3', R, 5'- GGGTCAGCTGTACAGGCATC -3'), PDHE1α (F, 5'- GGTGGCATCCCGTCATTTTG -3', R, 5'- CGAACGGTCTGCATCATCCT -3'), PDP1 (F, 5'- GTTGTGGATGTTGTCGGCTC -3', R, 5'- TGCAGTGCCATAGATTCTGCT -3'), PDP2 (F, 5'- CTGCTGTTTGGCATCTTCGAC -3', R, 5'- CTTTCCATGGCCTCCTCCATT -3'), YWHAZ (F, 5'-AGACGGAAGGTGCTGAGAAA-3', R, 5'-CGTTGGGGATCAAGAACTTT-3'), TBP (F, 5'- AGAATAAGAGAGCCCCGCAC-3', R, 5'- TTCACATCACAGCTCCCCAC-3'), RPS15 (F, 5'- ATCATTCTGCCCGAGATGGTG -3', R, 5'- TGCTTTACGGGCTTGTAGGTG -3'), GAPDH (F, 5'- CTGGCC AAGGTC ATCCAT-3', R, 5'- ACA GTCTTCTGGGTGGCAGT -3').* Expression values for the genes of interest were normalized to the geometric mean of reference genes: TATA-binding protein (TBP), Tyrosine 3-Monooxygenase/Tryptophan 5-Monooxygenase Activation Protein Zeta (YWHAZ), ribosomal protein S15 (RPS15), and Glyceraldehyde-3-Phosphate Dehydrogenase (GAPDH). Results were normalized to the geometric mean of the

reference genes using the comparative change of threshold cycles (ΔCT) method (CT gene of interest – CT reference gene)(229). The ΔCT values were calculated for group comparisons. Gene analysis was performed adhering to MIQE guidelines (230).

2.3.6 Western Blot Analysis. Protein lysates were prepared from semitendinosus muscle in ice-cold CelLytic MT Buffer (Sigma-Aldrich, St Louis, MO) containing additional protease and phosphatase inhibitors: 0.5 mM phenylmethane sulfonyl fluoride (Thermo Fisher Scientific), 2µg/mL Aprotinin (Sigma-Aldrich), 2.5µg/mL Leupeptin (Sigma-Aldrich), 100µM DL-Dithiothreitol (Sigma-Aldrich), and 5mM sodium vanadate (Thermo Fisher Scientific). Protein concentrations were measured with a Pierce BCA Protein Assay Kit (ThermoFisher Scientific). Fifty µg of protein from each animal was separated on a 10% polyacrylamide gel and transferred onto PVDF membranes (Bio-Rad, Hercules, CA). The membranes were blocked in a 5% (w/v) non-fat milk in Tris-buffered saline, 0.1% Tween (TBS-T) solution for 30 minutes at room temperature and then incubated overnight at 4°C with primary antibodies in 5% nonfat milk in TBS-T. The primary antibodies used are as follows: anti-Pyruvate Dehydrogenase Phosphatase 1 (1:3000; Abcam, ab198261, RRID:AB_2756338), anti- Pyruvate Dehydrogenase Phosphatase 2 (1:3000; Abcam, ab99170, RRID:AB_10670444), anti- Pyruvate Dehydrogenase-E1α (1:3000; Abcam, ab110334, RRID:AB_10866116), anti-phospho-Pyruvate Dehydrogenase-E1α (SER293, 1:3000; Abcam, ab177461, RRID:AB_2756339), anti-Pyruvate Dehydrogenase Kinase 1(1:3000; Abcam, ab90444, RRID:AB_2161150), anti-Pyruvate Dehydrogenase Kinase 4(1:3000; Abcam, ab110336, RRID:AB_10863042). Goat anti-rabbit IgG secondary antibodies conjugated with horseradish peroxidase (1:15,000; BioRad RRID AB_11125142) were detected with

Thermo Scientific™ SuperSignal West Pico Chemiluminescent Substrate and exposed to Blue Lite Autorad Film (VWR, Radnor, PA). Protein abundances were quantified using photographed images and densitometric analyses (Scion Image Software, Frederick, MD). Protein abundances of PDP1, PDP2, PDHE1α, phospho- PDHE1α, PDK1, and PDK4 were normalized to β-Tubulin (1:3000, Fisher Thermo Scientific, RB-9249-P, RRID:AB_722291). Phosphorylated PDHE1α was normalized to total PDHE1α. All samples were evaluated in triplicate and data are presented relative to control values.

2.3.7 Enzymatic Assays. PDH activity was measured in Biceps Femoris and Semitendinosus skeletal muscle, in triplicate, with the PDH Activity Assay Kit (MAK183, Sigma-Aldrich). Skeletal muscle (100mg) was homogenized in 1mL of ice-cold PDH Assay buffer, and 10µL of lysate was measured in triplicate reactions. Reactions were carried out at 37°C, and A_{450} was recorded every 5 minutes for 30 minutes. PDH activity rates are reported in nmol/min/mL as per assay protocol.

LDH activity was measured in Biceps Femoris and Semitendinosus skeletal muscle, in triplicate, with the LDH Activity Assay Kit (ab102526, abcam). Skeletal muscle (100mg) was homogenized according to the manufacturer's instructions. Reactions were carried out at 37°C, and A_{450} was measured every 2 minutes for 30 minutes. LDH activity rates are reported in nmol/min/mL, as per assay protocol.

CS activity was measured in Biceps Femoris and Semitendinosus skeletal muscle, in triplicate, with the Citrate Synthase Assay Kit (CS0720, Sigma-Aldrich) as described previously (201). Rates for citrate synthase are reported as nmol/min/mg protein.

2.3.8 Calculations and Statistical Analysis. The rate of umbilical blood flow (*f*; $ml \cdot min^{-1} \cdot kg^{-1}$) was calculated using the transplacental steady-state diffusion technique,

with tritiated water as the blood flow indicator, and normalized to fetal weight during the study(187). Net umbilical uptakes rates ($R_{f,p}$; $\mu mol \cdot min^{-1} \cdot kg^{-1}$) for oxygen, glucose, and lactate by the fetus from the placenta were calculated as the product of the umbilical blood (or plasma) flow and concentration difference between the umbilical vein (C_v) and umbilical artery (C_a) blood (O_2) or plasma (glucose and lactate) concentrations [$R_{f,p} = f(C_v - C_a)$].

Significant differences ($p < 0.05$) between groups (control and IUGR) were determined with a post hoc general linear means ANOVA and post hoc least significant distance test using general linear means procedures in the JMP Software System (JMP®, Version 14.0.0, SAS Institute Inc., Cary, NC, 1989-2018). Normality and skewness were ensured using a D'Agostino-Pearson normality test. The variance between groups for each condition (e.g. immunoblot and qPCR for each gene/protein) was equal between all groups in all conditions except for the immunoblot values for PDP1 (Levene's Test) and analyzed using the Wilcoxon Rank Sum test. Linear regression analyses for mRNA expression were performed using JMP14. Data are presented as mean ± standard error of the mean (SEM).

2.4 Results

2.4.1 Placental Insufficiency Causes an IUGR Phenotype. In IUGR fetuses blood oxygen, plasma glucose, plasma norepinephrine, and plasma insulin concentrations were lower than controls, while plasma lactate concentrations were not different (Table 1). Umbilical blood flow and rates of net umbilical oxygen uptake were not different between groups (Table 1). Rates of net umbilical glucose and lactate uptakes were significantly lower in IUGR fetuses compared to control fetuses (Table 1).

Fetal and placental mass were lower in IUGR fetuses than control fetuses (Table 2). Semitendinosus muscles weighed 51% less in IUGR fetuses than control fetuses but were similar relative to fetal weight (Table 2). Similarly, although brain weights in IUGR fetuses were 16% lower in IUGR fetuses, brain weight relative to fetal weight was 53% higher in IUGR fetuses compared to controls (Table 2).

2.4.2 Greater PDK1 and PDK4 mRNA expression in IUGR skeletal muscle. PDK1 and PDK4 mRNA concentrations were 1.3 and 2.8 fold greater, respectively, in IUGR semitendinosus muscle compared to control muscle (Figure 3). PDH, PDP1, and PDP2 mRNA concentrations were not different between groups (Figure 3).

PDK1 and PDK4 mRNA concentrations were positively associated with the transplacental (maternal-fetal) arterial oxygen concentration difference and negatively associated with fetal mass (Figure 4 a-d). PDH mRNA concentrations were negatively associated with the transplacental arterial oxygen concentration difference and positively associated with fetal mass (Figure 4 e-f). PDK1 mRNA concentrations were negatively associated with fetal oxygen content (R^2=0.3010, P<0.05). PDK4 mRNA was also negatively associated with fetal oxygen content (R^2=0.3788, P<0.05). PDH mRNA concentrations were positively associated with fetal oxygen content (R^2=0.4180, P<0.05) and fetal [glucose] (R^2=0.2884, P<0.05).

2.4.3 Lower phosphorylation status leads to greater PDH activity in IUGR muscle. No difference in PDK1, PDK4, PDP1, PDP2, or PDH protein concentrations were detected between groups (Table 3). Phosphorylated PDH (S^{293}) concentrations were 28% lower in IUGR semitendinosus muscle compared to control muscle (Figure 5). PDH

complex activity was 67% greater in IUGR muscle compared to control muscle (Figure 6A). CS and LDH activities were not different between groups (Figure 5B and 5C).

Table 1. Fetal metabolic parameters of control and IUGR fetuses

Measurement	**Control (8)**	**IUGR (8)**
Umbilical Blood Flow (mL/min/kg)	186 ± 23.3	159 ± 9.01
Arterial Blood O_2 Content (mM)	3.5 ± 0.1	1.4 ± 0.1*
Umbilical O_2 Uptake (umol/min/kg)	357 ± 16.7	313 ± 22.7
Arterial [Glucose] (mM)	1.02 ± 0.04	0.61 ± 0.06*
Umbilical Glucose Uptake (umol/min/kg)	27.3 ± 2.24	22.1 ± 0.97*
Arterial [Lactate] (mM)	2.34 ± 0.66	1.75 ± 0.21
Umbilical Lactate Uptake (umol/min/kg)	16.9 ± 3.23	8.35 ± 1.97*
Δ Maternal-Fetal O_2 Content (mM)	2.32 ± 0.13	4.58 ± 0.20*
Arterial Norepinephrine (pg/mL)	712 ± 183	4310 ± 920*
Arterial Insulin (ng/mL)	0.36 ± 0.06	0.16 ± 0.05*

Table 1. Fetal metabolic parameters of control and IUGR fetuses. Values are expressed as means ±SEM. * less than $P<0.01$

Table 2. Biometric measurements of control and IUGR fetuses

Measurement	Control (8)	IUGR (8)
Percent male fetuses (%)	50	37
Age at necropsy (days)	134 ± 1	133 ± 1
Fetal Weight (kg)	3.37 ± 0.16	1.57 ± 0.25*
Placental Weight (g)	363 ± 35.1	117 ± 14.3*
Brain Weight (g)	48.9 ± 1.24	41.4 ± 1.76*
Brain Weight (g)/ Fetal Weight (kg)	15.9 ± 0.86	27.5 ± 1.93*
Total Semitendinosus Weight (g)	12.5 ± 1.16	6.17 ± 0.69*
Semitendinosus Weight (g) / Fetal Weight (kg)	4.01 ± 0.20	3.71 ± 0.12
Total Biceps Femoris Weight (g)	32.1 ± 1.74	16.2 ± 2.28*
Biceps Femoris Weight (g) / Fetal Weight (kg)	9.74 ± 0.54	8.93 ± 0.37

Table 2. Biometric measurements of control and IUGR fetuses. Values are expressed as means ±SEM. * less than $P<0.01$

Table 3. Protein Concentrations Relative to Control Fetuses

Protein	Control (8)	IUGR (8)
PDK1	1.0±0.06	0.97±0.04
PDK4	1.0±0.09	0.85±0.08
PDH	1.0±0.06	0.94±0.03
pPDH(ser^{293}):PDH ratio	1.0±0.08	0.74±0.04*
PDP1	1.0±0.06	0.96±0.03
PDP2	1.0±0.04	1.1±0.05

Table 3. Protein concentrations relative to control fetuses. Values are relative to control and expressed as means ± SEM. * less than $P<0.05$

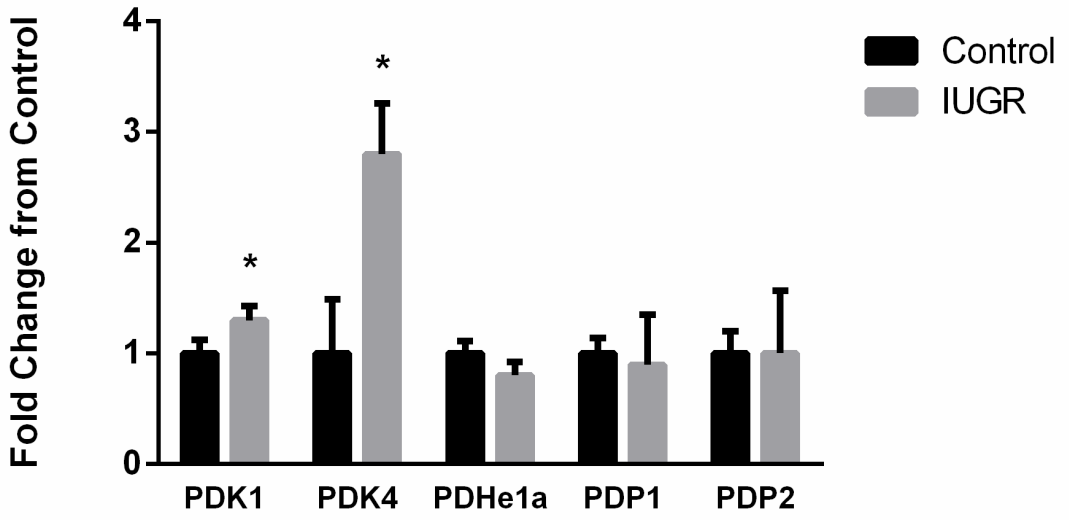

Figure 3. Fold change for mRNA expression relative to control fetuses. Fold changes relative to control mRNA concentrations are presented for PDK1, PDK4, PDH, PDP1, and PDP2. Values are expressed as means ± SE. *Differences ($P < 0.05$) between groups. IUGR, intrauterine growth restriction; PDH, pyruvate dehydrogenase; PDK, pyruvate dehydrogenase kinase; PDP, pyruvate dehydrogenase phosphatase.

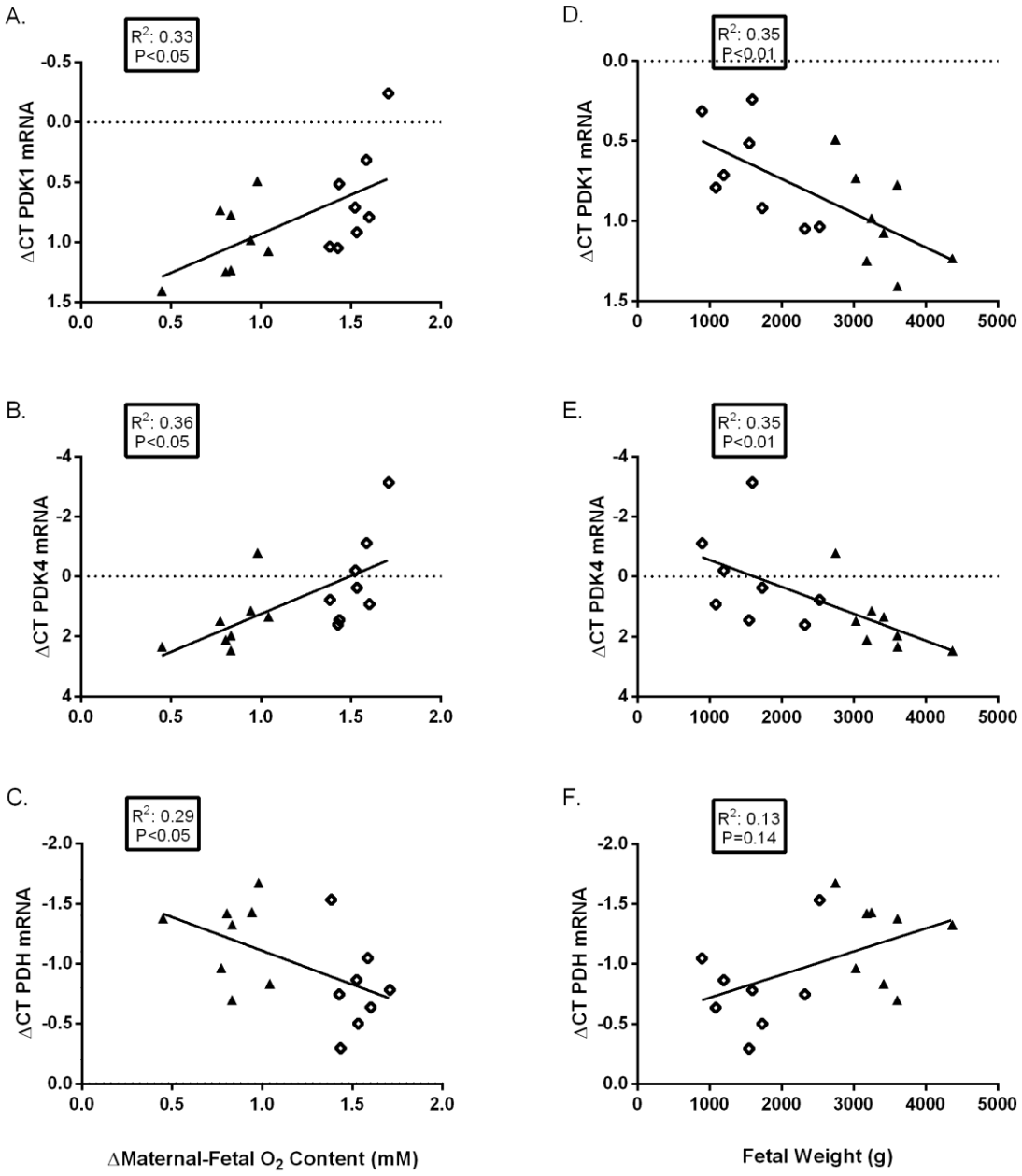

Figure 4. Gene expression correlates with parameters of placental insufficiency and intrauterine growth restriction (IUGR). Correlations are presented for pyruvate dehydrogenase kinase (PDK)1, PDK4, and pyruvate dehydrogenase (PDH) with the maternal-fetal arterial O_2 content difference (millimolar; *A–C*) and with fetal weight (grams; *D–F*). The maternal-fetal O_2 content gradient was used as a marker of placental insufficiency and fetal weight was used as a measure of IUGR for mRNA correlations. mRNA data (*y*-axis) are presented as the comparative change of threshold cycles (ΔCT) values of the gene of interest relative to the geometric mean of the reference genes for control (closed triangles, $n = 8$) and IUGR (open diamonds, $n = 8$). Linear regression was performed with JMP 14 and R^2, and *P* values are indicated.

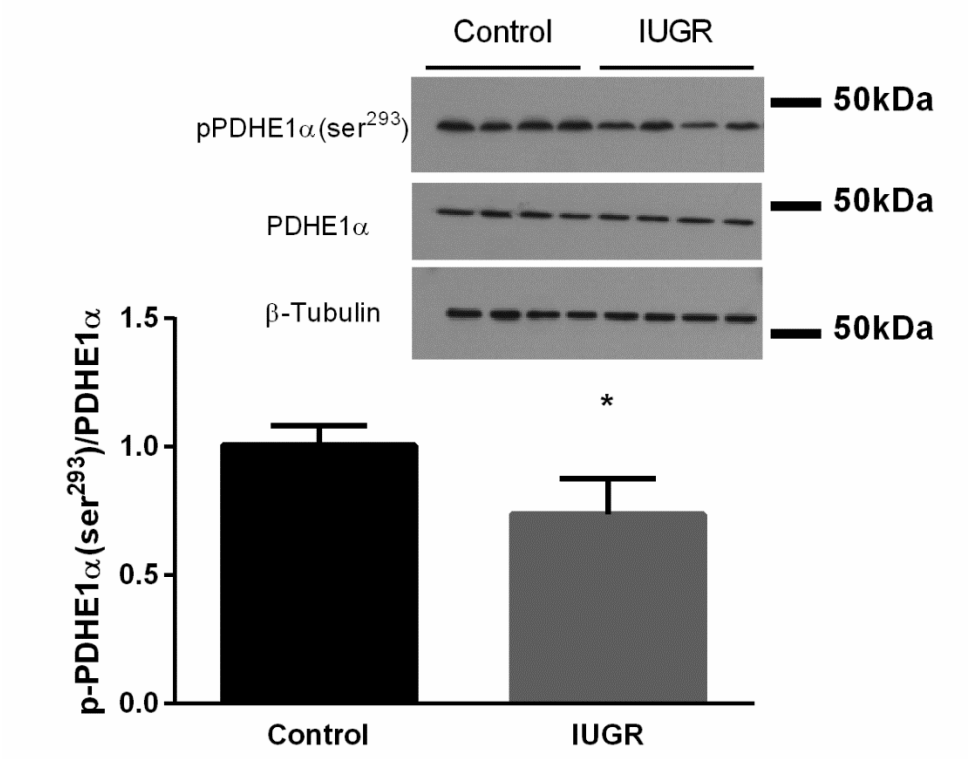

Figure 5. Lower phosphorylated pyruvate dehydrogenase (PDH) E1α (p-PDHE1α) (Ser^{293}) concentrations in intrauterine growth restriction (IUGR) semitendinosus muscle. p-PDH (Ser^{293}) concentrations are presented relative to total PDH for the semitendinosus muscle from control and IUGR fetuses (n = 8/group). Representative immunoblots are shown for p-PDH (Ser^{293}) and β-tubulin in four control and four IUGR fetal muscle samples. Values are expressed as means ± SE. *Differences ($P < 0.05$) between groups.

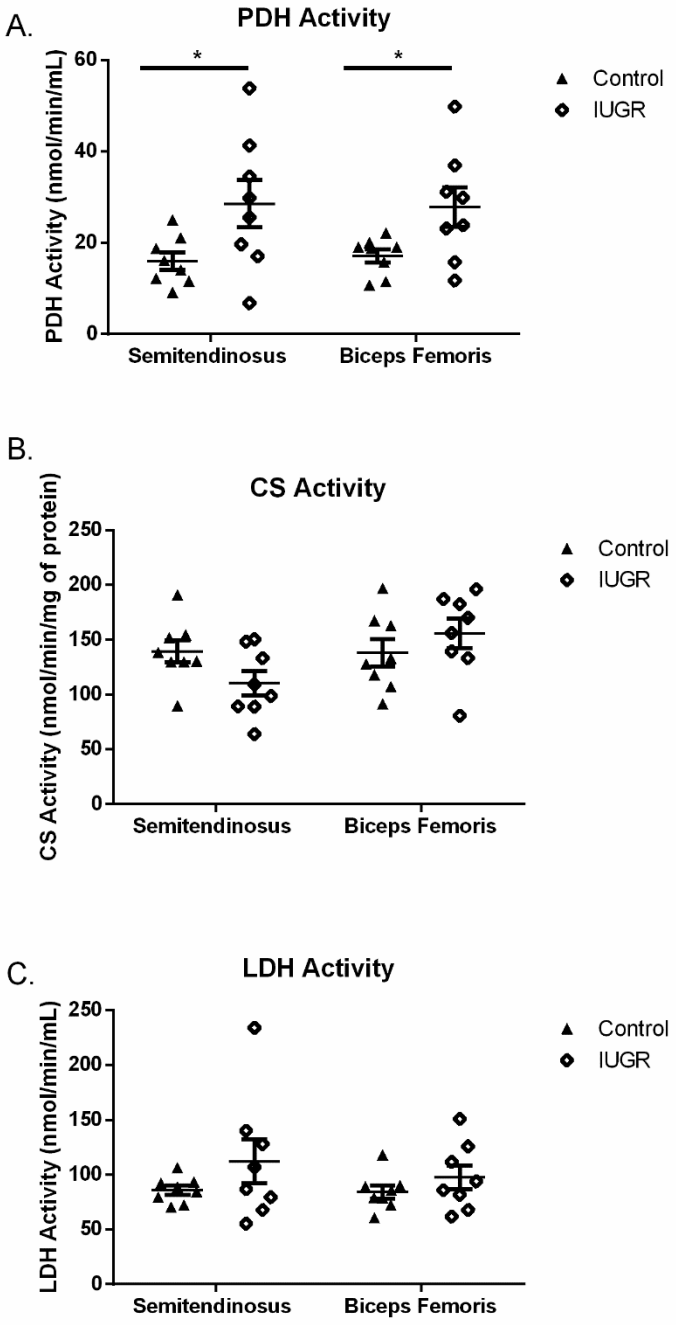

Figure 6. Pyruvate dehydrogenase (PDH), lactate dehydrogenase (LDH), and citrate synthase (CS) activity in control and intrauterine growth restriction (IUGR) skeletal muscles. PDH activity (*A*), CS activity (*B*), and LDH activity (*C*) were measured in semitendinosus and biceps femoris muscles from control and IUGR fetuses (n = 8/group). Individual fetal muscle activities are presented with the means ± SE for the groups. The asterisks and bar indicate differences between groups within muscles ($P < 0.05$).

2.5 Discussion

Although our data are consistent with previous reports showing greater PDK4 mRNA expression in IUGR skeletal muscle, protein concentrations of PDK4 did not parallel mRNA expression (197,200). Instead, we demonstrate that the PDH complex has a reduced phosphorylation status and greater enzymatic activity in skeletal muscle from IUGR fetuses. Furthermore, PDK1 mRNA concentrations were elevated in IUGR skeletal muscle, but the increase in PDK1 mRNA is also incongruent with PDK1 protein concentrations. We also show that the depressed phosphorylation status of PDH (E1α S293) was not explained by increases in mRNA and protein concentrations of PDH, PDP1 and PDP2 in muscle from IUGR fetuses. These findings indicate that skeletal muscle pyruvate metabolism may be higher due to increased PDH complex activity, a response that likely normalizes metabolism in the hypoglycemic IUGR fetus (76).

Transcription of both PDK1 and PDK4 are regulated, in part, by hypoxia, which explains the higher mRNA expression in IUGR fetuses (231–235). Under acute hypoxic conditions, HIF-1α increases the expression of these kinases, which serves to maintain ATP production under low oxygen tension by promoting gene expression for anaerobic metabolism and reducing mitochondrial oxygen consumption (231–233,236–239). Interestingly, although there is evidence of increased prolyl hydroxylase domain (PHD) expression in IUGR fetuses, HIF-1/2α activity is increased in IUGR fetuses compared to control fetuses(240–242). This most likely represents a new hypoxic set-point in response to chronic hypoxemia in IUGR tissues; consequently, the expression of genes regulated by hypoxia-response element (HRE), such as PDK1, are increased in IUGR fetuses (240–244). PDK1, through altered hypoxemic signaling may contribute to the reprogramming

of glucose metabolism in skeletal muscle from oxidative phosphorylation to anaerobic glycolysis by increasing the activities of hexokinase and phosphofructose kinase 1, the latter is known to be expressed at greater concentrations in muscle from IUGR fetuses (197,200,240,245). In contrast to PDK1, PDK4 transcription is also regulated by insulin (246,247). High insulin concentrations decreased PDK4 mRNA expression skeletal muscle, and increase glucose catabolism in accordance with availability (231,232,245,248–252). Considering that the IUGR fetus is hypoglycemic, hypoxemic, and hypoinsulinemic, the upregulation of both PDK1 and PDK4 mRNA are plausible metabolic adaptations to a challenging *in utero* environment.

Greater PDK1 and PDK4 mRNA expression in the semitendinosus muscle of IUGR fetuses did not translate into increased protein concentrations or activities. Interestingly, greater PDH complex activity in IUGR muscle may explain *in vivo* observations that show the lactate + glucose-oxygen quotient is maintained across the hindlimb of the IUGR fetus, even though the individual quotients indicate higher rates of glucose uptake and lactate output per mole of oxygen consumed by the IUGR hindlimb (76). Reduced phosphorylation of PDH is explained by decreased pyruvate dehydrogenase kinase activity or increased pyruvate dehydrogenase phosphatase activity in IUGR skeletal muscle rather than their actual protein concentrations. Short-term, transient pyruvate dehydrogenase kinase activity is regulated by allosteric effectors such as high acetyl-CoA:CoA and NADH:NAD+ concentration ratios, and is suppressed by high pyruvate or lactate concentrations generated by glycolysis (253). Furthermore, PDP1/2 is transiently activated by insulin-dependent phosphorylation by Protein Kinase C (PKC), and this is thought to be the major mechanism of activation for these

phosphatases in both the liver and skeletal muscle (254). Since we do not observe a difference in protein concentration for pyruvate dehydrogenase kinases or phosphatases between groups, we hypothesize that the activities of these kinases would be decreased in IUGR skeletal muscle.

Pyruvate dehydrogenase activity is higher in IUGR skeletal muscle, but may not correct the defect in whole body fractional glucose oxidation (196,197). Although the IUGR fetuses are hypoinsulinemic, they have been shown to have greater insulin sensitivity in skeletal muscle (104,196,216). Greater insulin sensitivity might explain the disconnect between fractional glucose oxidation rates and PDH complex activity as insulin would activate PDP1 and PDP2 and inactivate PDK4 (254). Also, since this demonstrates a mechanism by which the IUGR fetus adapts to sustained hypoglycemia, it might also adapt to chronic hypoxemia. Likewise, changes in pyruvate carboxylase (PC) regulation would affect the glucose oxidation fraction. Decreased PC expression, or activity, while having normal PDH expression and activity, would cause shunting of pyruvate to lactate production. The shunting of pyruvate to lactate would provide a sufficient glycolytic-derived carbon source to maintain plasma glucose concentration via the Cori Cycle; however, we found no differences in LDH activity between groups in both semitendinosus and biceps Femoris skeletal muscle (255,256). Although there are no differences in plasma lactate concentrations, or LDH activity, between groups, this might be representative of a new metabolic set point between skeletal muscle lactate production and hepatic gluconeogenesis in the IUGR fetus (196).

We have previously shown less type I oxidative muscle fibers, but no differences in type II muscle fibers, in semitendinosus and biceps femoris muscle in IUGR fetuses

compared to controls (215). Skeletal muscles can undergo fiber type switching in response to mitochondrial dysfunction, namely type I to type II; this is an effective adaptation in IUGR fetuses as type II muscle fibers have lower mitochondrial contents compared to type I fibers(257,258). Therefore, it is expected that skeletal muscles that have less type I fibers will have reduced glucose metabolism and decreased PDH expression and/or activity. However, using citrate synthase activity measurements as a proxy for mitochondrial number, our findings do not support dramatic changes in mitochondrial content of these representative, mixed fiber type muscles similar to previous observations (223). Therefore, we propose that the change in PDH activity and phosphorylation status outweigh the potential fiber type switching in the skeletal muscles of IUGR fetuses, and this may be a direct result of decreased PDK activity rather than expression (259,260).

The findings in this study demonstrate that IUGR fetal sheep have higher PDH complex activity. Despite greater PDK1 and PDK4 mRNA concentrations in IUGR skeletal muscle, there were no differences in protein concentrations of the kinases and phosphatases that regulate the PDH complex. In fact, phosphorylation of PDH Eα1 was lower and enzymatic activity higher in skeletal muscle from IUGR fetuses. These data indicate that the PDH complex is upregulated to normalize pyruvate metabolism in IUGR fetuses with hypoglycemia.

Chapter 3

Lower Oxygen Consumption and Complex I Activity in Mitochondria Isolated from Skeletal Muscle of Fetal Sheep with Intrauterine Growth Restriction

The contents of this chapter have been accepted for publication in the American Journal of Physiology-Endocrinology and Metabolism.

The full citation is given below.

Pendleton AL, et al. Lower oxygen consumption and Complex I activity in Mitochondria Isolated from Skeletal Muscle of Fetal Sheep with Intrauterine Growth Restriction. Accepted for publication in Physiology- Endocrinology and Metabolism (2020).

3.1 Abstract

Fetal sheep with placental insufficiency-induced intrauterine growth restriction (IUGR) have lower hind-limb oxygen consumption rates (OCR), indicating depressed mitochondrial oxidative phosphorylation capacity in their skeletal muscle. We hypothesized that OCRs are lower in skeletal muscle mitochondria from IUGR fetuses due to reduced electron transport chain (ETC) activity and lower abundances of Tricarboxylic Acid (TCA) cycle enzymes. IUGR sheep fetuses (n=12) were created with mid-gestation maternal hyperthermia and compared to control fetuses (n=12). At 132±1 days of gestation, biceps femoris muscles were collected, and the mitochondria were isolated. Mitochondria from IUGR muscle have 47% lower State 3 (Complex-I dependent) OCRs than controls, while State 4 (proton leak) OCRs were not different between groups. Furthermore, Complex I, but not Complex II or IV, enzymatic activity was lower in IUGR fetuses compared to controls. Proteomic analysis (n=6/group) identified 160 differentially expressed proteins between groups with 107 upregulated and 53 downregulated mitochondria proteins in IUGR fetuses compared to controls. Although no differences were identified in ETC subunit protein abundances, abundances of key TCA cycle enzymes (IDH3B, SUCLA2, and OGDH) were lower in IUGR mitochondria. IUGR mitochondria had a greater abundance of a hypoxia inducible protein, NADH dehydrogenase 1 alpha subcomplex 4-like 2, NDUFA4L2, which is known to incorporate into Complex I and lower Complex I-mediated NADH oxidation. Our findings show that mitochondria from IUGR skeletal muscle adapts to hypoxemia and hypoglycemia by lowering Complex I activity and TCA cycle enzymes concentrations, which together act to lower OCR and NADH production/oxidation in IUGR skeletal muscle.

3.2 Introduction

Intrauterine growth restricted (IUGR) fetuses have reduced lean mass and impaired glucose metabolism compared to normally growing counterparts (213). Many cases of IUGR are caused by reductions in placental function leading to fetal nutrient restriction resulting in fetal hypoglycemia, hypoxemia, and maladaptive sarcopenia (96,261–263). Moreover, it has been proposed that nutrient and oxygen restriction to the fetus during development is associated with permanent alterations in whole-body metabolism, and a fixed functional capacity of vital organs in postnatal life (264,265). Our ovine model of hyperthermia-induced placental insufficiency successfully recapitulates several aspects of the human IUGR phenotype (185). These maladaptations to IUGR *in-utero* can eventually lead to complications later in life, as these adults are more prone to develop metabolic syndrome (266).

Normally, the oxidation of glucose and lactate accounts for >50% of whole-fetus oxygen consumption, underscoring the importance of these substrates in fetal metabolism (218). When placental transport capacity for glucose and oxygen are limited, the IUGR fetus prioritizes growth of neurological tissues at the expense of peripheral tissue growth through metabolic and endocrine adaptations(14,15,267). This is evidenced in the IUGR fetus by lower hindlimb skeletal muscle mass and weight-specific oxygen consumption rates (OCRs) even though hindlimb weight-specific glucose uptake is similar to uptake in control fetuses (76). Body weight-specific glucose utilization rates are also similar between IUGR and control fetuses despite lower fractional glucose oxidation rates that have been shown to persist in skeletal muscle of IUGR lambs (196,197,268). Importantly, higher glucose extraction efficiencies and expression levels of glycolytic enzymes

maintain normal hindlimb glucose-oxygen quotients, but further reduction in the lactate-oxygen quotient indicates greater lactate output per mole of oxygen consumed (76,104,269). These findings imply that IUGR fetuses have lower skeletal muscle oxidative metabolic capacity.

Mitochondria, the site of cellular respiration and oxidative phosphorylation, are central to metabolism. Within the mitochondrial matrix, the conversion of pyruvate, the primary metabolite from glucose, into acetyl-CoA is the first step in a series of redox steps that ultimately lead to the production of NADH and $FADH_2$ within the Tricarboxylic Acid (TCA) cycle (270). Although the TCA cycle does not directly consume oxygen, it is considered aerobic because the NADH and $FADH_2$ produced by acetyl-CoA metabolism must transfer their electrons to the electron transport chain (ETC) at Complexes I and II, respectively, in order to regenerate NAD+ and FADH for further revolutions of the TCA cycle (271,272). Regeneration of these redox cofactors through oxidation at the ETC relies upon the terminal electron transfer to oxygen at Complex IV (273–275). Thus, the TCA cycle is indirectly dependent upon oxygen for function. If sufficient electron transfer does not occur within the ETC (e.g. post-translational modification of ETC subunits), mitochondrial oxygen consumption rates decrease; however, this leads to alterations in cellular metabolism and substrate selection that hinder TCA cycle function (276–280). As such, the TCA cycle and the ETC are linked, and decreasing mitochondrial metabolism to conserve oxygen would concomitantly lower glucose metabolism.

Given that the IUGR fetuses have less lean body mass than their appropriately grown counterparts, it is not surprising that previous studies have shown that IUGR

skeletal muscle metabolically adapts *in-utero* (76,77,197,214,268). Glucose metabolism and oxygen consumption are linked through the TCA cycle and subsequent oxidative phosphorylation, and previous findings in IUGR models with placental restriction indicates reduced mitochondrial function in the fetal skeletal muscle (77,223). However, mitochondrial metabolic capacity has not yet been examined comprehensively in the skeletal muscle of IUGR fetuses.

The objective of this study was to uncover differences between IUGR and control skeletal muscle mitochondrial metabolism by: 1) measuring OCRs and ETC subunit activities on isolated mitochondria as a means to quantitatively measure ETC function, and 2) using a proteomic-based approach to measure differences in protein abundances within the mitochondria-proteome between IUGR and control fetuses. Since IUGR fetuses have previously been reported to possess lower hind-limb OCRs, we tested the hypothesis that OCRs are lower in skeletal muscle mitochondria from IUGR fetuses due to reduced ETC activity and lower abundances of TCA cycle enzymes.

3.2 Materials and Methods

3.2.1 Fetal Sheep Model of IUGR. Studies on pregnant Columbia-Rambouillet ewes were approved by the University of Arizona Institutional Animal Care and Use Committee and performed at the Agricultural Research Complex, which is accredited by the American Association for Accreditation of Laboratory Animal Care International. The experimental design of this study was performed in accordance with the Animals in Research: Reporting In Vivo Experiments (ARRIVE) guidelines (281). Columbia-Rambouillet crossbred ewes with singleton pregnancies were purchased from the

University of Arizona Sheep Unit and transported to the laboratory at 35 ± 2 days of gestation age (dGA). The ewes were two to four years of age with unknown parity. Singleton fetuses were determined by ultrasonography prior to group assignment. Ewes were assigned by a simple randomization method into one of two groups, control and IUGR. Placental insufficiency-induced IUGR fetuses (n=15) were created by exposing pregnant ewes to elevated ambient temperatures (40°C for 12 h; 35°C for 12 h; dew point 22 °C) from 40 ± 1 dGA to 91 ± 1 dGA (term 149 dGA) as described previously (172). Control fetuses (n=12) were from ewes maintained 22 ± 1°C that were fed alfalfa pellets to the average *ad libitum* feed intake of ewes in the IUGR group. Water and salt were available to ewes *ad libitum.* After the hyperthermic exposure, all ewes were maintained in a thermoneutral environment alongside ewes in the control group. Three IUGR fetuses were lost prior to surgery, making the final animal numbers for the experimental groups: Control (n=12), and IUGR (n=12).

3.2.2 Surgical Preparation and Fetal Physiological Studies. At day 123±1, each fetus underwent a sterile, surgical procedure to place indwelling, polyvinyl arterial and venous catheters for blood sampling and infusion as described previously (196). Animals were allowed to recover for at least 5 days prior to *in vivo* physiological experimentation to determine rates of fetal glucose, oxygen, and lactate umbilical uptakes. Fetal catheters for blood sampling were placed in the abdominal aorta via hindlimb pedal arteries and the umbilical vein. Infusion catheters were placed in the femoral veins via the saphenous veins. Maternal catheters were placed in the femoral artery and vein for arterial sampling and venous infusions. All catheters were tunneled subcutaneously to the ewe's flank, exteriorized through a skin incision, and kept in a plastic mesh pouch sutured to the ewe's

skin. At induction of all surgical procedures, ewes received an intramuscular injection of penicillin G procaine injectable suspension (24,000 units/kg; Agri-Cillin, Huvepharma, Inc., Peachtree City, GA) and intravenous injection of Ketofen (2 mg/kg; Zoetis Kalamazoo, MI). Ewes were given post-operative analgesics intravenously (10 mg/kg/day phenylbutazone, VetOne Boise, ID) for 3 days. The vascular catheters were flushed daily with heparinized saline solution (100 U/mL heparin in 0.9% NaCl solution, Vedco, Inc, St. Joseph, MO).

Rates of umbilical (net fetal) uptake for oxygen, glucose, and lactate were measured at 130±1 days of gestation. Umbilical blood flows were measured by steady state tritiated water diffusion and normalized to fetal weight for the study (New England Nucleotides; PerkinElmer Life Sciences, Boston, MA). After a priming bolus of 50 μCi $^{3}H_2O$, the intravenous $^{3}H_2O$ infusion (0.83 μCi/min) began 60 minutes before sampling commenced. Four sets of blood samples were collected at 10-min intervals to determine umbilical blood flow, blood gasses, blood oximetry, plasma metabolites, and hormone concentration. At the start of tracer infusion, an infusion of maternal blood (10 mL/h) was given to the fetus to avoid fetal anemia from sampling. Two control and two IUGR animals were not included in the physiological studies due to failure of catheter patency. The animal numbers for blood gas, hormone, and metabolite collection were: Control (n=10) and IUGR (n=10).

Arterial blood gases and oximetry for each sample was measured with an ABL 825 (Radiometer, Copenhagen, Denmark), and values were temperature-corrected to 39.1°C. Plasma glucose and lactate concentrations were measured with the YSI model 2700 SELECT Biochemistry Analyzer (Yellow Springs Instruments, Yellow Springs,

OH, USA). Additionally, plasma concentrations of insulin (ovine insulin ELISA; ALPCO Diagnostics, Windham, NH; intra- and inter-assay coefficients of variation <6%; sensitivity 0.14 ng/mL) and norepinephrine (noradrenaline ELISA; Labor Diagnostika Nord GmbH & Co., KG, Germany; intra- and inter-assay coefficients of variation <14%; sensitivity 35 pg/mL) were measured.

3.2.3 Tissue Collection. At day 132±1, the ewe and the fetus were euthanized with an intravenous administration of sodium pentobarbital (86 mg/kg) and phenytoin sodium (11 mg/kg; Euthasol; Virbac Animal Health). Fetal organs and skeletal muscles (biceps femoris) were dissected and weighed. The tissue that was not used immediately for mitochondrial isolations was then snap frozen in liquid nitrogen and stored at -80°C for *in vitro* experiments.

The large muscle groups of the body (e.g. biceps femoris, latissimus dorsi, etc) have a proportionally greater impact on glucose metabolism due to mass compared with smaller muscles. Additionally, these large muscle groups are also comprised of mixed fiber types (215,282–284)**.** Therefore, we chose the biceps femoris (BF) muscle as the representative muscle group for this study.

3.2.4 Skeletal Muscle Moisture Content. Tissue water content was quantified with the wet/dry ratio utilizing the BF muscle. 300 mg of BF muscle (n=12/group) was placed drying oven set at a temperature of +40°C until reaching constant weight. Muscles were then reweighed (dry weight), and the percentage of water mass was calculated using the following equation: (wet weight – dry weight)/wet weight * 100.

3.2.5 Isolation of Mitochondria. Fresh BF muscle from each fetus was cleaned of fascia and three grams of cleaned BF was minced, homogenized, and mitochondria were

isolated by density gradient centrifugation according to established protocols using "Isolation Buffer 1 " and "Isolation Buffer 2"(285). Isolation Buffer 1 consists of a final concentration of: 67mM sucrose, 50mM Tris/HCl, 50mM 1 M KCl, 10mM EDTA, and .02% w/v BSA, in distilled water and adjusted to pH 7.4. Isolation Buffer 2 consists of a final concentration of: 250mM sucrose, 3mM EGTA, and 1mM Tris, in distilled water and adjusted to pH 7.4. Oxygen consumption rates were measured in "Experimental Buffer" which was prepared by mixing: 10 mM Tris/HCl, 5 mM $MgCl_2$, 2 mM Pi, 0.02 mM EGTA, and 250 mM sucrose, in distilled water and adjusted to pH 7.4.

3.2.6 Mitochondrial Oxygen Consumption Rate. Following isolation, mitochondria were incubated on ice in Isolation Buffer 2 for 30 minutes prior to OCR measurements to ensure sufficient wash-out of respiratory substrates (285). For each OCR analysis, pelleted mitochondria were resuspended in 1:3 (v/v) in Experimental Buffer that was prewarmed to 39.1ºC. The resulting solution was divided evenly into three separate chambers of a Fluorescence Lifetime Micro Oxygen Monitoring System (Instech Laboratories, Inc., Plymouth Meeting, PA, USA) that were prewarmed to 39.1ºC, as previously described (286).

Partial pressure of O_2 (PO_2) in each chamber was recorded over time using fiber optic sensors and NeoFox viewer software (Instech Laboratories, Inc.). Oxygen consumption rates (OCRs; nmol O_2 min^{-1}) were determined from the slope of PO_2 disappearance over time for State 3 and State 4 and were calculated using the average of triplicate measurements for each condition. Maximum Complex I-linked respiration (State 3) was measured in the presence of 5 mM glutamate, 5 mM malate, and 100 µM ADP. For each mitochondria preparation, OCRs were recorded for 5 minutes prior to the

addition of ADP (+glutamate/malate, -ADP; State $4_{Low\ ADP}$), to ensure sufficient use/washout of respiratory substrates for each sample prior to the addition of 100 µM ADP, State 3 measurements. To measure OCR in the absence of oxidative phosphorylation (State $4_{Oligomycin}$), an ATP synthase inhibitor, oligomycin A (5µM final concentrations) was added after State 3 measurements (287). All OCRs at State $4_{Low\ ADP}$ were not different of their respective State $4_{Oligomycin}$ measurements. The respiratory control ratio (RCR) was calculated as the ratio of State 3 to State $4_{Oligomycin}$ OCRs (287).

Integrity of the mitochondria preparations of each sample was determined by the addition of 100µM cytochrome c during State 3 OCR measurements and confirmed by less than a 16% increase in OCRs (Sigma). Following OCR analysis, the isolated mitochondria were collected from each chamber, and protein concentrations were measured with a Pierce BCA Protein Assay Kit (Thermo Fisher) for OCR normalization to protein concentration.

3.2.7 In-solution Tryptic Digestion of Mitochondria. To determine changes in the mitochondrial proteome associated with IUGR, 50 µg of mitochondrial isolates were supplemented with dithiothreitol (DTT) at a final concentration of 5 mM and incubated at 56°C for 30 minutes. Samples were cooled to room temperature for 10 minutes and incubated with 15 mM acrylamide for 30 minutes at room temperature while protected from light. The samples were supplemented with additional DTT at a final concentration of 5 mM and incubated in the dark for 15 minutes to quench the alkylation reaction. Six volumes of pre-chilled 100% acetone were added to the samples and incubated for one hour at -20°C to precipitate proteins followed by centrifugation at 16,000 x g for 10 minutes at 4°C. 400 □L of pre-chilled 90% acetone was added to the protein pellet and

vortexed followed by centrifugation at 16,000 x g for 5 minutes at 4°C. The remaining acetone was removed, and the protein pellets were air dried for 2-3 minutes. The protein pellet was resuspended in 50 µL of Digestion Buffer (50 mM NH4HCO3, 1% sodium deoxycholate (SDC)) and sonicated for 5 minutes. One □g of Lys-C was added to each sample and incubated at 37°C for 2 hours while shaking at 300 rpm. Afterwards, 50 □L of 50mM ammonium bicarbonate and 2 µg of trypsin were added to each sample and incubated at 37°C overnight while shaking at 300 rpm. 14.7 µL of 40% Formic Acid (FA) /1% Heptaflourobutyrate (HFBA) was added to each sample and incubated for 10 minutes (final concentration is 4% FA/0.1% HFBA) to simultaneously stop trypsin digestion and cause precipitation of the SDC contained in the digestion buffer. The SDC was pelleted by centrifuging at 12,000 x g for 10 minutes and the peptide-containing solution was extracted. The samples were desalted with Pierce Peptide Desalting Spin Columns per the manufacturer's protocol (ThermoFisher Scientific, cat no. 89852) and the peptides were dried by vacuum centrifugation. The dried peptides were resuspended in 20 µL of 0.1% FA (v/v) and the peptide concentration was determined with the Pierce Quantitative Colorimetric Peptide Assay Kit per the manufacturer's protocol (ThermoFisher Scientific, cat no. 23275). 600 ng of the final sample was analyzed by mass spectrometry.

3.2.8 Mass Spectrometry and Data Processing. HPLC-ESI-MS/MS was performed in positive ion mode on a Thermo Scientific Orbitrap Fusion Lumos tribrid mass spectrometer fitted with an EASY-Spray Source (Thermo Scientific, San Jose, CA). NanoLC was performed using a Thermo Scientific UltiMate 3000 RSLCnano System with an EASY Spray C18 LC column (Thermo Scientific, 50cm x 75 µm inner diameter,

packed with PepMap RSLC C18 material, 2 µm, cat. # ES803); loading phase for 15 min at 0.300µL/min; mobile phase, linear gradient of 1–34% Buffer B in 119 min at 0.220 µL /min, followed by a step to 95% Buffer B over 4 min at 0.220 µL /min, hold 5 min at 0.250 µL/min, and then a step to 1% Buffer B over 5 min at 0.250 µL /min and a final hold for 10 min (total run 159 min); Buffer A = 0.1% FA/H_2O; Buffer B = 0.1% FA in 80% Acetonitrile. All solvents were liquid chromatography mass spectrometry grade. Spectra were acquired using XCalibur, version 2.3 (ThermoFisher Scientific).

3.2.9 Label-free Quantitative Proteomics. Progenesis QI for proteomics software (version 2.4, Nonlinear Dynamics Ltd., Newcastle upon Tyne, UK) was used to perform ion-intensity based label-free quantification similar to as previously described (288). In brief, in an automated format, .raw files were imported and converted into two-dimensional maps (y-axis = time, x-axis =m/z) followed by selection of a reference run for alignment purposes. An aggregate data set containing all peak information from all samples was created from the aligned runs, which was then further narrowed down by selecting only +2, +3, and +4 charged ions for further analysis. The samples were then grouped in Control versus IUGR. A peak list of fragment ion spectra was exported in Mascot generic file (.mgf) format and searched against the *Ovis aries* UniProt database (27,372 entries) using Mascot (Matrix Science, London, UK; version 2.6). The search variables that were used were: 10 ppm mass tolerance for precursor ion masses and 0.5 Da for product ion masses; digestion with trypsin; a maximum of two missed tryptic cleavages; variable modifications of oxidation of methionine and phosphorylation of serine, threonine, and tyrosine; 13C=1. The resulting Mascot .xml file was then imported into Progenesis, allowing for peptide/protein assignment, while peptides with a Mascot

Ion Score of <25 were not considered for further analysis. Precursor ion-abundance values for peptide ions were normalized to all proteins. For quantification, proteins must have possessed at least one or more unique, identifying peptide.

The subcellular localization database, COMPARTMENTS, was used to identify mitochondrial proteins using a confidence score of 3 or greater (289). Of those mitochondrial specific proteins, comparisons were made to identify differential expression (DE) between groups. Perseus software platform was used to generate PCA plots and heat maps to compare and visualize differences between samples, and a pseudo-count of 1 was added to the abundance scores to avoid a logarithm of zero (290). Volcano plot visualizations were constructed to summarize protein abundance between the two experimental groups. The figure was generated using statistical software R (v3.3.3), and plotting fold change (x-axis, log2 scale) against p-value (y-axis, -log10 scale) obtained from conducting a two-sample t-test on the log (base 2) normalized abundances.

DAVID was used to identify the significant biological themes within Gene Ontology (GO) Terms and KEGG pathways, for DE proteins (Supplemental Tables S2-S5) (291–297). Graphs for the individual, significantly enriched annotations within GO sub-ontologies (Biological Processes (BP), Cellular Component (CC), and Molecular Function (MF)) and KEGG pathways were plotted as fold enrichments against log10 adjusted P-values. Pathways were summarized to reduce redundant non-physiologically relevant terms.

3.2.10 Enzymatic Assessment of Mitochondrial Function. Complex I, II, and IV activities were measured in biceps femoris muscle from the same subset of 12 animals used for proteomic analysis (n=6/group). Measurements were recorded, in triplicate, with

the Complex I (cat # ab109721, Abcam), Complex II (cat # ab109908, Abcam), Complex IV (cat # ab109909, Abcam) Enzyme Activity Kits and all were analyzed using a SpectraMax M2 plate reader (Molecular Devices, San Jose CA). Skeletal muscle (100 mg) was homogenized in cold Phosphate Buffered Saline (PBS), and the protein concentration was measured using a Pierce BCA Protein Assay Kit. Samples were adjusted to recommended protein concentrations, and the proteins were extracted from the samples using 10X detergent provided by the manufacturer. Samples were then centrifuged at 12000 x g for 20 minutes at 4°C. Sample concentrations were verified to be ~5 mg/mL. Samples were loaded into the wells at a concentration of 100 µg/200µL (Complex I Assay), 60µg/50µL (Complex II), or 10µg/200µL (Complex IV), along with appropriate positive and negative controls.

For each assay, plates were incubated at recommended temperatures, and activity was extrapolated by optical density in a kinetic mode: Complex I (1-minute intervals at 450nm for 30 min), Complex II (20 second intervals at 600 nm for 60 min), and Complex IV (1-minute intervals at 550 nm for 120 min). The linear rate of absorbance was then calculated and normalized to whole protein concentration.

3.2.11 Western Blot Analysis. Mitochondrial protein expression was evaluated in the same subset of 12 animals used for proteomic analysis (n=6/group). Protein lysates were prepared from biceps femoris muscle or isolated mitochondria in ice-cold CelLytic MT Buffer (Sigma-Aldrich, St Louis, MO) containing additional protease and phosphatase inhibitors: 0.5 mM phenylmethane sulfonyl fluoride (Thermo Fisher Scientific), 2µg/mL Aprotinin (Sigma-Aldrich), 2.5µg/mL Leupeptin (Sigma-Aldrich), 100µM DTT, and 5mM sodium vanadate (Thermo Fisher Scientific). Protein

concentrations were measured with a Pierce BCA Protein Assay Kit. 50 µg of protein from each animal was separated on a 15% polyacrylamide gel and transferred onto PVDF membranes (Bio-Rad, Hercules, CA). The membranes were blocked in a 5% (w/v) non-fat milk in Tris-buffered saline, 0.1% Tween (TBS-T) solution for 30 minutes at room temperature and then incubated overnight at 4°C with primary antibodies in 5% nonfat milk in TBS-T. The primary antibodies used on isolated mitochondrial preps are as follows: anti-COXIV (1:3000; RRID: AB_879754), anti-IDH3B (1:3000; RRID:AB_2819360) , anti-NDUFA4L2 (1:3000; RRID: AB_2761150), anti-OGDH (1:3000; RRID:AB_2156766), anti-SUCLA2 (1:3000; RRID:AB_2819117). The primary antibodies used on whole BF protein lysate are as followed: Total OXPHOS Rodent WB Antibody Cocktail (1:3000; RRID: AB_2629281). Specificity of antibodies was verified by the presence of a single band at the expected molecular weight, and Total OXPHOS antibody mixture was used as previously described (298). Goat anti-rabbit or anti-mouse IgG secondary antibodies conjugated with horseradish peroxidase (1:15,000; BioRad RRID AB_11125142) were detected with Thermo Scientific™ SuperSignal West Pico Chemiluminescent Substrate and exposed to Blue Lite Autorad Film (VWR, Radnor, PA). Protein concentrations were quantified using photographed images and densitometric analyses (Scion Image Software, Frederick, MD). Protein concentrations were normalized to Citrate Synthase (1:3000, Santa Cruz, RRID: AB_2813783). All samples were evaluated in triplicate and data are presented relative to control values.

3.2.12 Measurements for Skeletal Muscle Mitochondria Density. Mitochondrial DNA (mtDNA) was co-purified with genomic DNA (nDNA) from 100 mg of biceps femoris from the same subset of 12 animals used for proteomic analysis (n=6/group).

DNA concentration and purity were determined from absorbance measurements with a NanoDrop ND-1000 Spectrophotometer (NanoDrop, Wilmington, DE). 12.5 ng of total DNA was used per reaction. DNA was amplified using a QuantiTect SYBR® Green PCR Kit (Qiagen, Venlo, Netherlands) and a CFX Connect Real-Time PCR Detection System (Bio-Rad). Optimal annealing temperatures for primer pairs were determined. Primer specificity was confirmed with nucleotide sequencing of the cloned PCR products (pCR 2.1-TOPO vector; Thermo Fisher Scientific). Primer efficiencies and sensitivities were measured with serial cDNA dilutions. All primers had efficiency ≥93%. After an initial 15-minute incubation at 96°C, all reactions went through 40 cycles of denaturation (96°C for 30 seconds), annealing temperature (60°C for 30 seconds), and extension and read (72°C for 10 seconds). Primers synthesized for PCR are as follows for mtDNA and nDNA, respectfully: ND1 [Forward (F): 5'-CCAGCATGACCCCTAGCAAT-3', Reverse (R): 5'-AGAATAGGGCGAATGGTCCG-3'], S15 [Forward(F, 5'-TGAGCAACTGATGCAGCTATACA-3'), Reverse (R): 5'-AAGGTCTTGCCGTTGTAGACG-3']. mtDNA copy number was calculated using a standard curve and normalizing to nDNA copy number. Gene analysis was performed adhering to MIQE guidelines (230).

Citrate synthase (CS) activity was measured, in triplicate, in whole biceps femoris muscle with the Citrate Synthase Assay Kit (cat. no. CS0720, Sigma-Aldrich), as described previously (201). Rates for CS are reported as $nmol \cdot min^{-1} \cdot mg$ of muscle $protein^{-1}$.

3.2.13 Statistical Analysis. Significant differences ($P < 0.05$) between groups (control and IUGR) for morphometric data were determined with an ANOVA and post

hoc least-significant difference test using general linear model procedures in JMP Software (version 14.0.0; SAS Institute, Cary, NC). Data for OCRs, enzyme assays, immunoblots, DNA ratio, was analyzed using unpaired t-test between groups after testing for the homogeneity of variance. Normality and skewness were ensured using a D'Agostino-Pearson normality test. The variance between groups for each condition (e.g., morphometry, OCR, immunoblot, etc) was similar between groups in all conditions.

The male to female ratio (male:female) ratio for OCR experiments and biometric measurements (n=12/group) was 5:7 for both IUGR and Control groups. The male to female ratio for blood flow studies (n=10/group) was 4:6 for both IUGR and Control groups. The male to female ratio for the first 6 animals per group used in the proteomic analysis, enzymatic activities, mitochondria density comparison, and immunoblots was 3:3 for both IUGR and Control groups. When data were analyzed to include fetal sex as a variable in our ANOVA, we did not find significant differences and sex was, therefore, not included in the model. Data are presented as mean ± standard error of the mean (SEM).

3.3 Results

3.3.1 Placental Insufficiency Lowers Glucose Uptake and Fetal Weight. Blood oxygen, plasma glucose, and plasma insulin concentrations were lower in IUGR fetuses than controls (Table 4). Plasma norepinephrine concentrations were 5.6-fold higher in IUGR fetuses compared to controls, similar to our previous studies and other models of IUGR (172,185,187,269,299). Plasma lactate concentrations were not different between groups. Weight-specific umbilical blood flow and umbilical (net fetal) oxygen uptakes

were not different between groups. In IUGR fetuses, rates of umbilical glucose and lactate uptakes were 24%, and 46% lower than controls, respectively.

Fetal and placental masses were 48% and 56% lower, respectively, in IUGR fetuses compared to control fetuses (Table 5). Gestational age at necropsy was not different between the groups. Total BF muscle weight was 55% lower in IUGR fetuses than control fetuses; however, BF moisture content was not different between groups (Table 5). Although brain weight was lower in IUGR fetuses compared to controls, brain weight relative to fetal body weight was 68% higher in IUGR fetuses.

3.3.2 Lower Mitochondrial Oxygen Consumption Rates in IUGR Skeletal Muscle. Mitochondrial respiration rates in State 3 conditions were 47% lower in mitochondria isolated from the IUGR skeletal muscle than controls (Figure 7A). No differences were observed between groups for State $4_{oligomycin}$ conditions (Figure 7B). The RCR was 40% lower for IUGR mitochondria compared to control fetuses (Figure 7C). In the biceps femoris muscle, mitochondrial DNA copy number and CS activity were not different between groups (Figure 8).

3.3.3 Lower Complex I Electron Transport Chain Activity in IUGR Mitochondria. In a subset of animals (n=6/group), function and expression of the individual complexes in the ETC were evaluated. Complex I activity was 18% lower in IUGR muscle compared to control muscle (Figure 9A). No differences in activity between groups were found for Complexes II or IV (Figure 9B-C). To assess total ETC expression, representative OXPHOS (Complexes I-V) proteins were evaluated by immunoblot analysis on whole BF muscle lysates; however, there were no differences in the abundances of representative OXPHOS proteins between groups (Figure 9D).

Furthermore, Complex I activity was positively associated with State 3 OCRs for both groups (Figure 10).

3.3.4 IUGR Mitochondria Proteomic Profiles Identify Mechanisms for Complex I Inhibition. Within our 12 samples, proteomic analysis identified 2691 total, unique proteins. Of those, 1112 were identified as mitochondrial specific proteins by a confidence of 3 or greater using COMPARTMENTS (Supplemental Table S1)(289). Within the mitochondrial-specific proteins, organic, hierarchical clustering of the DE proteins grouped the control and IUGR samples showing 107 upregulated proteins and 53 downregulated proteins in IUGR mitochondria compared to control mitochondria (Figure 11 A-C). Enriched GO terms for the differentially expressed proteins were found in all three GO sub-ontologies (biological process (BP), cellular component (CC), and molecular function (MF)) as well as KEGG Pathways (Figure 5D). GO-BP and KEGG Pathways each had 10 enriched pathways, and both overlap in the terms: “TCA Cycle”, “Glycolysis/Gluconeogenesis”, and “Pyruvate Metabolism” (Supplemental Table S2 and S5). GO-CC and GO-MF each had 3 and 9 enriched pathways, respectively (Supplemental Table S3 and S4).

KEGG pathway analysis of the 160 DE proteins showed 17 proteins were connected to “Carbon Metabolism”: 7 proteins were upregulated and 10 proteins were downregulated in IUGR mitochondria compared to controls (Supplemental Table S5). Furthermore, KEGG pathway analysis identified 8 proteins connected to “TCA Cycle”, and all 8 of these proteins were downregulated in IUGR mitochondria, and all 8 proteins were found within “Carbon Metabolism” pathway (Supplemental Table S5).

Additionally, of these 8 downregulated proteins, 5 overlap with “2-oxocarboxylic Acid Metabolism” (Supplemental Table S5).

Proteomic analysis also showed a downregulation of proteins involved in pyruvate flux into the TCA cycle in IUGR mitochondria. These proteins include Mitochondrial Pyruvate Carrier 2 (MPC2), Pyruvate Dehydrogenases 2 and 3 (PDK2,3), and pyruvate carboxylase (PC; Figure 12). Additionally, the results identified lower abundances of enzymes involved in amino acid metabolism such as Branched Chain Aminotransferase 2 (BCAT2) and Branched Chain Keto Acid Dehydrogenase Kinase (BCKDK) in IUGR mitochondria compared to controls (Figure 12).

No upregulated proteins in IUGR mitochondria were directly involved in the TCA cycle, Amino Acid Metabolism, or β-oxidation. However, two upregulated proteins in IUGR mitochondria were identified as potential regulatory factors for metabolism: NDUFA4L2 and LDHB, which are centrally located in mitochondrial metabolism (Figure 12).

3.3.5 Immunoblot Confirm Reductions in TCA Cycle Enzymes and Elevated NDUFA4L2. NADH dehydrogenase 1 alpha subcomplex 4-like 2 (NDUFA4L2) was selected as an upregulated protein in IUGR mitochondria that also affects ETC function at Complex I. NDUFA4L2 concentrations were 3-fold higher in IUGR mitochondria compared to control mitochondria (Figure 13A).

TCA cycle enzymes, Isocitrate Dehydrogenase 3B (IDH3B), Succinate-CoA Ligase ADP-Forming Subunit Beta (SUCLA2), and, Oxoglutarate Dehydrogenase (OGDH), were validated with immunoblots (Figure 13 B-D). IDH3B, SUCLA2, and

OGDH abundances were 55%, 38%, and 54% lower in IUGR mitochondria, respectively, compared to Control (Figure 13 B-D).

Data supplements can be found here:

https://figshare.com/s/15f93a5720ba0e300c8c

Table 4. Metabolic and hormone concentrations, and umbilical uptakes for control and IUGR fetuses

Measurement	Control (10)	IUGR (10)
Male to Female Ratio (Male: Female)	4:6	4:6
Umbilical Blood Flow (mL/min/kg)	200.9 ± 24.2	167.6± 8.6
Blood O_2 Content (mM)	3.4 ± 0.1	1.1 ± 0.1*
Umbilical Oxygen Uptake (μmol/min/kg)	355.1± 16.4	318.7 ± 14.0
Plasma Glucose (mM)	1.03 ± 0.04	0.63 ± 0.05*
Umbilical Glucose Uptake (μmol/min/kg)	30.4 ± 0.8	23.2 ± 1.2*
Plasma Lactate (mM)	2.15 ± 0.12	2.73 ± 0.39
Umbilical Lactate Uptake (μmol/min/kg)	19.3 ± 2.2	10.4 ± 1.8*
Plasma Norepinephrine (pg/mL)	770 ± 140	4340 ± 1020*
Plasma Insulin (ng/mL)	0.37 ± 0.02	0.15 ± 0.02*

Values are expressed as means ± SE. Significant differences ($P < 0.05$) between groups were determined by ANOVA and post hoc least-significant difference test using general linear model procedures. IUGR, intrauterine growth restriction.
*$P < 0.05$, difference between groups.

Table 5. Body and organ masses of control and IUGR fetuses at necropsy.

Measurement	Control (12)	IUGR (12)
Male to Female Ratio (Male: Female)	5:7	5:7
Age at necropsy (days)	132± 1	132 ± 1
Fetal Weight (kg)	3.33 ± 0.21	1.73 ± 0.12*
Placental Weight (g)	425 ± 43.4	188 ± 47.2*
Brain Weight (g)	51.9 ± 1.4	43.0 ± 1.5*
Brain Weight (g)/ Fetal Weight (kg)	15.2 ± 0.8	25.6± 2.8*
Total Biceps Femoris Weight (g)	34.5 ± 1.3	15.6 ± 1.6*
Total Biceps Femoris Weight (g)/ Fetal Weight (kg)	10.9 ± 0.4	8.94 ± 0.3*
Biceps Femoris Wet/Dry Ratio (%)	77.7 ± 2.1	75.8 ± 2.6

Values are expressed as means ± SE. Significant differences ($P < 0.05$) between groups were determined by ANOVA and post hoc least-significant difference test using general linear model procedures. IUGR, intrauterine growth restriction.
*$P < 0.05$, difference between groups.

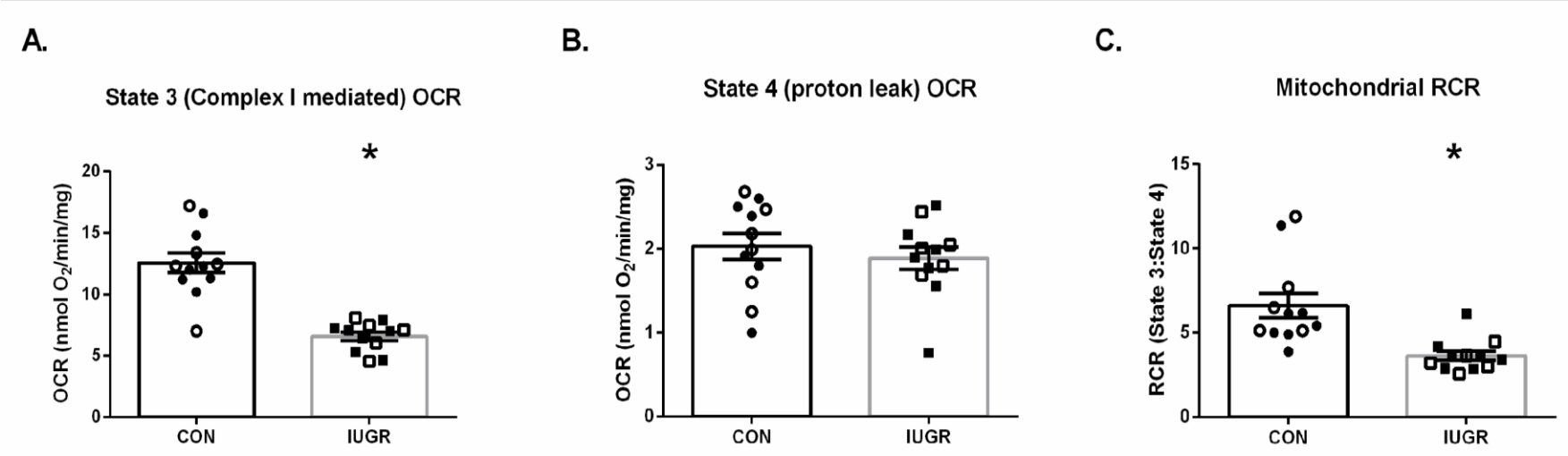

Figure 7. Reduced mitochondrial oxygen consumption rates (OCRs) in intrauterine growth restriction (IUGR) skeletal muscle. Mitochondria isolated from biceps femoris muscle of IUGR (n = 12) and control (CON; n = 12) fetuses were evaluated. Oxygen consumption rates (OCRs) normalized to mitochondrial protein concentrations were measured at State 3 conditions (Complex I mediated; A) and State 4 conditions (proton leak; B). C: the respiratory control ratio (RCR; State 3:State 4 ratio) is presented. The data were analyzed using unpaired t test between groups, and data are presented as the means ± SE, with *P < 0.05 denoting group differences.

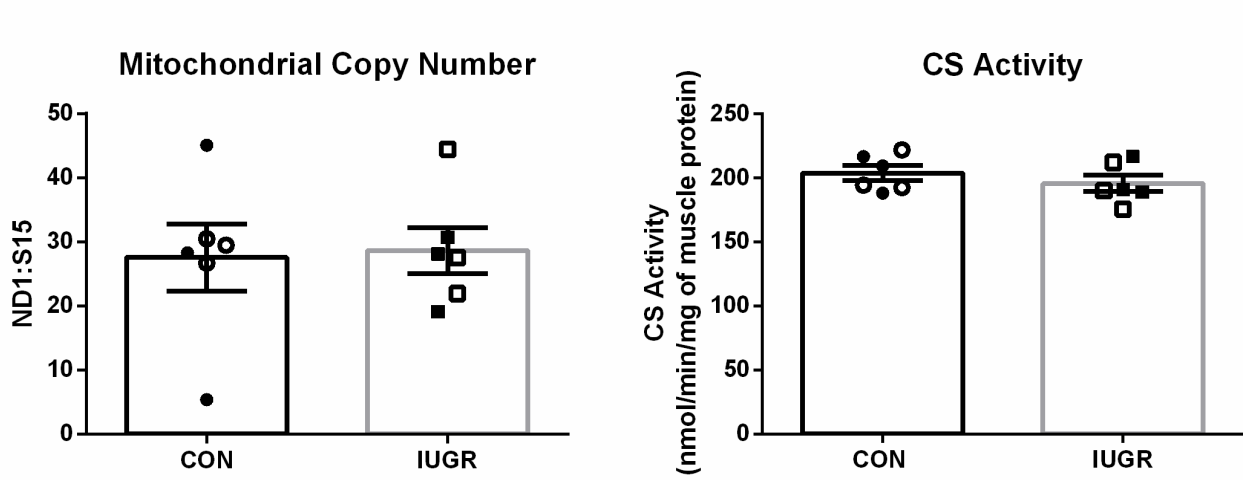

Figure 8. Mitochondrial density was unaffected in intrauterine growth restriction (IUGR) skeletal muscle. Left: mitochondrial DNA copy number to nuclear DNA copy number in the biceps femoris muscle is represented as a ratio of NADH-ubiquinone oxidoreductase subunit 1 (*ND1*):(RPS15) genes for control (CON; $n = 6$) and IUGR ($n = 6$) fetuses. Right: citrate synthase (CS) activity normalized to milligrams of whole biceps femoris tissue is presented for CON and IUGR fetuses. The data were analyzed using unpaired *t* test between groups, and data are presented as the means ± SE; there were no significant differences observed between groups.

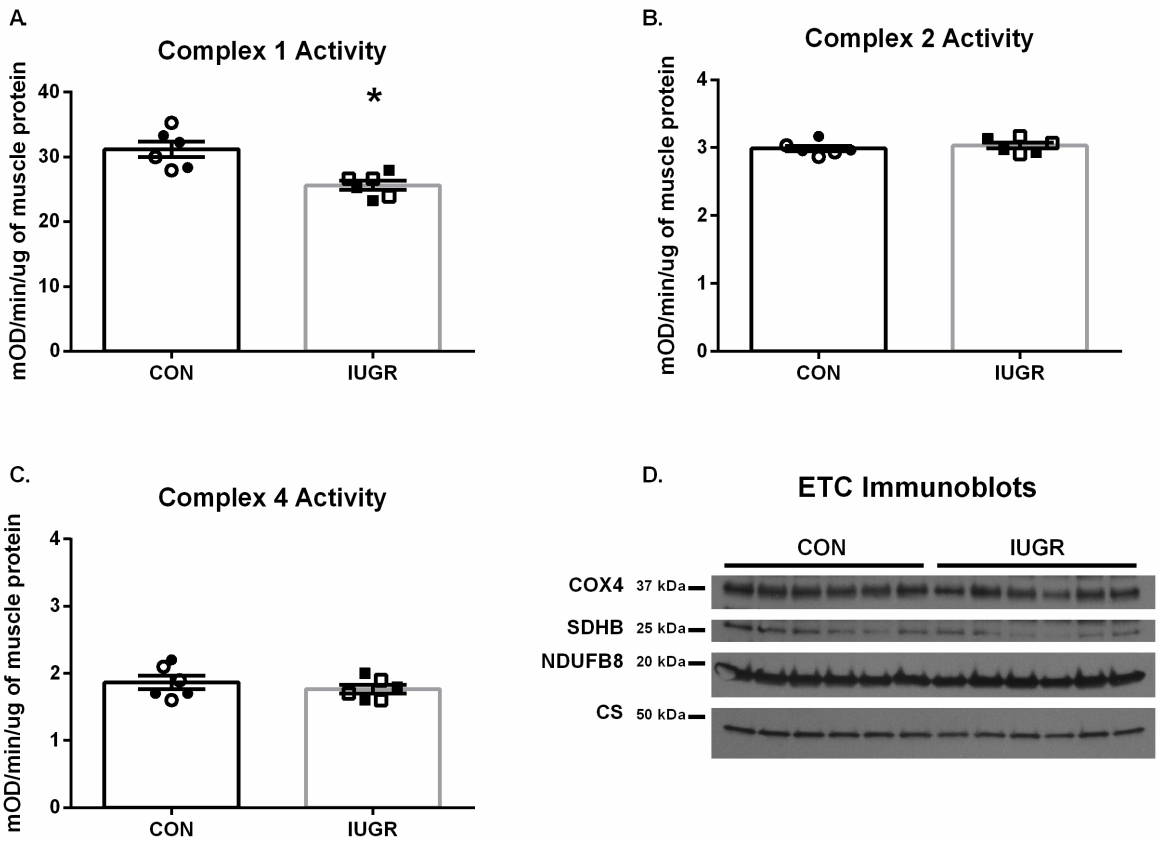

Figure 9. Reduced electron transport chain activity rates, but not complex abundances in intrauterine growth restriction (IUGR) mitochondria. Complex I (*A*), Complex II (*B*), and Complex IV (*C*) activities of the electron transport chain (ETC) were determined for biceps femoris muscle of IUGR and control (CON) fetuses. *D*: representative immunoblots are presented for Complex I [NADH dehydrogenase 1β subcomplex subunit 8 (NDUFB8)], Complex II [succinate dehydrogenase B (SDHB)], and Complex IV (COX4) subunits and citrate synthase (CS) for whole biceps femoris muscle protein lysate. No differences in protein concentrations were observed between groups by immunoblot analysis. For each group, males are represented by open symbols, and females are represented by closed symbols. The data were analyzed using unpaired *t* test between groups after testing for equal variance, and the data are presented as the means ± SE. *$P <$ 0.05 denotes significance differences between groups. mOD denotes milli optical density.

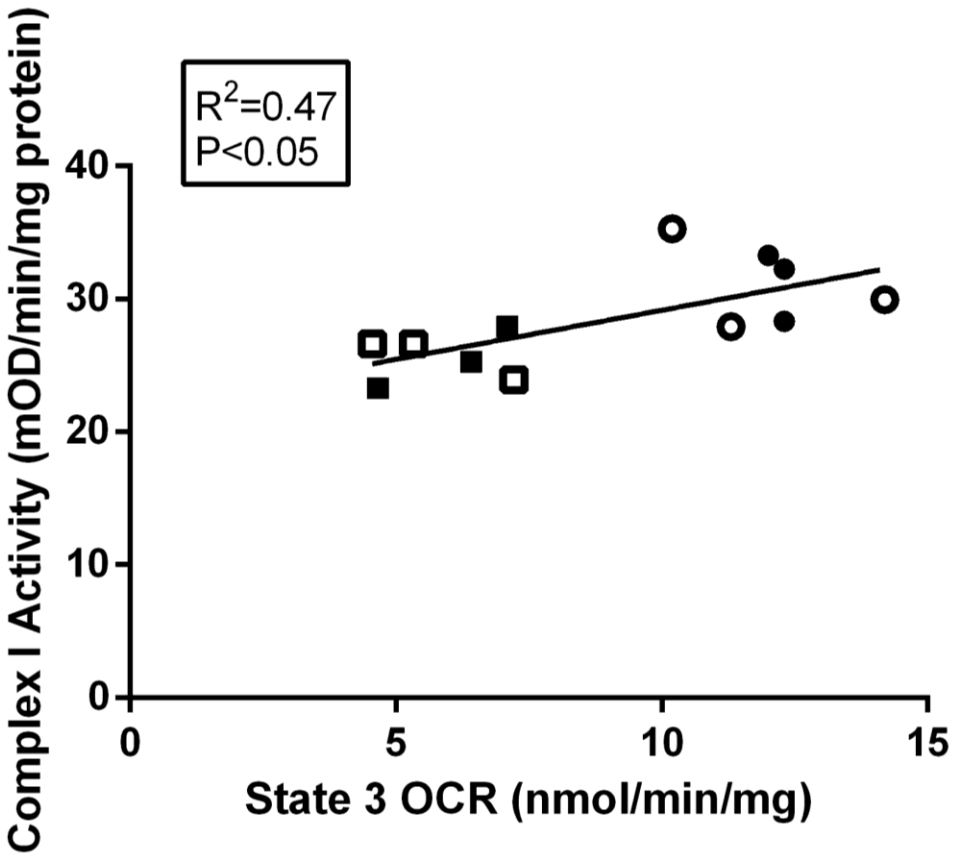

Figure 10. Correlation of mitochondrial oxygen consumption rates (OCRs) and State 3 Complex I activity. State 3 oxygen consumption rates (OCRs) plotted against Complex I activity rates for the subset of intrauterine growth restriction (IUGR; squares, $n = 6$) and control (CON; circles, $n = 6$). For each group, males are represented by open symbols, and females are represented by closed symbols. Linear regression was performed with JMP 14, and R^2 and P values are indicated. mOD denotes milli-optical density.

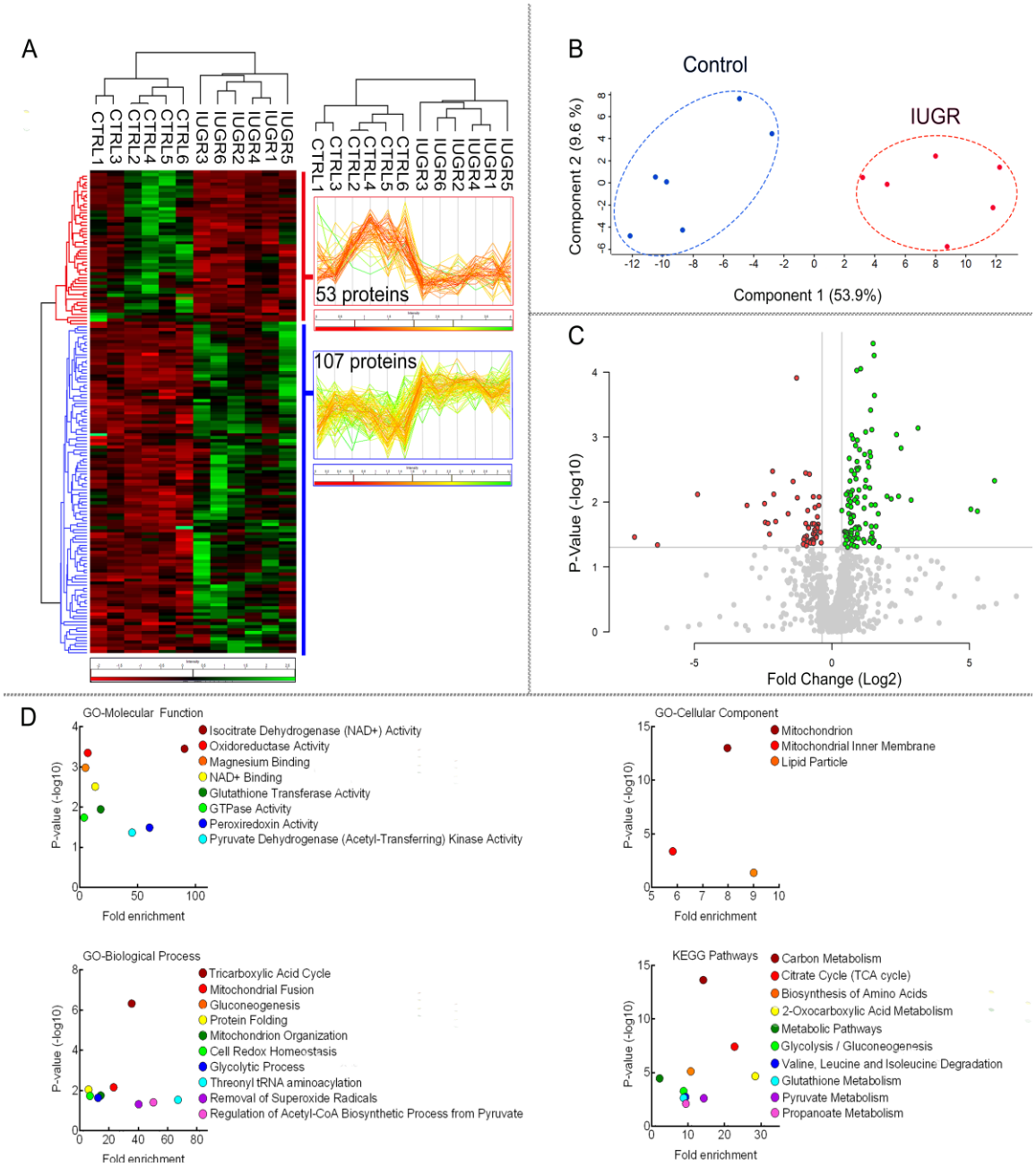

Figure 11. Proteomic analysis reveals 160 differentially expressed proteins in intrauterine growth restriction (IUGR) skeletal muscle mitochondria. A: expression patterns for the differentially expressed (DE) proteins are present in the heatmap that shows organic, hierarchical clustering of the significant DE proteins between control (CTRL) and IUGR mitochondria. Lower protein abundances are shown in red, and higher protein abundances are shown in green for IUGR versus control comparison. Hierarchical clustering of the 107 upregulated (blue) and 53 downregulated (red) for control versus IUGR comparison is displayed on either side of the heatmap. B: a principal component analysis (PCA) plot shows distinct separation between control (blue) and IUGR (red) mitochondria protein abundances. C: for the control and IUGR comparison, the volcano plot for log2 fold change plotted against log10 adjusted P values identifies all significant DE proteins with lower (red) and higher (green) protein abundances of IUGR mitochondria. D: the P values for each Gene Ontology (GO) term and Kyoto Encyclopedia of Genes and Genomes (KEGG) pathway for all DE proteins (both up- and downregulated) for the control vs. IUGR comparison were graphed against their individual fold enrichment scores. The protein list for each GO term or KEGG pathway can be found in Supplemental Tables S2–S5.

A.

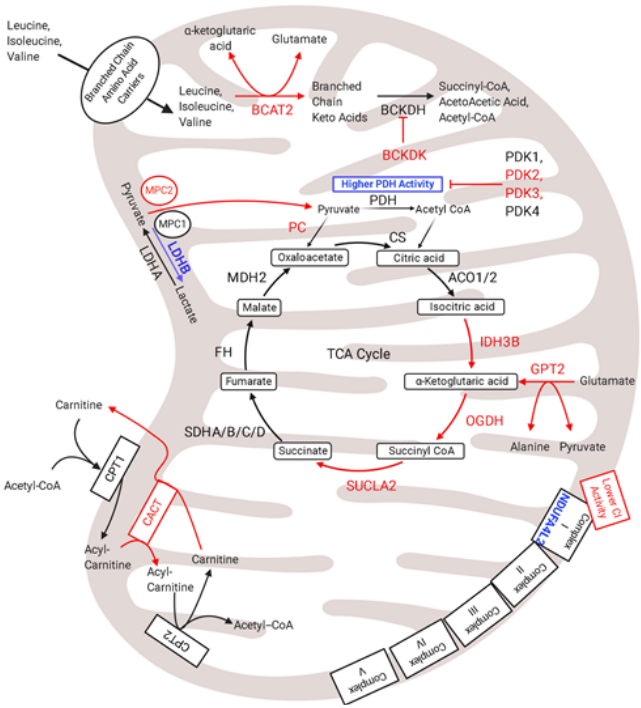

B.

Protein Name	Log Fold Change Relative to CON
Isocitrate Dehydrogenase 3B (IDH3B)	-1.6
2-Oxoglutarate Dehydrogenase (OGDH)	-1.4
Mitochondrial Pyruvate Carrier 2 (MPC2)	-1.7
Glutamic-Pyruvic Transaminase 2 (GPT2)	-2.4
Lactate Dehydrogenase B (LDHB)	+2.5
NADH Dehydrogenase 1 Alpha subcomplex 4-like 2 (NDUFA4L2)	+5.7
Branched Chain Keto-Acid Dehydrogenase Kinase (BCKDK)	-1.98
Branched Chain Amino Acid Transaminase 2 (BCAT2)	-1.01
Pyruvate Carboxylase (PC)	-1.6
Carnitine/Acylcarnitine Translocase (CACT)	-1.0
Pyruvate Dehydrogenase Kinase 2 (PDK2)	-1.6
Pyruvate Dehydrogenase Kinase 3 (PDK3)	-1.8

Figure 12. Changes in mitochondrial metabolic enzymes in response to intrauterine growth restriction (IUGR) relative to control (CON). *A*: the schematic outlines major mitochondrial enzymes and their processes in the tricarboxylic acid (TCA) cycle (ETC), fatty acid oxidation, or branched chain amino acid metabolism, created using BioRender.com. In the schematic, lower protein abundances (red) and greater protein abundances (blue) for IUGR mitochondria are indicated, whereas enzymes that are not different are in black text. Proposed decreased metabolic fluxes in IUGR mitochondria are shown with red arrows. *B*: fold changes are presented for each differentially expressed (DE) protein of interest. ACO1/2, aconitate hydratase 1/2; BCKDH, branched-chain α-keto acid dehydrogenase; CPT1,2, carnitine palmitoyltransferase 1,2; CS, citrate synthase; FH, fumarate hydratase; LDHA, lactate dehydrogenase A; MDH2, malate dehydrogenase 2; MPC1, mitochondrial pyruvate carrier 1; PDH, pyruvate dehydrogenase; PDK1,4, pyruvate dehydrogenase kinases 1,4; SDHA–D, succinate dehydrogenase A–D; SUCLA2, succinate-CoA ligase ADP-forming subunit β.

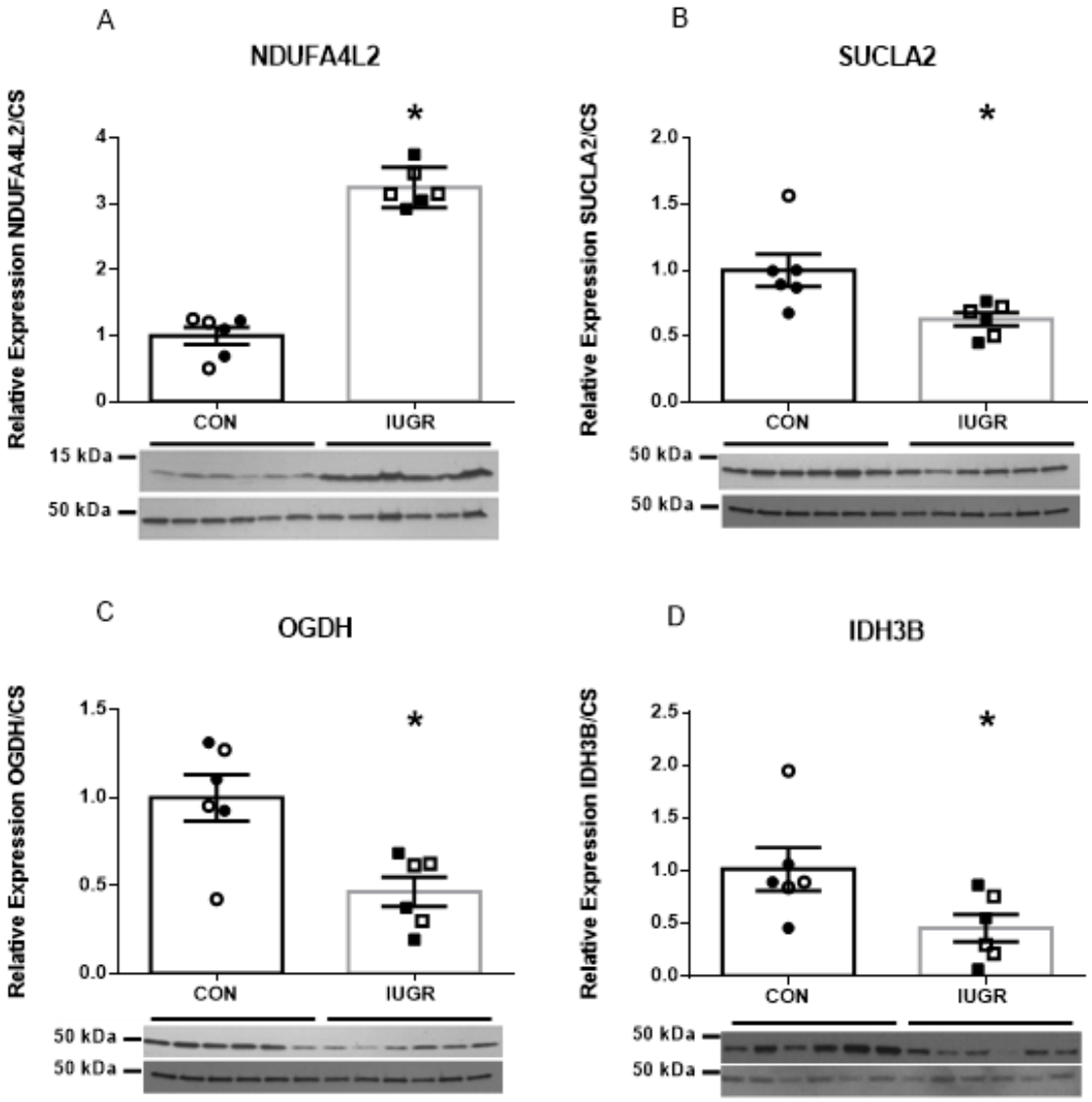

Figure 13. Immunoblots of differentially expressed (DE) proteins confirm proteomic results. Representative immunoblots are presented for NADH dehydrogenase 1α subcomplex 4-like 2 (NDUFA4L2; *A*), succinate-CoA ligase ADP-forming subunit β (SUCLA2; *B*), oxoglutarate dehydrogenase (OGDH; *C*), and isocitrate dehydrogenase (NAD^+) 3 noncatalytic subunit β (IDH3B; *D*). The relative abundances to citrate synthase (CS) are shown for control (CON) and intrauterine growth restriction (IUGR; $n = 6$/group). For each group, males are represented with open symbols, and females are represented by closed symbols. The data were analyzed using unpaired *t* test between groups after testing for equal variance, and the data are presented as the means ± SE. $*P < 0.05$ denotes significance differences between groups.

3.4 Discussion

To adapt to low nutrient and oxygen conditions *in-utero*, skeletal muscle mitochondria from IUGR fetuses have a lower maximal Complex I-mediated respiratory rates and reduced Complex I activity compared to controls. The reductions in Complex I activity in IUGR mitochondria was associated with greater NDUFA4L2 concentrations because abundances of other representative ETC proteins remain unchanged. Induction of NDUFA4L2 during hypoxia has been shown to decrease cellular respiration by reducing the functional capacity of Complex I(300–302). ETC function, and subsequent energy production, relies on adequate supplies of reducing equivalents, primarily from the TCA cycle (271,303). Interestingly, our proteomic and western analysis shows that mitochondria isolated from skeletal muscle of IUGR fetuses have lower concentrations of TCA cycle enzymes compared to controls. Lower OCR, Complex I activity, and TCA cycle enzyme abundances in IUGR skeletal muscle mitochondria may serve as an avenue for substrate (e.g. pyruvate) conservation in IUGR skeletal muscle in response to nutrient and oxygen restriction induced by placental insufficiency.

3.4.1 Mitochondrial Oxygen Consumption. Glucose metabolism and oxygen consumption are entwined via mitochondrial metabolism. IUGR fetuses are not only hypoxemic, hypoglycemic, and smaller than control fetuses, but they also exhibit decreased rates of growth, protein accretion, as well as lower whole-fetus glucose oxidation rates (76,95,185,197,206,221,263,304,305). In the present study, mitochondria from IUGR skeletal muscle have lower State 3 (Complex-I mediated) OCRs compared to controls, supporting previous observations of globally reduced energy status in their skeletal muscle and lower fetal hind-limb oxygen consumption rates (76,77). The

reduction in State 3 OCR of IUGR mitochondria was independent of Complex II and IV activities, but OCRs correlated with lower Complex I activity (Figure 4). State 4 OCRs (proton leak) were not different between groups, thus showing that the lower NADH-coupled respiration in IUGR mitochondria was due to lower State 3 OCRs (Figure 1). Furthermore, the defect in IUGR State 3 OCR was also independent of ETC proteins because abundances examined by immunoblots and proteomic analyses were not different for several protein subunits of the ETC complexes. Together, these findings indicate that lower mitochondria respiration rates in IUGR skeletal muscle are, in part, related to inhibition of Complex I of the ETC.

Complex I mediated oxygen consumption, which accounts for the majority of mitochondrial oxygen consumption, relies upon an adequate supply of O_2, NADH, Pi, and ADP (306). Consisting of 45 subunits, Complex I is the largest, most complicated, and least understood component of the ETC, and its activity is regulated in response to nutrient and oxygen availability (127,307). The regulation of Complex I activity has yet to be fully elucidated, but it appears to be governed by its active/dormant (A/D) transition state in response to substrate and oxygen supply: the A-form operates at physiological temperatures and substrates, but Complex I transitions into the D-form if oxygen/substrates become limiting (308–310). The mechanism behind the Complex I A/D transition is unknown, but it may be due to post translational modifications or a decrease in core catalytic subunit expression (306,311,312). Intriguingly, our proteomic analysis of isolated mitochondria indicates that neither of these mechanisms is responsible for reduced State 3 OCRs in IUGR mitochondria. However, we observed greater NDUFA4L2 abundance in skeletal muscle mitochondria from IUGR fetuses,

which has been shown to inhibit Complex I activity and may serve as a potential adaptive response mechanism to conditions of placental insufficiency and IUGR(300–302). The expression of NDUFA4L2 is stimulated by hypoxia inducible factor 1α (HIF-1α), the expression of which is a primary adaptive response to decreases in available oxygen (300,301). Although IUGR fetuses are hypoxemic, increased prolyl hydroxylase domain expression, which opposes the actions of HIF-1α, is observed in IUGR tissues; however, increased prolyl hydroxylase domain expression is matched by increased HIF1/2α activity in IUGR tissues, which most likely represents a new metabolic set-point in response to chronic hypoxia in IUGR fetuses (240–244). While the physiological function of NDUFA4L2 remains to be fully elucidated, when it is expressed, NDUFA4L2 is inserted into Complex I and reduces ROS generation and oxygen consumption by decreasing electron flux (300,301). Furthermore, due to its strategic position downstream of NADH production, increased NDUFA4L2 expression would reduce OCRs regardless of fuel origin. Importantly, increased NDUFA4L2 expression would keep total substrate oxidation lower thereby conserving substrates for vital tissues at the expense of skeletal muscle metabolism.

IUGR fetal skeletal muscle is depleted in purines, ribose, oxygen, glucose metabolites, and key amino acids, indicating a lower energy status (76,77). However, a depletion of skeletal muscle metabolites may be consequential to, and not a cause of, decreased skeletal muscle mass in IUGR fetuses. One mechanism likely to reduce accretion rates and metabolism is a reduction in skeletal muscle OCR. Since the rate of oxygen consumption by mitochondria *in vivo* is determined by the phosphorylation potential (log(ATP/ADP*Pi)), electrons will only be donated to oxygen if ADP is

concomitantly phosphorylated to ATP (313–316). As such, the rate of oxidative phosphorylation is coupled to the rate of ATP utilization. Therefore, a reduction in OCR will reduce ATP production and force established fetal muscle fibers to reduce energy (ATP) expenditure, of which a significant portion is devoted to protein synthesis (317–319). Taken together, the adaptation of IUGR skeletal muscle to a hypoxic, nutrient restricted environment decreases its need for energy and metabolic requirements at the expense of its growth.

Although Complex I activity and State 3 (Complex I mediated) OCRs were highly correlated (Figure 4), the magnitude of reduction in IUGR fetuses was not equivalent for each measurement (18% lower Complex I activity vs 47% lower State 3 OCRs in IUGR fetuses compared to controls). The measurements of Complex I activity demonstrates a lower rate in the NADH redox capability; however, the ability of Complex I to transfer protons to the intermembrane space or transfer electrons within Complex I (or between Complex I and coenzyme Q) was not investigated. Alterations in either of these processes may explain the discrepancy between State 3 OCR and Complex I activity measurements in this study. Interestingly, *in vivo* experiments show weight-specific hindlimb oxygen uptakes are 29% lower in IUGR fetuses compared to controls (76). Although these *in vivo* hindlimb OCRs are higher than the State 3 OCRs for isolated mitochondria, this result is expected because the *in vivo* measurements include Complex II activity (FADH redox), which also contributes to the total OCR. In contrast, the *in vitro* State 3 OCRs for isolated mitochondria were performed in the absence of Complex II activity.

3.4.2 The link between the Electron Transport Chain and Energy Conservation. Due to the low energy status of IUGR skeletal muscle, it is not surprising that the TCA

cycle enzyme abundances are lower in IUGR mitochondria (Figure 12)(77). A decrease in OCRs would result in a reduction in electron flow through the ETC, and this would subsequently inhibit the flow of glycolytic substrates through mitochondrial metabolism since oxidative phosphorylation is dependent upon reducing equivalents, namely NADH. Consequently, reduced ETC function reduces NADH oxidation, increases the [NADH]:[NAD+] ratio, and inhibits key TCA cycle enzymes such as IDH and OGDH, both of which, along with CS, represent the rate-limiting steps of the TCA cycle(320). Interestingly, both IDH and OGDH are downregulated in IUGR mitochondria (Figure 13). Although NADH and ATP only allosterically inhibit IDH and OGDH, the downregulation of these proteins in our data set could represent adaptation to a lower energy requirement in IUGR skeletal muscle (77).

Intriguingly, IUGR mitochondria appear to conserve glutamate by decreasing the abundances of enzymes which use glutamate, or glutamate derivatives, such as BCAT2, GPT2, OGDH, and BCKDK (Figure 6). Since amino acid oxygen quotients are lower in the IUGR hindlimb, these fetuses may conserve amino acids rather than use them in energy producing pathways, such as the TCA cycle. Although these data are consistent with current studies, speculation on amino acid metabolism in IUGR skeletal muscle mitochondria is beyond the scope of this study (76,77).

Due to their relative mass, larger muscle groups have a proportionally greater impact on glucose metabolism and are composed of mixed fiber types (282–284). The BF was chosen as the representative muscle group for this study. However, the IUGR BF muscle has fewer Type I fibers compared to control BF muscle, and Type 1 fibers are known to have higher mitochondrial density compared to Type II fibers, which indicates

that changes in muscle composition might impact mitochondrial content (215). The citrate synthase activity assay, along with other measurements in whole BF muscle (DNA ratio and immunoblots for mitochondrial ETC proteins) performed in this study serve as proxies for mitochondrial density. Furthermore, using both immunoblot and proteomic measurements, no differences in citrate synthase abundances were observed between groups. This implies that mitochondrial density in the biceps femoris is similar between groups, and the abundance of citrate synthase per mitochondria is similar between groups. Together, these measurements do not support reductions in mitochondrial content in the BF muscle of IUGR fetuses. This might reflect that in the IUGR sheep fetus, there is a smaller proportion of Type 1 fibers to total fiber number, and the 5% reduction in this population, which is <20% in the BF muscle, does not lead to major declines in mitochondrial density (215).

3.4.3 Pyruvate Metabolism and OCR. Although we found a decrease in the abundances of various TCA cycle enzymes, we did not find a significant increase in the abundances of the enzymes that inhibit pyruvate catabolism into acetyl-CoA. In fact, the abundances of Pyruvate Dehydrogenase, Pyruvate Dehydrogenase Phosphatase 1, and Pyruvate Dehydrogenase Phosphatase 2 were not different between groups (Supplemental Table S1). Furthermore, the abundances of Pyruvate Dehydrogenase Kinases were either lower or unchanged in IUGR mitochondria compared to controls, supporting our previous findings (269) (Figure 12, Supplemental Table S1). However, we did find lower pyruvate carboxylase (PC) abundance in IUGR mitochondria, which may be due to the decrease in demand of NADH by the ETC.

Increased, or normal, pyruvate catabolism in IUGR skeletal muscle runs contrary to speculation of IUGR glucose metabolism and activation of the Cori cycle (197,221). Intuitively, increased pyruvate catabolism should increase substrate available to the ETC, though greater NDUFA4L2 expression is expected to limit the capacity of IUGR skeletal muscle to oxidize NADH. Remarkably, we show lower Mitochondrial Pyruvate Carrier 2 (MPC2) abundance in IUGR mitochondria compared to controls. MPC2 and Mitochondrial Pyruvate Carrier 1 (MPC1) are highly conserved pyruvate transporters, and are thought to be the primary pyruvate transporters on the inner mitochondrial membrane (321,322). Regulation of MPC2 is yet to be fully understood; however, it is hypothesized that acetylation of MPC2 occurs under hypoxia, thereby reducing oxygen consumption under stress (303,323). Although IUGR skeletal muscle has increased PDH activity, this may be a result of decreased pyruvate flux across the mitochondrial membrane due to decreased MPC2 abundance (269). Therefore, the increase in PDH activity in IUGR skeletal muscle mitochondria may act to maintain pyruvate flux to meet minimal skeletal muscle energy requirements. The reduction in MPC2, along with the reduction in ETC function via NDUFA4L2, may represent a co-adaptive response by IUGR skeletal muscle mitochondria as a coping mechanism to a low nutrient environment.

Chapter 4

Dimming the Powerhouse: Mitochondrial Dysfunction in Liver and Skeletal Muscle of Intrauterine Growth Restricted Fetuses

The contents of this chapter have been submitted for publication in Frontiers in Endocrinology.

4.1 Abstract

Intrauterine growth restriction (IUGR) of the fetus, resulting from placental insufficiency (PI), is characterized by low fetal oxygen and nutrient concentrations that stunt growth rates of metabolic organs. Numerous animal models of IUGR recapitulate several of the pathophysiological conditions found in human fetuses with IUGR. These models provide insight into the metabolic dysfunction in skeletal muscle and liver. For example, cellular energy production and metabolic rate are decreased in the skeletal muscle and liver of IUGR fetuses. These metabolic adaptations demonstrate that the fundamental processes of mitochondria, such as substrate utilization and oxidative phosphorylation, are tempered in response to low oxygen and nutrient availability. As a central metabolic organelle, mitochondria coordinate cellular metabolism by coupling oxygen consumption to substrate utilization in concert with tissue energy demand and accretion. In IUGR fetuses, reducing mitochondrial metabolic capacity in response to nutrient restriction is advantageous to ensure fetal survival. If permanent, however, these adaptations may predispose IUGR fetuses toward metabolic diseases throughout life. Furthermore, these mitochondrial defects may underscore developmental programming that results in the sequela of metabolic pathologies. In this review, we will examine how reduced nutrient availability in IUGR fetuses impacts skeletal muscle and liver substrate catabolism, and discuss how enzymatic processes governing mitochondrial function, such as the Tricarboxylic Acid Cycle and Electron Transport Chain, are regulated. Considering the importance of the skeletal muscle and the liver to later life metabolic dysfunction, understanding the deficiencies in oxygen and substrate metabolism in response to placental restriction is essential to understanding the pathogenesis of IUGR.

4.2 Introduction

Many cases of intrauterine growth restriction (IUGR) of the fetus are caused by reductions in placental mass and function resulting in lower fetal nutrient and oxygen availability. Fetal development and growth are particularly vulnerable to perturbations in the *in utero* environment, and it is proposed that lower nutrient availability during gestation significantly impacts short- and long-term metabolic regulation (46,266,324–326). Glucose is an important and primary substrate for oxidative metabolism in the fetus (53,218). Consequently, early studies in "small for gestational age" or IUGR neonates have focused on describing the negative effects from hypoglycemia and malnutrition on neonatal growth and metabolism (207,327–331). These studies laid the foundation for our understanding of neonatal metabolism and the potential responses associated with fetal growth restriction. However, there are gaps in our knowledge regarding how organ specific effects coordinate whole-body substrate utilization in the IUGR fetus.

Prenatal development establishes the foundation for global metabolic regulation and substrate utilization in fetal tissues. Glucose, lactate, and amino acids comprise the primary oxidizable substrates used for energy production and tissue growth in the fetus (332). When the placental transport capacity for nutrient and oxygen flux becomes limited in IUGR pregnancies, metabolic and endocrine responses are initiated in the fetus to ensure survival (188,333). As a result, two major physiological responses occur out of necessity: stunted growth and metabolic adaptation. Slowing growth lowers the global metabolic burden on the fetus and prioritizes substrate availability for essential organs such as the brain and heart. The skeletal muscle and liver each comprise a small amount of the total fetal weight near term (~10% for skeletal mass, and 3-4% for liver mass)

(334–337). However, combined, these tissues are responsible for 40-50% of the total fetal oxygen consumption, underscoring their importance as two of the largest metabolic organs in the fetus (334,338). Therefore, these tissues are at greater risk for developing persisting metabolic adaptations when IUGR occurs.

IUGR neonates are born with less muscle and liver masses (107–112,339). The deficiencies in lean mass are retained through adulthood, despite adequate nutrient availability after birth (107,109,110,113–115). This observation is especially important considering that tissue growth is dictated by energy homeostasis, and this balance is governed by substrate utilization and oxidative phosphorylation (119,120,122,123). Interestingly, IUGR infants have higher rates of resting energy expenditure, measured within the first few weeks after delivery, and are predicted to increased body mass (catch-up growth) (116,117). However, these neonates fail to increase adequate muscle mass, which potentiates subcutaneous and hepatic fat deposition, and represents a modified metabolic phenotype (119–124,340,341). The greater adiposity may further serve as a comorbidity that exacerbates the metabolic strain throughout the life-course, including the predisposition to nonalcoholic fatty liver disease (39,125,340–343). The life-long metabolic strain induced by postnatal catch up growth manifests as an increased risk of developing impaired glucose tolerance, dyslipidemia, and hypertension (342,344). Thus, individuals born IUGR are at risk of increased morbidities due to impaired substrate metabolism combined with lower lean mass and greater adiposity. These observations highlight that prenatal conditions from placental restriction negatively affect postnatal energy balance.

Comprehensive studies evaluating whole-body metabolism and the coordinated tissue-specific responses in IUGR fetuses are beginning to define the impacts of nutrient and oxygen restriction during gestation. However, despite the growing number of experimental models and studies investigating IUGR metabolism, much remains unknown. Given the importance and centrality of mitochondria to substrate utilization and energy balance, the metabolic aberrations observed in IUGR fetuses implies mitochondrial metabolism is adjusted to low nutrient and oxygen concentrations. In this review, we will discuss our current understanding of mitochondrial metabolism in the skeletal muscle and liver of IUGR fetuses and present gaps in the field.

4.2.1 Maintenance of Oxidative Phosphorylation in Mitochondria. Oxidative metabolism is predicated on mitochondrial function. Within the mitochondria, carbohydrate (pyruvate), amino acid, and fatty acid metabolism intersect in the Tricarboxylic Acid (TCA) cycle, which requires oxygen, to produce the primary cellular energy currency: adenosine triphosphate (ATP). However, utilization of substrates within the mitochondrion is not equal. Some metabolites, like lysine and leucine, only enter the TCA cycle only as acetyl-CoA, while other substrates, like valine and glutamate, can only enter as TCA cycle intermediates via specific carriers (anaplerosis). Oxidative phosphorylation is generally limited by the presentation of ADP to the mitochondrion (free ADP), and changes in the concentration of any one substrate would affect the utilization of other substrates (345).

In the mitochondrion, ATP is synthesized from the oxidation of carbohydrates, proteins, and lipids. To be utilized, these substrates must diffuse through, or be transported across, the outer and inner mitochondrial membranes. Once inside the

mitochondrial matrix, metabolic substrates can enter the TCA cycle as acetyl-CoA or as an intermediate; however, the oxidation of acetyl CoA produces a majority of the cellular NADH/$FADH_2$, as less NADH is produced from intermediates that enter later in the TCA cycle compared to acetyl-CoA. The NADH produced from each pass through the TCA cycle is subsequently oxidized at the electron transport chain (ETC) to produce ATP. While the oxidative potential of TCA cycle intermediates is not as great as acetyl-CoA , a greater abundance of TCA cycle intermediates is beneficial for several reasons. First, these anaplerotic reactions increase the acetyl CoA "carrying capacity" of the TCA cycle, allowing more acetyl CoA to be oxidized. Additionally, anaplerotic reactions refill TCA cycle intermediates that are lost through cataplerosis. Therefore, substrate oxidation and anaplerotic inputs ensure efficient TCA cycle function, where it continuously works to produce NADH and $FADH_2$ for the ETC.

The net effects of catabolism and anabolism on energy production define mitochondrial function. The TCA cycle and ETC are intrinsically linked through the redox cycle of NADH and $FADH_2$ (271,278). Normally, the flow of electrons starts with the oxidation of NADH and $FADH_2$, at Complexes I and II, respectively. As electrons are transported through the ETC, protons move from the matrix to the intermembrane space, creating the proton motive force. The journey of electrons through the ETC ends with their terminal transfer onto oxygen at Complex IV (oxygen consumption). Simultaneously, the proton motive force is used by ATP synthase to catalyze ATP from ADP and inorganic phosphate (P_i). The integrated nature of the ETC and TCA cycle means the rate of oxygen consumption in mitochondria is coupled to the phosphorylation potential (log [ATP]/[ADP] [P_i]), which means ATP production and utilization is coupled

to oxygen consumption rate (OCR) (235,272,273,278,346–348). As such, conditions that reduce the electron flux through the ETC will also reduce the production of ATP as well as the regeneration of NAD+/FADH due to reduced NADH/$FADH_2$ oxidation (235,272,278). Consequently, both cytosolic and mitochondrial enzymes that rely on hydrogen carriers to function, including those in the TCA cycle, are impacted by perturbations in ETC function, which subsequently reduces oxygen consumption and energy production.

4.3 Animal Models of IUGR with Metabolic Dysfunction

Measuring whole-body, tissue, and cellular metabolism requires invasive experiments. As a result, animal models that recapitulate human IUGR are needed to study the link placental insufficiency and the metabolic phenotype IUGR fetuses. Similar to human IUGR, several animal models of IUGR have been developed that exhibit reductions in lean body mass, lower blood nutrient and/or oxygen concentrations, and develop metabolic syndromes later in life (129,141,149,349,350).

4.3.1 Rats. Three well-defined rat models of IUGR show fetal and persistent postnatal metabolic consequences in skeletal muscle and hepatic tissue due to reduced nutrient availability during gestation. Gestational maternal caloric restriction (CR), gestational maternal low protein (LP), and uterine artery ligation (UAL) at embryonic day 19 (E19), each cause significant (10-50%) reductions in lean mass which persist into adulthood (113,121,128,129,131–133). The persistent disparity in lean mass may serve as an IUGR trait that underscores metabolic defects in skeletal muscle and liver function leading to glucose intolerance, fatty liver disease, and altered amino acid metabolism in

juveniles with IUGR (115,129,136,140–144). In addition to low bodyweight, IUGR fetal rats possess defects in oxidative phosphorylation and nutrient signaling in both the skeletal muscle and liver (114,115,139,351,121,128,133–138). Therefore, although the exact mechanisms behind the development of metabolic dysfunction in IUGR rats are unclear, altered mitochondrial function acquired during fetal life is a likely a contributing cause to the development of metabolic aberrations later in life.

4.3.2 Sheep. Experimental models have been developed to induce IUGR in sheep by either reducing placental structure/function or preventing normal placental development. Models that reduce placental structure or function, such as carunclectomy or placental embolization, mimic placental insufficiency and yield fetuses with 15-66% growth restriction compared to matched controls (166–168). Models that inhibit placental development, such as maternal hyperthermia and over-nourished adolescent ewes, also produce IUGR of the fetus. Fetal weights in these sheep models of IUGR are reduced by 30-60% when measured at 0.9 gestation (169,171,172,352).

Factors that match closely with the gradual onset of IUGR found in human pregnancies are recapitulated in sheep models (190–192). Placental insufficiency-induced IUGR sheep fetuses have severe nutrient restriction in late gestation that results in hypoxemia, hypoglycemia, as well as reduced transport of amino acids (185–189). To ensure survival, the IUGR sheep fetus copes with lower nutrient and oxygen availability by slowing skeletal muscle growth and increasing hepatic glucose production rates (76,200,214). These *in-utero* adaptations lead to postnatal metabolic dysfunction where young lambs afflicted with IUGR continue to have lower lean masses and skeletal muscle protein contents, altered glucose metabolism and liver function, and greater adiposity

(106,201–204). Considering mitochondria are the primary site for oxidative metabolism, these adaptations imply IUGR fetuses have altered hepatic and skeletal muscle mitochondrial function.

4.3.3 Piglets. Natural runting of piglets (IUGR) arises from a disproportionate supply of nutrients along the uterine horn causing growth restriction of 15-20% of piglets from each litter (148). As a result of *in utero* nutrient restriction, runted piglets exhibit asymmetric growth restriction, increased liver:brain weight ratio, reduced bodyweight at birth, and metabolic perturbances which last into adulthood (149–152). Consistent with human IUGR pathophysiology, the lower lean mass present in IUGR piglets at birth is never fully rectified in adulthood (153,154). IUGR piglets at term also have a lower capacity for skeletal muscle protein accretion and protein synthesis (155,156). The impact of IUGR not only decreases liver and skeletal muscle growth, but also decreases the abundances of proteins involved in intermediate metabolism in the liver and energy production in the skeletal muscle (155). As adults, energy production, amino acid catabolism, and glucose metabolism remain dysregulated in both the liver and skeletal muscle (149,157).

Clues to metabolic adaptation of IUGR piglets may be found in studies using nutrient supplementations. Specifically, mid-gestation arginine/glutamine supplementation of pregnant gilts simultaneously increases litter size and reduces the number of IUGR piglets per litter (156). Alternatively, neonatal supplementation of amino acids to IUGR piglets results in hyperammonemia, elevated blood urea concentrations, and death (158). Moreover, during the first 21 days post-parturition, postnatal glucose injections increased IUGR piglet bodyweight compared to non-

supplemented IUGR piglets (159). Based on these observations, IUGR piglets may have predetermined fuel preferences that is programmed *in utero*. Thus, in IUGR piglets, the asymmetric growth restriction and metabolic dysfunction indicates defects in mitochondrial function that continue postnatally (160–165).

4.4 Mitochondrial Metabolism and Dysfunction in Animal Models of IUGR

The conservation and scavenging of oxygen and nutrients from expendable metabolic processes, such as systemic growth, is a necessary adaptation during IUGR to meet basal metabolic demands. Accordingly, because protein synthesis during the latter half of gestation accounts for ~18% of fetal oxidative metabolism, and protein synthesis is an ATP consuming process, slowing protein accretion may be a primary mechanism of conserving energy, oxygen, and nutrients in IUGR fetuses (194,195). On the other hand, IUGR fetuses have increased rates of hepatic glucose production, an ATP demanding process, that is activated to counteract hypoglycemia (221,351). These two observations show that differential metabolic adaptations are needed to IUGR fetal survival. Further, these pathways likely have tissue-specific regulation that depends on differential enzyme expression in skeletal muscle and liver. From this, a critical question arises: how are these metabolic processes regulated in skeletal muscle and the liver of IUGR fetus?

4.4.1 Skeletal Muscle.

In fetal sheep with IUGR, reductions in skeletal muscle oxidative phosphorylation result from chronic reductions in both the ETC activity and TCA cycle protein abundances (353). A modulator of electron transfer to the ETC is NADH dehydrogenase 1 alpha subcomplex, 4-like 2 (NDUFA4L2) (301,302). NDUFA4L2 is driven by hypoxia-inducible factor 1α (HIF1α), and it incorporates into

Complex I and lowers the electron flux through the ETC by functioning as an inhibitor of oxidative phosphorylation (Figure 14) (300–302,353). NDUFA4L2 expression is increased in skeletal muscle of IUGR sheep fetuses, likely due to chronically sustained HIF1α activity, thereby exerting a global impact on suppressing whole-body metabolism (240–242). First, the lower electron flux through the ETC and complex 1 will lower the production of reactive oxygen species (ROS), which will potentially protect against oxidative stress found in several pathologies, including IUGR, as a result of chronic hypoxia ((1), Figure 14) (302,354). Second, the lower electron flux through the ETC will reduce OCR, as evidenced by the lower Complex I activity and state 3 (Complex I-mediated) flux observed in the skeletal muscle mitochondria of IUGR sheep fetuses ((2), Figure 14) (353). Third, lower ETC electron flux and lower OCR will reduce $NADH/FADH_2$ regeneration thereby inhibiting TCA cycle enzymes that use NAD+ as a cofactor ((3), Figure 14). This is evidenced by lower abundances of key NAD+ consuming TCA cycle enzymes isocitrate dehydrogenase (IDH) and 2-oxo-glutarate dehydrogenase (OGDH) (Figure 14) (353). Fourth, and finally, concomitantly lowering $NADH/FADH_2$ production and oxidation may place the skeletal muscle in a lower steady state by limiting energy (ATP) production and ADP rephosphorylation, and may have significant consequences on global cellular metabolic rates ((4), Figure 14). The impact of NDUFA4L2 on whole-body metabolism is demonstrated in transgenic mice with NDUFA4L2 overexpression in skeletal muscle (302). NDUFA4L2 reduces skeletal muscle mass by ~20%, mirroring the slow muscle growth in IUGR fetuses (302). These adjustments to mitochondrial function lowers rates of ATP production in sync with other processes, such as lower Na+/K+ ATPase activity, and depresses protein synthesis and

accretion in IUGR skeletal muscle (355). While skeletal muscle in IUGR fetuses has lower ETC flux to match lower oxygen availability, this process is tied to ADP/ATP utilization, and the IUGR skeletal muscle may have lower ADP availability to match lower ATP utilization.

Alterations to energy homeostasis in the IUGR skeletal muscle are made more interesting in the context of substrate oxidation, which are associated with hypoxemia and subsequently greater NDUFA4L2 expression. Oxygen uptake relative to hindlimb mass is 29% lower in IUGR fetuses compared to control which is consistent with depressed metabolic rates based on oxygen consumption (76). The lower oxygen uptake rates in IUGR fetuses also implies lower substrate utilizations. Substrate utilization relative to the metabolic rate (substrate oxygen quotients) were comprehensively evaluated in IUGR fetal sheep (76). Here, substrate oxygen quotients were calculated by dividing the whole blood arterial–venous difference in substrate concentration by the arterial–venous difference in oxygen content, then multiplying by the number of oxygen molecules needed to oxidize one molecule of the nutrient (76,356). Despite similar glucose + lactate oxygen quotients across the hindlimb of the IUGR fetal sheep, the glucose uptake and lactate output per mole of oxygen consumed by the hind limb are greater (76). Interestingly, the hindlimb amino acid oxygen quotient is significantly reduced in IUGR fetal sheep (76). When the sum of these oxidizable substrates is calculated, they modestly exceed the oxygen consumption rate (nutrient to oxygen quotient is approximately 1), meaning the substrates are meeting the minimal energy requirement of the muscle, but are not contributing to tissue accretion (76). The results from the fetal sheep hindlimb reflect findings in the whole fetus where lower fetal uptake

of amino acids is the dominant factor limiting growth and is associated with hypoxemia (356). Although the hypoxic induction of NDUFA4L2 will lower oxygen consumption in the mitochondria, additional mechanisms are likely responsible for the reduction in amino acid uptake and oxidation (76,213,300,302,356). As a result, the skeletal muscle of IUGR fetuses is in a lower metabolic state that is fine-tuned towards maintenance rather than growth by matching oxygen availability to substrate utilization (76,77).

4.4.2 Liver. In the IUGR fetus, the liver also has lower rates of growth, modified protein synthesis rates, and a lower mitochondrial redox state coupled with lower concentrations of TCA cycle intermediates (104,114,155,357). Although IUGR sheep hepatocytes are postulated to have lower energy production, the abundances of the hepatic ETC and TCA cycle metabolites appear unaffected, although the expression profile of ETC enzyme abundances are presently unknown (Figure 15) (357). Moreover, the IUGR sheep liver has a lower abundance of IDH mRNA which may slow TCA cycle functionality upstream of α-ketoglutarate(357). These differences may reflect the dynamic role of the liver during placental restriction. Unlike muscle, the liver must maintain energy requirements for gluconeogenesis. However, achieving this metabolic goal presents a unique problem to the IUGR liver when trying to conserve nutrients and energy utilization. Specifically, energy production relies on constant revolutions of the TCA cycle to reduce cofactors, but the high rate of gluconeogenesis demands a high flux of oxaloacetate out of the TCA cycle as well as energy (ATP and NADH). To complicate the matter further, as oxaloacetate leaves the mitochondrial matrix, it must be replenished to retain the functionality of the TCA cycle. Pyruvate is both the primary source for energy production (via acetyl-CoA) and gluconeogenesis (via oxaloacetate), and

increased lactate flux from the skeletal muscle likely counterbalances pyruvate deficits in the IUGR liver (197,200). Even so, increased HGP likely requires additional TCA cycle intermediates for both the gluconeogenic substrates and the energy production requirements needed to sustain gluconeogenesis. This may include increased utilization and oxidation of amino acids to supply the carbon and energy substrates for gluconeogenesis, as demonstrated in studies with hypoglycemia-induced gluconeogenesis in the fetus (338). The lower IDH mRNA abundance in the IUGR liver may act to redirect pyruvate flux towards gluconeogenesis, but allow downstream substrates, like amino acids, to enter the TCA cycle. Thus, in the IUGR fetus the liver may have an increased reliance upon anaplerotic substrates compared to skeletal muscle.

4.5 Pyruvate: Differential Regulation of Pyruvate Oxidation in IUGR Tissues.

Glucose and lactate oxidation account for ~65% of oxygen consumption in the normally developing sheep fetus (218,358). However, glucose metabolism in the skeletal muscle and liver are distinctly regulated. In the fetus, the muscle is major consumer of glucose, in contrast to the liver which is small net consumer of glucose and is capable of producing glucose.

The IUGR fetus has tissue specific differences in insulin sensitivity for glucose metabolism(359). IUGR fetuses, studied under basal conditions, have normal or near normal rates of weight-specific, whole-body glucose utilization even with ~30% lower umbilical glucose uptake (53,196). This reflects the early activation of endogenous glucose production to meet the fetal demand for glucose utilization(200,360). Furthermore, at the whole-body level, IUGR fetuses have increased insulin sensitivity for

glucose utilization given the normal utilization of glucose at lower insulin levels and higher utilization rates at high insulin doses when tested under hyperinsulinemic-euglycemic conditions to measure insulin sensitivity(221,360). Lastly, the early activation of hepatic glucose production in IUGR fetuses is not suppressed by insulin, demonstrating the early development of liver-specific insulin resistance (104,196,206,216,221,361). Together, these studies demonstrate that tissues like skeletal muscle are insulin-sensitive for glucose utilization, while the liver has developed insulin resistance and produces glucose for the IUGR fetus.

The utilization of pyruvate, the oxidative product of glycolysis, has profound effects on energy status, redox state, and overall homeostasis. After glycolysis, pyruvate has two primary fates: entrance into the TCA cycle or conversion into lactate. For TCA cycle entry, pyruvate flux is regulated by pyruvate carboxylase (PC) and pyruvate dehydrogenase (PDH). PDH converts pyruvate to acetyl CoA, and PC is used for the anaplerotic “backfill” of oxaloacetate. Alternatively, lactate dehydrogenase (LDH) facilitates the interconversion of pyruvate and lactate, both of which can be excreted. The pyruvate flux into the mitochondrion is regulated by PDH, and PDH activity is inhibited its phosphorylation status via pyruvate dehydrogenase kinases (PDKs) and pyruvate dehydrogenase phosphatases (PDPs), which inactivate or activate PDH, respectively. In IUGR sheep fetuses, skeletal muscle and liver glycolytic capacity appears normal or increased (77,197,352). However, because the skeletal muscle and liver have different metabolic roles in normal fetuses and during IUGR, adaptations in enzymes that regulate pyruvate metabolism are expected to differ (Figures 14 and 15) (197,352,353).

4.5.1 Skeletal Muscle. Although the skeletal muscle of IUGR fetal sheep has 3-4 fold higher PDK4 mRNA expression than controls, it has normal PDK4 protein abundance and higher PDH activity (197,352,353). Conversely, the protein and mRNA expression of PC is lower in the IUGR sheep skeletal muscle (197,353). The lower PC expression and higher PDH activity in the skeletal muscle is conflicting as the lower expression of PC represents lower anaplerosis and the higher activity PDH pathway represents enhanced pyruvate oxidation. However, this response may indicate, in part, that the minimal needs of the muscle can be met with pyruvate conversion to acetyl CoA making the IUGR skeletal muscle less reliant upon anaplerotic reactions through PC. These data may explain the disassociation between glucose utilization and oxidation discussed above.

Alternatively, normal rates of pyruvate oxidation with greater PDH activity indicates deficiencies in pyruvate transport into the mitochondria of IUGR skeletal muscle. The abundance of mitochondrial pyruvate carrier 2 (MPC2) is lower in IUGR sheep skeletal muscle mitochondria (Figure 14) (353). Less MPC2 will restrict the transport of pyruvate into the mitochondria for PDH conversion. Due to the normal glycolytic capacity in IUGR sheep skeletal muscle, the inhibition of pyruvate flux into the mitochondrial matrix will lead to multiple metabolic outcomes (77). First, pyruvate will be converted to lactate prior to the TCA cycle, and this outcome is associated with greater intramuscular pyruvate concentrations and normal or increased plasma lactate concentrations in IUGR sheep fetuses (77). Second, by preventing pyruvate entry into the mitochondrial matrix, the matrix pyruvate concentrations will be lower, which will inhibit PDK4 activity, thereby leading to higher PDH activity, as evidenced by lower

phosphorylation of PDH in IUGR sheep skeletal muscle (352). Another fate for pyruvate may be conversion to alanine, consistent with increased Cahill cycling and is associated with higher plasma alanine concentrations in the human and sheep IUGR fetus (77,324). Cahill cycling will keep skeletal muscle pyruvate oxidation low while also providing gluconeogenic substrates to the liver (357).

4.5.2 Liver. In the fetal liver, under normal conditions, substrates are stored in the form of glycogen, used in protein synthesis, or used for energy production. Importantly, the fetal liver also normally has a high uptake of gluconeogenic substrates, yet it does not perform gluconeogenesis. The largest carbon sources for the fetal liver come from amino acids and lactate, with lesser contribution from glucose and a net output of pyruvate (338,362,363). However, under abnormal conditions, such as IUGR, increased gluconeogenesis is required to subsidize placental deficits in glucose supply to the fetus. While the carbon sources for increased gluconeogenesis are not known, if the IUGR fetus used pyruvate or lactate, this would necessitate an increased pyruvate to glucose conversion by modulating the abundances of enzymes that govern hepatic pyruvate metabolism to support gluconeogenic flux (Figure 15). In support of this, the IUGR sheep liver has increased PFK1 (Phosphofructokinase 1), PDK4, PC mRNA expression when compared to controls, along with increased gluconeogenic genes, Phosphoenolpyruvate carboxykinase 1 and 2 (PCK1 and PCK2) (197). Curiously, IUGR fetuses also have increased LDHA mRNA expression which is suspected to increase intrahepatic lactate production(197). Taken together, these data suggest that increased PDK4 inhibits PDH and, with increased PC, favors conversion of pyruvate to oxaloacetate. Oxaloacetate is shuttle to the cytosol where PCK1 catalyzes the rate limiting step in gluconeogenesis and

the resulting phosphoenolpyruvate (PEP) is used to synthesize glucose. Increased PCK2 also may catalyze the mitochondrial conversion of Oxaloacetate to PEP. Additionally, increased LDHA may be important to produce lactate and regenerate NAD+ to sustain increased glycolysis via predicted increased PFK1 activity and maintain redox balance. Overall, these adaptations would permit a shift in substrate metabolism and energy production to support glucose production.

4.5.3 Liver-Muscle Crosstalk. Evidence supports tissue-specific responses in liver and skeletal muscle metabolism and crosstalk between these organs. Insight into interdependent metabolic regulation is realized from experiments from genetically engineered mice utilizing a skeletal muscle knockout (skmKO) of the MPC1 gene. Here, utilizing a skmKO of MPC1 reduces pyruvate flux through the MPC complex because MPC1 and MPC2 are both necessary and sufficient for the functional MPC (323). Moreover, a knockout of MPC1 leading to a dysfunctional MPC, may result in an increased reliance upon pyruvate-alanine cycling for forward TCA cycle flux, rather than anaplerotic filling via PC, as well as adaptive glutaminolysis (364). The former parallels the enzyme profile and predictions for alanine production in IUGR skeletal muscle, whereas the latter pathway is not expected in IUGR muscle for reasons presented below (Figure 14) (364). Furthermore, this knockout model exhibits greater skeletal muscle lactate production, hepatic glucose production, and peripheral glucose disposal, all of which are found in the IUGR fetus (364). $MPC1^{skm-/-}$ mice also have greater skeletal muscle fatty acid oxidation which acts to supplement acetyl CoA and succinate; this adaptation is likely specific to adult—rather than fetal—physiology (364). Due to lower rates of fatty acid oxidation in fetal tissues, the same metabolic flexibility observed in

adult skeletal muscle is not likely to exist in IUGR fetuses. Nonetheless, the MPC1 mutation in skeletal muscle enhances Cori and Cahill Cycle activity and indicates an intricate level of metabolic regulation between the skeletal muscle and liver that may be representative of aspects found in IUGR metabolism.

4.6 Amino Acids: Divergent Metabolic Responses in Skeletal Muscle and Liver of the IUGR Fetus.

The metabolic potential of amino acids is fully realized through anaplerotic/cataplerotic reactions within the mitochondrion and support oxidative phosphorylation and gluconeogenesis. Within the mitochondrial matrix, all 20 standard, proteinogenic amino acids (except cysteine, alanine, and histidine) have metabolic pathways which enter the TCA cycle. Though cysteine, alanine, and histidine do not enter matrix, they can be converted into pyruvate, or other amino acids, which can then be degraded in the TCA cycle. In normally developing fetuses, amino acids are critical oxidative substrates and the accretion of amino acids into proteins is an essential component for fetal growth. Studies measuring amino acid metabolism and concentrations in IUGR fetuses remains conflicting. However, a common, overlapping feature between human IUGR and animal models of IUGR is reduced placental transfer of certain essential amino acids (104,365–368). Although amino acids are critical substrates, specific mitochondrial amino acid metabolism in skeletal muscle and liver of IUGR fetuses is largely unexplored. Furthermore, tissue-specific differences for amino acid utilization are expected in the IUGR fetus.

4.6.1 Skeletal Muscle. In skeletal muscle of IUGR sheep fetuses, substrate oxidation is modified through lower isocitrate dehydrogenase 3B (IDH3B), Succinate CoA ligase (SUCLA2), and OGDH abundance (Figure 14). Within the TCA cycle, IDH and OGDH act as rate limiting enzymes that regulate the rate the oxidation to meet the energy needs of the cell. Moreover, OGDH and SUCLA2 act as key anaplerotic gateways controlling much of the amino acid flux into the TCA cycle through the oxidation of α-ketoglutarate and Succinyl-CoA, respectively. Therefore, downregulating the abundances of all of these enzymes establishes a complex substrate regulating system: the oxidation of upstream TCA cycle intermediates, including acetyl CoA, is inhibited by low IDH and OGDH abundances, and the anaplerotic flux of amino acids into downstream TCA cycle intermediates is inhibited by low OGDH and SUCLA2 abundances. In addition to the lower IDH, OGDH, and SUCLA2 concentrations, abundances of enzymes involved in BCAA metabolism are lower, which will further reduce TCA cycle activity as BCAAs enter as acetyl CoA (Leucine and Isoleucine) or succinyl CoA (Isoleucine and Valine). Not only is TCA cycle activity depressed in IUGR fetal skeletal muscle, but it also appears to be less reliant upon amino acid substrates (76,77)

IUGR sheep fetal hindlimbs have lower net uptake rates of a variety of amino acids such as BCAAs, alanine, glycine, and glutamine (77). Coupled with the observation of lower abundances of mitochondrial enzymes associated with amino acid metabolism, amino acid oxidation is generally lower in IUGR skeletal muscle (76). In the muscle mitochondria of the IUGR sheep fetus, the first step of BCAA metabolism appears to be hindered by low expression of branched-chain aminotransferase 2 (BCAT2) (77,353)(Figure 16). Conversely, the expression of the negative regulator, Branched

Chain Keto Acid Dehydrogenase Kinase (BCKDK), is either lower or unchanged in both rat and sheep IUGR models (133,353). These observations are conflicting, but clues to why these adaptations are advantageous to the IUGR skeletal muscle may lie within nitrogen disposal (Figure 16). In IUGR sheep fetuses, the abundance of glutamate-pyruvate transaminase 2 (GPT2) is lower in skeletal muscle mitochondria, but the abundances of glutamate dehydrogenase (GDH), glutamate synthetase (GLS), and aspartate amino transferase (GOT2) are all unchanged (77,353). Together, these alterations to enzyme abundances may represent an adaption by IUGR skeletal muscle to increase nitrogen disposal and increase the efflux gluconeogenic amino acids to the liver as they are all linked through the use of α-ketoglutarate and glutamate (77). Unfortunately, on its own, this enzyme profile is insufficient to decipher substrate flux, which identifies critical gaps for future studies to elucidate the amino acids metabolism in IUGR skeletal muscle.

4.6.2 Liver. In normally growing fetuses, the hepatic uptake of essential and gluconeogenic amino acids is high (362,363). Though amino acids are necessary to fetal metabolism, studies in fetal lambs and neonatal piglets show lower amino acid degradation and lower mitochondrial activity in the IUGR liver (357,369). Further metabolomic studies of hepatic amino acid utilization in IUGR sheep fetuses shows higher concentrations of BCAAs and alanine, while aspartate concentrations are comparably lower (357). Interestingly, although amino acid degradation is lower in the IUGR liver, the lower amino acid degradation was primarily associated arginine, histidine, proline, and tryptophan metabolic pathways—these first three pathways converge exclusively at α-ketoglutarate and indicate lower anaplerotic flux through α-

ketoglutarate (Figure 17) (133). Furthermore, lower hepatic aspartate concentrations observed in the IUGR liver are indicative of adaptations intended to mitigate high nitrogen concentrations. Specifically, the IUGR skeletal muscle continually provides the liver with ammoniagenic amino acids such as glutamine and alanine as an adaptation to rid itself of ammoniagenic amino acids, but also provide energy substrates for gluconeogenesis (77).

As the liver uses ammoniagenic amino acids as energy substrates, they are deaminated, and ammonia is produced as a byproduct. Ammonia is toxic and is therefore typically excreted from the liver as innocuous urea. As a result, a common complication of being born IUGR is hyperammonaemia (370,371). This indicates that increased deamination of ammoniagenic amino acids may persist due to lower abundances of enzymes responsible for the preceding steps of hepatic urea production in the mitochondria (Figure 17) (370–373). This presents a difficult situation for the IUGR liver. The IUGR skeletal muscle excretes excess ammonia in the form of gluconeogenic amino acids. However, due to costs associated with high hepatic gluconeogenesis in the IUGR fetus, the liver must use those ammoniagenic amino acids, but it becomes inundated with ammonia. Therefore, additional mechanisms are needed to manage excess hepatic ammonia concentrations. One relevant pathway to manage nitrogen balance is the malate-aspartate shuttle, which is also a primary energy shuttle between the mitochondria and cytosol (Figure 15).

Gluconeogenesis relies on oxaloacetate as a substrate. However, the mitochondrial membrane is impermeable to oxaloacetate, and oxaloacetate must be converted to either malate or aspartate for transport (Figure 15). Although commonly

grouped together as the “malate-aspartate shuttle,” each component has a distinct function. The malate shuttle requires a reducing step to carry oxaloacetate and electrons in the form of malate. Alternatively, the aspartate shuttle relies on the availability of glutamate and α-ketoglutarate to carry oxaloacetate and nitrogen in the form of aspartate. These distinctions are important as the proportion of oxaloacetate carried by each of the shuttles additionally depends on the cytosolic redox state (NADH:NAD+ ratio) as well as the mitochondrial redox state. Moreover, the source of gluconeogenic fuels impacts which shuttle is used. If pyruvate is derived from lactate, the cytosolic NADH/NAD+ ratio will remain stable or increase, and the need for cytosolic reducing equivalents will be low, so oxaloacetate transport via the aspartate shuttle will predominate. Conversely, if pyruvate is derived from amino acids, no cytosolic reducing equivalents are produced. However, because gluconeogenesis requires glyceraldehyde-phosphate dehydrogenase, and this enzyme requires NADH, transport of oxaloacetate via the malate shuttle is necessary.

In IUGR sheep fetuses, the proportions of lactate and amino acids used for hepatic gluconeogenesis is unknown (104,206,357,359). Studies investigating liver bioenergetics in IUGR rat fetuses have found uncoupled cytosolic and mitochondrial redox states (113,114). Lower cytosolic, but higher mitochondrial, redox states suggest the malate shuttle is the preferred system used by IUGR mitochondria to produce cytosolic reducing equivalents and sustain gluconeogenesis. However, the aspartate shuttle may also be used to rid the IUGR hepatic mitochondria of excess ammonia (357). Additional investigations on mitochondrial metabolomics and proteomics are required to define adaptations in liver mitochondrial function.

4.7 Lipids: A Minor Role in Fetal Metabolism

Compared to other metabolites discussed lipid metabolism remains relatively unexplored in both normally grown and IUGR fetuses. During pregnancy, maternal triglyceride (TAG) and free fatty acids (FFAs) concentrations in the plasma range from 0.2-0.3 M for rats, sheep, and humans (374). Fetal plasma concentrations of FFAs are substantially lower than maternal concentrations: 0.16 M for rats, 0.04 M for sheep, and 0.1 M for humans (374). The concentration gradient might reflect low rates of placental transfer, although small FFAs are able to cross the human placenta (375). However, fetal uptakes of FFA represent <10% of the total daily umbilical carbon uptake in both sheep and human fetuses (332,376). Predictably, the FFA oxidation rate in the fetus is relatively low indicating FFA are incorporated into membranes or stored in the liver (377,378). Despite low lipid oxidation rates, based on the relative contribution to the fetal metabolic rate (oxygen consumption), a small contribution to energy production may potentially affect the IUGR fetal outcomes. Interestingly, hepatic lipid content in IUGR fetal sheep is similar to controls (357), yet some studies demonstrate increased hepatic lipid accumulation in SGA or preterm human neonates (340,341). Furthermore, the expression of lipid synthesis enzymes are lower in IUGR sheep fetuses suggesting that any lipids stored in the liver are exogenous and are supplied from the placenta(357). Conversely, maternal nutrient restriction in pregnant ewes leads to greater intramuscular triglyceride (IMTG) stores of the fetus (379). These observations imply that lipid oxidation, although already low in normal fetuses, is further reduced in IUGR fetuses. Moreover, the IUGR skeletal muscle and liver have different mechanisms to reduce lipid oxidation. In skeletal muscle, IUGR sheep fetuses have a lower abundance of Carnitine-acylcarnitine

translocase (CACT), which is responsible for the transport of carnitine and carnitine-fatty acid complexes across the inner mitochondrial membrane (Figure 14) (353). Lower CACT concentrations would promote acetyl CoA oxidation from pyruvate or amino acids rather than FFAs. Therefore, lipid oxidation is likely regulated in a tissue-specific manner in IUGR fetuses.

4.8 Conclusion

Animal models of IUGR provide valuable insight into the developmental origins of metabolic dysfunction. These models, while diverse in their etiology of IUGR, provide considerable evidence of irregularities in mitochondrial function. Skeletal muscle and liver serve as major metabolic tissues but exhibit distinct metabolic responses to fetal conditions causing IUGR. In skeletal muscle of the IUGR fetus, the adaptations culminate in the creation of a “thrifty phenotype” that is slow growing with a low-energy demand. Phenotypic changes in IUGR muscle indicate that rates of glucose utilization and oxidation disjointed and that the metabolic rate, measured with hindlimb oxygen consumption, is depressed. The greater utilization rates were hypothesized to promote anaerobic energy production via glycolysis(197). However as presented in this review, mitochondrial dysfunction is a primary site for metabolic dysregulation and programming. Specifically, in IUGR skeletal muscle there is evidence for reduced TCA and ETC activity. Evidence for lower TCA is founded on reduced abundances of several enzymes and MPC2, whereas the ETC inhibition of Complex 1 activity result from the induction of the hypoxic-induced NDUFA4L2 inhibition. In contrast, to meet the increased energy demands associated with hepatic glucose production, the IUGR liver must utilize gluconeogenic substrates, likely a combination of pyruvate and amino acids,

to provide the carbon substrates and energy co-factors to fuel gluconeogenesis. The mitochondrial metabolic adaptations of the skeletal muscle and liver are important in ensuring minimal energy requirements in the IUGR fetus. However, as global metabolic aberrations develop in the fetus, they promote persistent adaptations that are deleterious throughout the individual's life course.

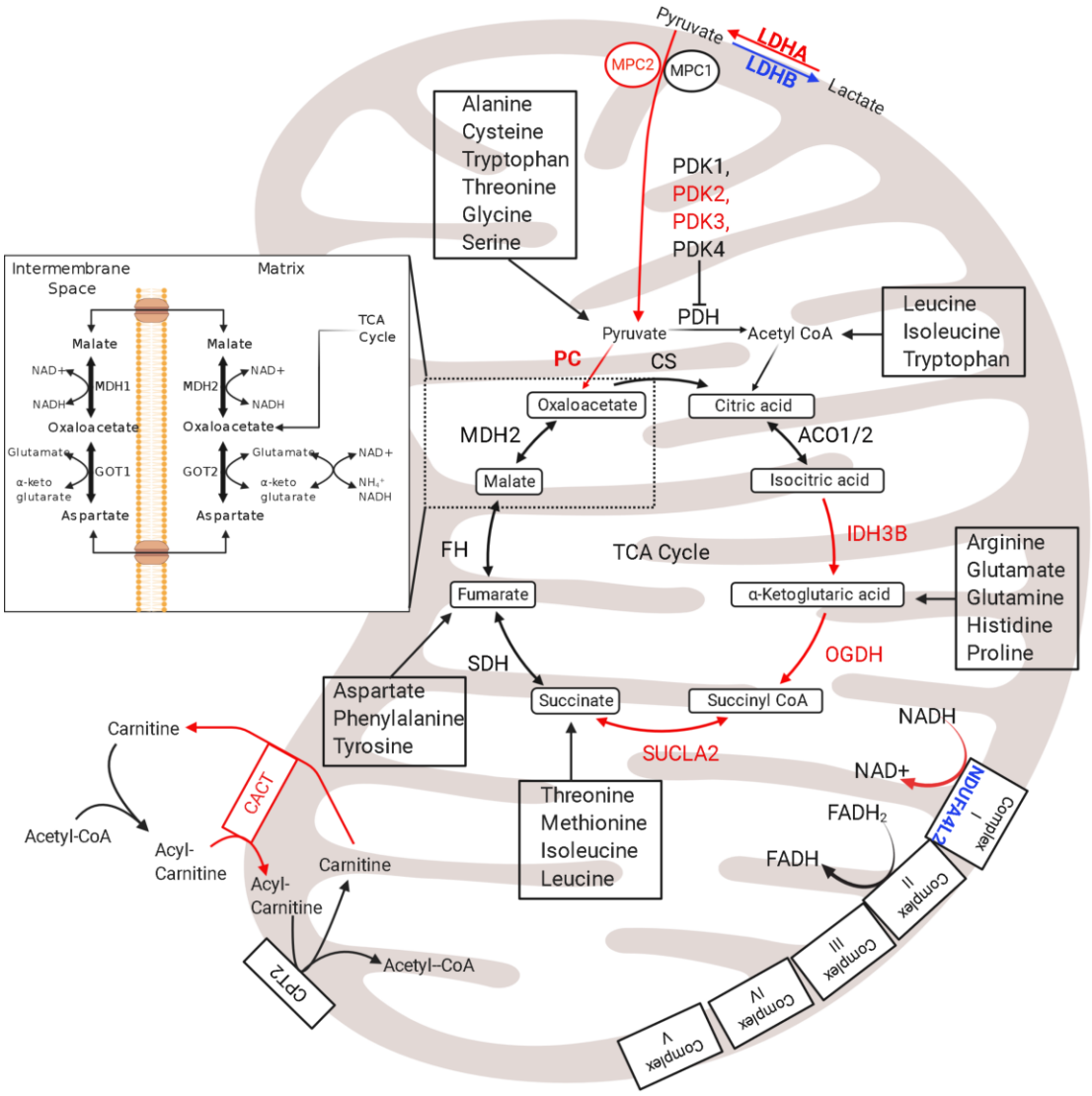

Figure 14. Enzymatic profile for skeletal muscle mitochondria in the IUGR fetus. The schematic outlines major mitochondrial enzymes and their processes in the tricarboxylic acid (TCA) cycle and in the electron transport chain (ETC). Lower abundances (red text) and greater abundances (blue text) for IUGR mitochondria are indicated, whereas enzymes that are not different from control mitochondria are in black text. Proposed decreased metabolic fluxes in IUGR mitochondria are shown with red (lower) and blue (higher). ACO1/2†, aconitate hydratase 1/2(353); CACT†, Carnitine-Acylcarnitine Carrier(353); CPT2†, carnitine palmitoyltransferase 1,2(353); CS†, citrate synthase(353); FH†, fumarate hydratase(353); GOT1, Glutamic-oxaloacetic transaminase 1; GOT2†, Glutamic-oxaloacetic transaminase 2(353); IDH†, Isocitrate Dehydrogenase(353); LDHA‡, lactate dehydrogenase A(353); LDHB†, lactate dehydrogenase B(353); MDH1, malate dehydrogenase 1(353); MDH2†, malate dehydrogenase 2(353); MPC2†, mitochondrial pyruvate carrier 2(353); NDUFA4L2†, NDUFA4 Mitochondrial Complex Associated Like 2(353); OGDH†, Oxoglutarate Dehydrogenase(353); PC#, pyruvate carboxylase(77,353); PDH†, pyruvate dehydrogenase(353); PDK1-4#, pyruvate dehydrogenase kinases 1-4(352,353); SDHA–D†, succinate dehydrogenase A–D(353); SUCLA2†, succinate-CoA ligase ADP-forming subunit β(353). †denotes protein data, ‡denotes mRNA data, #denotes protein and mRNA data. The image was created in BioRender.com.

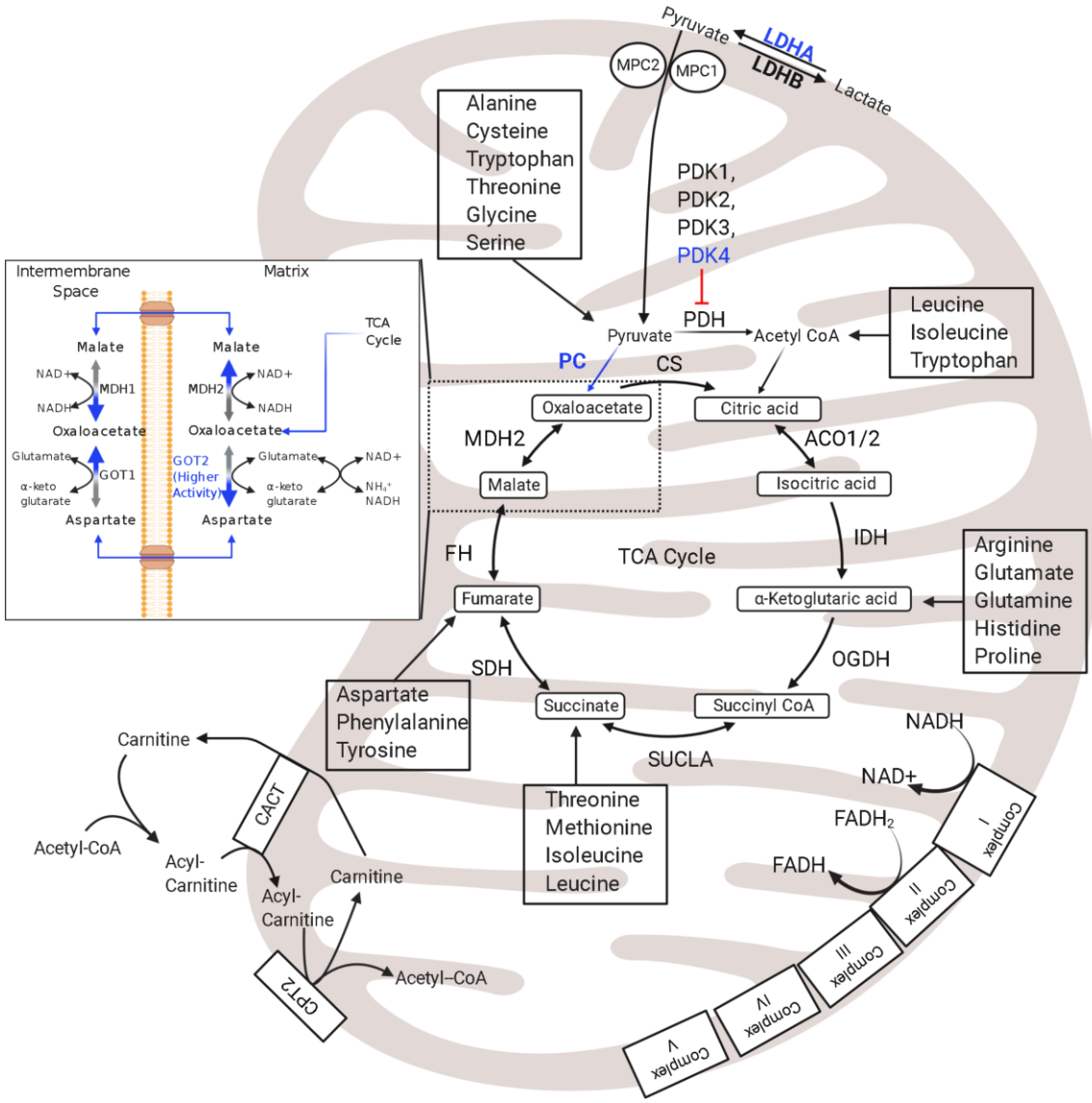

Figure 15. Enzymatic profile for liver mitochondria in the IUGR fetus. The schematic outlines major mitochondrial enzymes and their processes in the tricarboxylic acid (TCA) cycle and electron transport chain (ETC). Lower abundances (red text) and greater abundances (blue text) for IUGR mitochondria are indicated, whereas enzymes that are not different from control mitochondria are in black text(197,357,373). Proposed decreased metabolic fluxes in IUGR mitochondria are shown with red (lower) and blue (higher) arrows. ACO1/2, aconitate hydratase 1/2; CACT, Carnitine-Acylcarnitine Carrier; CPT2, carnitine palmitoyltransferase 1,2; CS, citrate synthase; FH, fumarate hydratase; GOT1, Glutamic-oxaloacetic transaminase 1; GOT2•, Glutamic-oxaloacetic transaminase 2 (373); IDH, Isocitrate Dehydrogenase; LDHA‡, lactate dehydrogenase A; LDHB, lactate dehydrogenase B; MDH1, malate dehydrogenase 1; MDH2, malate dehydrogenase 2; MPC2, mitochondrial pyruvate carrier 2; OGDH, Oxoglutarate Dehydrogenase; PC‡, pyruvate carboxylase(197); PDH‡, pyruvate dehydrogenase(197); PDK1-4‡, pyruvate dehydrogenase kinases 1-4 (197); SDHA–D, succinate dehydrogenase A–D; SUCLA2, succinate-CoA ligase ADP-forming subunit β. ‡denotes mRNA data, •denotes activity data. The image was created in BioRender.com.

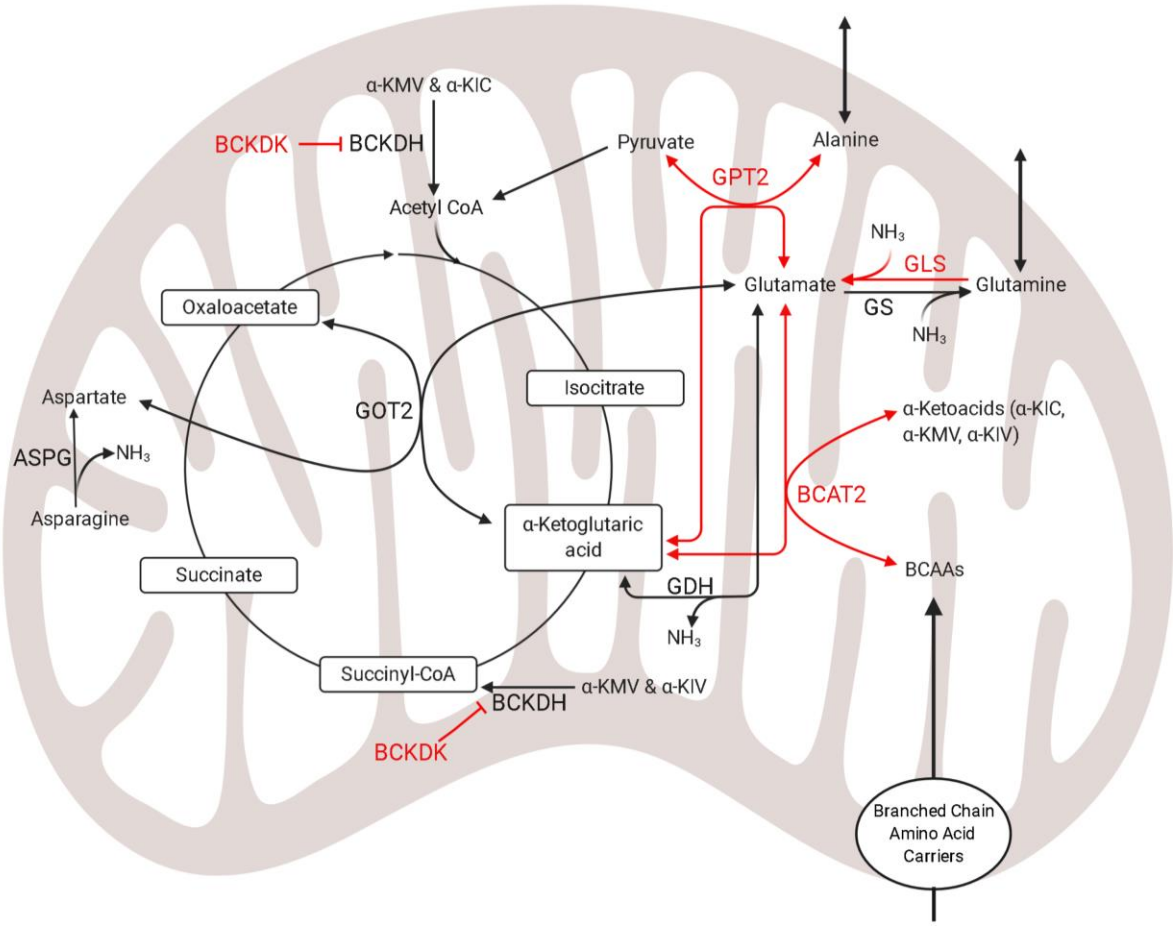

Figure 16. Amino acid and nitrogen-balance enzymes in IUGR skeletal muscle. The schematic outlines major mitochondrial enzymes and their processes in amino acid metabolism and nitrogen balance, created using BioRender.com. Lower abundances (red text) and greater abundances (blue text) are indicated for IUGR mitochondria compared to control mitochondria, whereas enzymes that are not different are in black text(77,157,353). Proposed decreased metabolic fluxes in IUGR mitochondria are shown with red (lower) and blue (higher) arrows. ASPG, Asparaginase; BCAT2[#], Branched Chain Amino Acid Transaminase 2(77,353); BCKDK[†], Branched Chain Keto Acid Dehydrogenase Kinase(353); GDH[†], Glutamate dehydrogenase(353); GLS[‡], Glutaminase(77); GOT2[†], Aspartate aminotransferase(353); GPT2[†], Alanine aminotransferase 2(353); GS[#], Glutamine Synthetase(77,353). [†]denotes protein data, [‡]denotes mRNA data, [#]denotes protein and mRNA data. The image was created in BioRender.com.

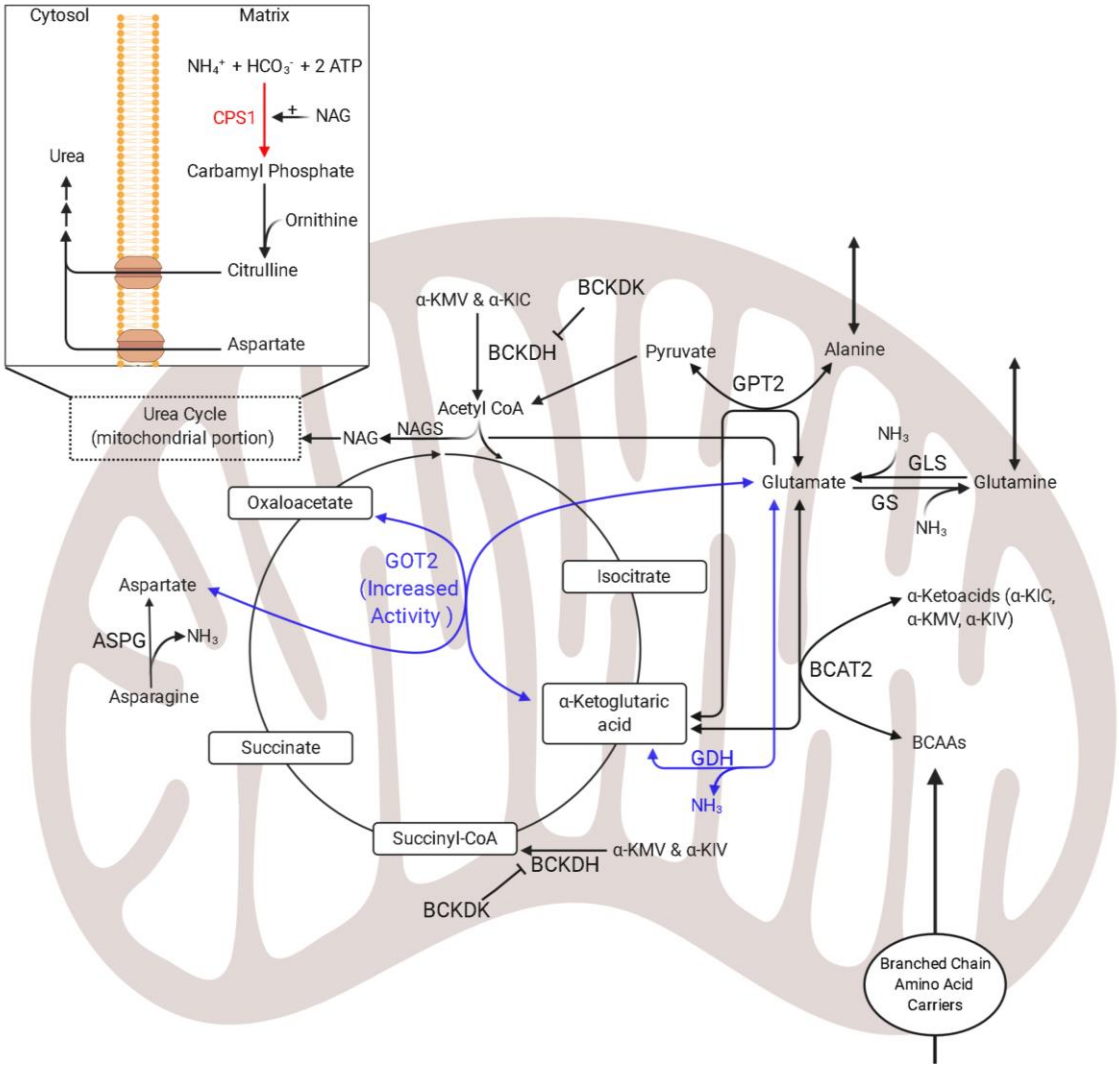

Figure 17. Amino acid and nitrogen-balance enzymes in IUGR liver. The schematic outlines major mitochondrial enzymes and their processes in amino acid metabolism and nitrogen balance, created using BioRender.com. Lower abundances (red text) and greater abundances (blue text) are indicated for IUGR mitochondria compared to control mitochondria, whereas enzymes that are not different are in black text(373). Proposed decreased metabolic fluxes in IUGR mitochondria are shown with red (lower) and blue (higher) arrows. ASPG, Asparaginase; BCAT2, Branched Chain Amino Acid Transaminase 2; BCKDK, Branched Chain Keto Acid Dehydrogenase Kinase; CPS1†, Carbamoyl-Phosphate Synthase 1(373); GDH†, Glutamate dehydrogenase(373); GLS, Glutaminase; GOT2†, Aspartate aminotransferase(373); GPT2, Alanine aminotransferase 2(353); GS, Glutamine Synthetase; NAGS, N-Acetylglutamate Synthase. †denotes protein data. The image was created in BioRender.com

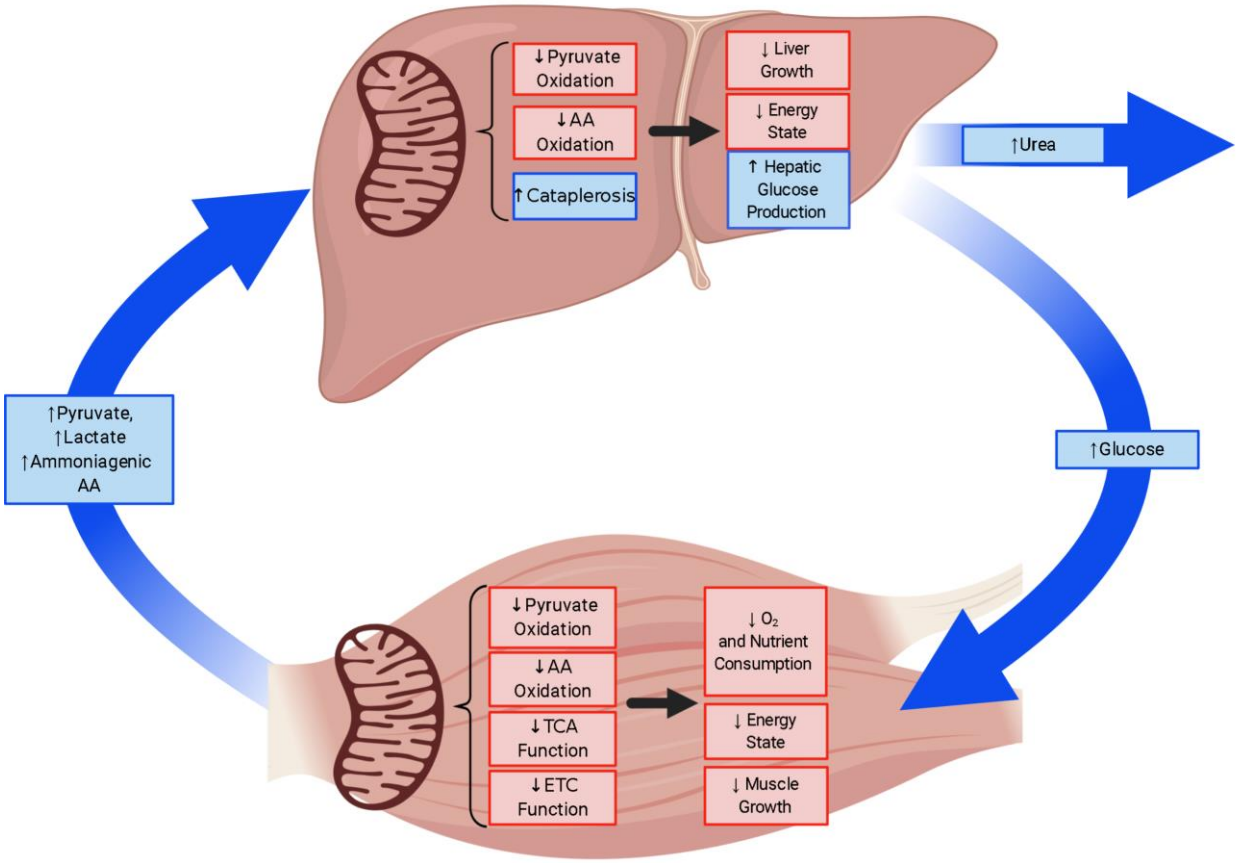

Figure 18. Skeletal muscle and liver metabolic interaction in IUGR fetuses. The schematic outlines the tissue metabolism outcomes due to mitochondrial adaptation in the skeletal muscle and liver of IUGR fetuses, created using BioRender.com. Lower responses (red) and greater responses (blue) are shown for IUGR mitochondria and whole tissue.

Chapter 5

Lower Oxygen Consumption Rate in Mitochondria Isolated from Satellite Cell-Derived Myotubes of Growth Restricted Lambs.

5.1 Introduction

Skeletal muscle accounts for ~40% of the body's mass and is a major determinant of energy expenditure (380–382). Individuals born small-for-gestational age (SGA) are at higher risk for sedentarism and low sports performance due to lower muscle mass compared to those born appropriate for gestational age (AGA) (383–389). Reduced skeletal muscle mass at birth persists and results in early exercise fatigue, decreased muscle strength, and impaired aerobic fitness (326,383,390–392). As a result, intrauterine growth restriction (IUGR) has been linked to the development of metabolic diseases later in life such as obesity, type 2 diabetes, and metabolic syndrome (393).

Placental insufficiency (PI), a common cause of IUGR, begins early in gestation and leads to a progressive reduction in the fetal nutrient supply by mid-gestation (394)(10,14,15). Low nutrient and oxygen availability in the fetus lowers metabolic requirements in peripheral tissues to ensure development of vital organs, and skeletal muscle growth is preferentially restricted (15,41,109,267). Fetal skeletal muscle adapts to placental restriction by lowing fractional glucose oxidation rates, fractional protein synthesis rates, and hind-limb oxygen consumption rates despite exhibiting greater insulin sensitivity for glucose uptake (76,196,360). Nutrient availability normalizes after birth, and PI-IUGR neonates typically experience compensatory catch-up growth; however, the body mass gain favors adipose deposition opposed to lean mass (110,342,349,395). Therefore, defects in skeletal muscle metabolism persist into postnatal life, which is evidenced by lower lean masses and fractional glucose oxidation rates IUGR lambs and lay the foundation for the onset of metabolic dysfunction later in life (102).

At the end of myogenesis (~110 days of gestation in sheep), the number of myofibers is established along with a complement of quiescent satellite (30,31,35). After this developmental milestone, skeletal muscle growth occurs by hypertrophy through the differentiation and fusion of satellite cells to myotubes (396). In adulthood, skeletal muscle is typically stable, and sporadic fusion of satellite cells compensates for muscle turnover caused by daily, sustained mechanical injury (30,31,35,51,397–399). Thus, satellite cells are critical to repair and the maintenance of lean mass in adulthood. In several animal models, nutrient restriction during mid to late-gestation lowers fetal myoblast proliferation, and reduced myofiber size at birth (214,400–402). Although the continued limitations in lean mass imply developmental programming of satellite cells, the effects of IUGR on this stem cell population are unknown.

When activated satellite cells proliferate, differentiate, and fuse with myocytes, differentiation also includes mitochondrial biogenesis, which is a prerequisites for myofiber growth (36,403)(403–407). In the IUGR fetus, metabolic abnormalities in skeletal muscle mitochondria lower mitochondrial oxygen consumption rate, inhibit Complex 1 activity, and reduce abundances of Mitochondrial Pyruvate Carrier 2 (MPC2) and key Tricarboxylic Acid Cycle enzymes (352,353) (76,77). Together, these adaptations concomitantly lower energy production (e.g. substrate oxidation) and specifically lower glucose oxidation in the IUGR fetus. In 1-month old IUGR lambs, the lower fractional glucose oxidation rates are coupled with normal skeletal muscle citrate synthase activity (102). This indicates that defects in mitochondria, specifically glucose oxidation, persist in IUGR offspring and are due to impaired oxidative phosphorylation. Moreover, the fusion of metabolically compromised satellite cells into existing muscle

fibers may explain the persistent onset of metabolic dysfunction observed in IUGR individuals.

We hypothesized that satellite cell-derived myotubes isolated from 1-month old IUGR lambs will resemble the bioenergetic profile of fetal skeletal muscle with lower TCA cycle enzyme abundances and lower ETC function. Our ovine model of hyperthermia-induced placental insufficiency and IUGR successfully recapitulates several aspects of human IUGR, including reduced skeletal muscle mass and impaired fractional glucose oxidation that persists postnatally. Oxygen consumption rates (OCRs) were measured on whole cell-derived myotubes and isolated myotube mitochondria from IUGR and control lambs. Finally, a proteomic-based approach was employed to identify differentially expressed proteins in mitochondria from IUGR myotubes.

5.2 Methods

5.2.1 Ethical Approval and Experimental Groups. Animal procedures were approved by the Institutional Animal Care and Use Committee at The University of Arizona and conducted at the Agricultural Research Center, which is accredited by the American Association for Accreditation of Laboratory Animal Care International. Pregnant Columbia–Rambouillet crossbred ewes were purchased from Nebeker Ranch (Lancaster, CA, USA), and those carrying singleton pregnancies were identified by ultrasonography prior to being assigned to an experimental group. Ewes were transported to the laboratory at 35 ± 2 days of gestation age (dGA) and were 2–4 years of age with unknown parity. Animal husbandry was managed as previously described (268). Ewes (45 ± 2 kg) were assigned by a simple randomization method to the thermoneutral control

group or the placental insufficiency-induced IUGR group. Lambs in the placental insufficiency-induced IUGR group (IUGR lambs; n = 14) were produced using the maternal hyperthermia model(268). Briefly, pregnant ewes were exposed to elevated ambient temperatures (40°C for 12 h; 35°C for 12 h; dew point 22°C) from 38 ± 1 to 87 ± 1 days of gestation. Following the environmental heat stress, ewes were maintained at 22 ± 1°C until parturition. Lambs born from the control group (n=15) were from ewes that were maintained at 22 ± 1°C and pair fed to the average ad libitum feed intake of the hyperthermic group. All sheep were given ad libitum access to water and salt.

After delivery, lambs were removed from the ewe to eliminate confounding maternal variability and raised in individual pens adjacent to each other. Lambs received colostrum before being placed solely on milk replacer (Milk Specialties, Dundee, IL) with ad libitum access. Birth weights were measured within 3 h of birth, usually before the lamb suckled. Growth rates, physiological parameters, and in vivo experiments evaluating glucose homeostasis in these lambs were reported previously as part of a larger cohort (268). Lambs used in this study were blocked by sex (3 male and 3 female in each group) and selected at random.

5.2.2 Satellite Cell Isolation. The semimembranosus muscle was removed, washed in cold PBS containing 1% antibiotic–antimycotic (AbAm; Gibco Life Technologies, Grand Island, NY, USA) and 0.5% gentamicin (Gibco), and then hand-minced. Satellite cells were liberated from minced muscle with Protease type XIV from *Strept. griseus* (1.25 mg ml^{-1}; Sigma-Aldrich, St Louis, MO, USA) as previously described (214). Satellite cells were cultured on fibronectin-coated tissue culture plates (10 mg ml^{-1}; Sigma-Aldrich) in growth media: DMEM (GlutaMAX, Gibco)

supplemented with 20% fetal bovine serum (FBS, Atlas Biologicals, Ft Collins, CO, USA), 1% AbAm, and 0.5% gentamicin. At 50% confluency, satellite cells were removed from plates with 0.25% trypsin (Gibco), centrifuged (1500 × *g*, 5 min), and frozen in growth media with 10% dimethyl sulfoxide (Sigma-Aldrich). Viability was determined in thawed myoblasts by Trypan Blue (0.4% solution; MP Biomedicals, Solon, OH, USA). Purity (>90%) was determined with Pax7 immunostaining (AbCam, Cambridge, MA, USA) as previously described(214).

5.2.3 Satellite Cell-Derived Myotubes. For all experiments, satellite cells were plated in tissue-culture treated 150mm plates at 250,000 cells per plate. Satellite cells were grown in McCoy's media, supplemented with 20% FBS, until 70% confluent. Media was then changed to low glucose DMEM supplemented with 2% horse serum (Sigma Aldrich, USA) and treated with 1µmol/l A83-01, a TGFβ inhibitor. After 24 hours of inhibitor treatment, media was changed with fresh low glucose DMEM supplemented with 2% horse serum. After 48 hours (a total of 72 hours after the addition of A83-01), myotubes were harvested for oxygen consumption rate (OCR) or mitochondrial isolation experiments.

5.2.4 Oxygen Consumption Rates in Myotubes. Myotubes were washed once with warm PBS (37°C) and dissociated from the plate using TrypLE (30°C). Cells were centrifuged at 1200g for 5 minutes. Pelleted myotubes were resuspended in media, counted with a hemocytometer, and washed a second time to adjust the media volume. Oxygen consumption rates were measured on $1x10^6$ cells in DMEM with 10% FBS using a Fluorescence Lifetime Micro Oxygen Monitoring System (Instech Laboratories, Inc., Plymouth Meeting, PA) that was maintained at 39.1°C).

Partial pressure of O_2 (Po_2) in each chamber was recorded over time with the NeoFox viewer software (Instech Laboratories, Inc.). Oxygen consumption rates (nanomole O_2 per minute) were determined from the slope of Po_2 disappearance over time for State 3_{DMEM} and State 3_{CCCP} and were calculated using the average of triplicate measurements for each condition. OCRs were recorded for 5 min in DMEM (State 3_{DMEM}) before the addition of CCCP (State 3_{CCCP}). The respiratory reserve capacity (RRC) was calculated as the percent change State 3_{DMEM} -to- State 3_{CCCP} OCRs.

5.2.5 Oxygen Consumption Rates in Mitochondria. Satellite cell-derived myotubes were washed once with PBS pre-warmed to 37°C and dissociated from the plate with TrypLE (30°C). Mitochondria were isolated by density gradient centrifugation, according to established protocols using "Isolation Buffer : Cell" (55). Isolation Buffer Cell consists of a final concentration of the following: 0.5 M sucrose, 10 mM Tris-MOPS, 1mM EGTA in distilled water and adjusted to pH 7.4.

Following isolation, mitochondria were incubated on ice in "Isolation Buffer : Cell" for 30 min before OCR measurements to ensure sufficient washout of respiratory substrates (55). For each OCR analysis, pelleted mitochondria were resuspended in 1:3 (v/v) Experimental Buffer that was prewarmed to 39.1°C. Experimental Buffer pH 7.4 contains 10 mM Tris/HCl, 5 mM MgCl2, 2 mM inorganic phosphate (Pi), 0.02 mM EGTA, and 250 mM sucrose. The resulting solution was divided evenly into three separate chambers of a Fluorescence Lifetime Micro Oxygen Monitoring System , which was prewarmed to 39.1°C, as previously described (56).

Mean OCRs (nanomole O2 per minute) were determined for State 3 and State 4, in triplicate for each animal. Maximum Complex I-linked respiration (State 3) was

measured in the presence of 5 mM glutamate, 5 mM malate, and 100 µM ADP. Before the addition of ADP (+glutamate/malate, −ADP; State $4_{Low\ ADP}$), OCRs were recorded for 5 min to ensure sufficient use/washout of respiratory substrates for each sample. To measure OCR in the absence of oxidative phosphorylation (State $4_{Oligomycin}$), an ATP synthase inhibitor, oligomycin A (5 µM final concentrations) was added after State 3 measurements. All OCRs at State $4_{Low\ ADP}$ were not different of their respective State $4_{Oligomycin}$ measurements.

Integrity of the mitochondria preparations of each sample was determined by the addition of 100 µM cytochrome c during State 3 OCR measurements and confirmed by less than a 15% increase in OCRs (Sigma). Following OCR analysis, the isolated mitochondria were collected from each chamber, and protein concentrations were measured with a Pierce Bicinchoninic Acid (BCA) Protein Assay Kit (Thermo Fisher) for OCR normalization to protein concentration.

5.2.6 In-solution Tryptic Digestion of Mitochondria. To determine changes in the mitochondrial proteome associated with IUGR, 50 µg of mitochondrial isolates were supplemented with dithiothreitol (DTT) at a final concentration of 5 mM and incubated at 56°C for 30 minutes. Samples were cooled to room temperature for 10 minutes and incubated with 15 mM acrylamide for 30 minutes at room temperature while protected from light. The samples were supplemented with additional DTT at a final concentration of 5 mM and incubated in the dark for 15 minutes to quench the alkylation reaction. Six volumes of pre-chilled 100% acetone were added to the samples and incubated for one hour at -20°C to precipitate proteins followed by centrifugation at 16,000 x g for 10 minutes at 4°C. 400 µL of pre-chilled 90% acetone was added to the protein pellet and

vortexed followed by centrifugation at 16,000 x g for 5 minutes at 4°C. The remaining acetone was removed, and the protein pellets were air dried for 2-3 minutes. The protein pellet was resuspended in 50 □L of Digestion Buffer (50 mM NH4HCO3, 1% sodium deoxycholate (SDC)) and sonicated for 5 minutes. One µg of Lys-C was added to each sample and incubated at 37°C for 2 hours while shaking at 300 rpm. Afterwards, 50 µL of 50mM ammonium bicarbonate and 2 µg of trypsin were added to each sample and incubated at 37°C overnight while shaking at 300 rpm. 14.7 µL of 40% Formic Acid (FA) /1% Heptaflourobutyrate (HFBA) was added to each sample and incubated for 10 minutes (final concentration is 4% FA/0.1% HFBA) to simultaneously stop trypsin digestion and cause precipitation of the SDC contained in the digestion buffer. The SDC was pelleted by centrifuging at 12,000 x g for 10 minutes and the peptide-containing solution was extracted. The samples were desalted with Pierce Peptide Desalting Spin Columns per the manufacturer's protocol (ThermoFisher Scientific, cat no. 89852) and the peptides were dried by vacuum centrifugation. The dried peptides were resuspended in 20 µL of 0.1% FA (v/v) and the peptide concentration was determined with the Pierce Quantitative Colorimetric Peptide Assay Kit per the manufacturer's protocol (ThermoFisher Scientific, cat no. 23275). 600 ng of the final sample was analyzed by mass spectrometry.

5.2.7 Mass Spectrometry and Data Processing. HPLC-ESI-MS/MS was performed in positive ion mode on a Thermo Scientific Orbitrap Fusion Lumos tribrid mass spectrometer fitted with an EASY-Spray Source (Thermo Scientific, San Jose, CA). NanoLC was performed using a Thermo Scientific UltiMate 3000 RSLCnano System with an EASY Spray C18 LC column (Thermo Scientific, 50cm x 75 µm inner diameter,

packed with PepMap RSLC C18 material, 2 µm, cat. # ES803); loading phase for 15 min at 0.300 µL/min; mobile phase, linear gradient of 1–34% Buffer B in 119 min at 0.220 µL /min, followed by a step to 95% Buffer B over 4 min at 0.220 µL /min, hold 5 min at 0.250 µ L/min, and then a step to 1% Buffer B over 5 min at 0.250 µL /min and a final hold for 10 min (total run 159 min); Buffer A = 0.1% FA/H_2O; Buffer B = 0.1% FA in 80% Acetonitrile. All solvents were liquid chromatography mass spectrometry grade. Spectra were acquired using XCalibur, version 2.3 (ThermoFisher Scientific).

5.2.8 Label-free Quantitative Proteomics. Progenesis QI for proteomics software (version 2.4, Nonlinear Dynamics Ltd., Newcastle upon Tyne, UK) was used to perform ion-intensity based label-free quantification similar to as previously described (288). In brief, in an automated format, .raw files were imported and converted into two-dimensional maps (y-axis = time, x-axis =m/z) followed by selection of a reference run for alignment purposes. An aggregate data set containing all peak information from all samples was created from the aligned runs, which was then further narrowed down by selecting only +2, +3, and +4 charged ions for further analysis. The samples were then grouped in Control versus IUGR. A peak list of fragment ion spectra was exported in Mascot generic file (.mgf) format and searched against the *Ovis aries* UniProt database (27,372 entries) using Mascot (Matrix Science, London, UK; version 2.6). The search variables that were used were: 10 ppm mass tolerance for precursor ion masses and 0.5 Da for product ion masses; digestion with trypsin; a maximum of two missed tryptic cleavages; variable modifications of oxidation of methionine and phosphorylation of serine, threonine, and tyrosine; 13C=1. The resulting Mascot .xml file was then imported into Progenesis, allowing for peptide/protein assignment, while peptides with a Mascot

Ion Score of <25 were not considered for further analysis. Precursor ion-abundance values for peptide ions were normalized to all proteins. For quantification, proteins must have possessed at least one or more unique, identifying peptide.

The subcellular localization database, COMPARTMENTS, was used to identify mitochondrial proteins using a confidence score of 3 or greater (289). Of those mitochondrial specific proteins, comparisons were made to identify differential expression (DE) between groups.

5.2.9 Statistical Analysis. Significant differences ($P < 0.05$) between groups (control and IUGR) for morphometric and OCR data were determined with an unpaired *t* test using general linear model procedures in JMP software (version 14.0.0; SAS Institute, Cary, NC) after testing for the homogeneity of variance. Normality and skewness were ensured using a D'Agostino-Pearson normality test. The variance between groups for each condition (e.g., morphometry, OCR, etc.) was similar between groups in all conditions. No sex differences were identified, and the effect was removed from each analysis.

5.3 Results

5.3.1 Lambs with IUGR Remains Smaller. At birth, IUGR lambs weighed 28% less than control lambs (Table 6). Age at necropsy was not different between the groups, but IUGR lambs remained 30% smaller than controls.

5.3.2 Lower Maximal OCR in IUGR Myotubes. Satellite cell-derived myotube respiration rates in State 3_{DMEM} were not different between groups (Figure 19). State 3_{CCCP} were lower in IUGR myotubes compared to controls (Figure 19). The reserve

respiratory capacity, State 3_{CCCP} respiration: State 3_{DMEM}, was 38% lower in IUGR myotubes compared to control myotubes (Figure 19).

5.3.3 Lower OCR in Mitochondria Isolated from IUGR Myotubes. In isolated mitochondria, State $3_{glutamate+malate}$ respiration rates were 44% lower in IUGR compared to controls (Figure 20). There was no difference for State $4_{Oligomycin}$ conditions between groups.

5.3.4 Proteomic Profiles Identify Mechanisms for Lower IUGR Myotube OCR. Within our 12 samples, proteomic analysis identified 4143 total, unique proteins. Of those, 1,033 proteins were identified as mitochondrial-specific proteins by a confidence of 3 or greater using COMPARTMENTS. Within the mitochondrial-specific proteins, including uncharacterized proteins, 15 proteins were differentially expressed between groups (Table 1). Nine proteins were down-regulated and five proteins were upregulated in IUGR mitochondria compared to control mitochondria.

Group (n)	Control (6)	IUGR (6)
Sex (M:F)	3:3	3:3
Birthweight (kg)	4.28 ± 0.28	3.23 ± 0.23*
Necropsy Age (days)	29±1	29±1
Necropsy Weight (kg)	12.5 ± 0.52	9.17 ± 0.78*
Hindlimb Weight at Necropsy (g)	0.94±0.19	0.83±0.06*
Semitendinosus Weight at Necropsy (g)	42.57 ± 3.7	25.00 ± 1.6*

Table 6: Morphometric data for IUGR and control lambs. Values are expressed as means ± SE. IUGR, intrauterine growth restriction $^{*}P < 0.01$.

Protein Name	Description	Fold Change Relative to Control	P-Value
PC	Pyruvate carboxylase	-1.36	0.00302
PARS2	Prolyl-tRNA synthetase 2, mitochondrial	-1.58	0.00995
HIBCH	3-hydroxyisobutyryl-CoA hydrolase, mitochondrial	-1.30	0.0105
SARDH	Sarcosine dehydrogenase	+1.67	0.0205
BCL2L2-PABPN1	BCL2L2-PABPN1 readthrough	-1.30	0.0251
SPTLC2	Serine palmitoyltransferase long chain base subunit 2	-1.30	0.0268
W5P4K5_SHEEP	Uncharacterized protein	+2.79	0.0275
W5PZ57_SHEEP	Uncharacterized protein	+1.52	0.0279
AARS2	Alanyl-tRNA synthetase 2, mitochondrial	-1.82	0.0294
NUDT2	Nudix hydrolase 2	+1.53	0.0296
GSTK1	Glutathione S-transferase kappa	-1.52	0.0312
CYB5B	Cytochrome b5 type B	-1.38	0.0378
MT-CO1	Cytochrome c oxidase subunit 1	-1.27	0.0430
NIT1	Nitrilase 1	+3.80	0.0459
W5Q285	Uncharacterized protein	+1.52	0.0477

Table 7: Proteomic analysis on isolated myotube mitochondria identifies 15 differentially expressed proteins between groups.

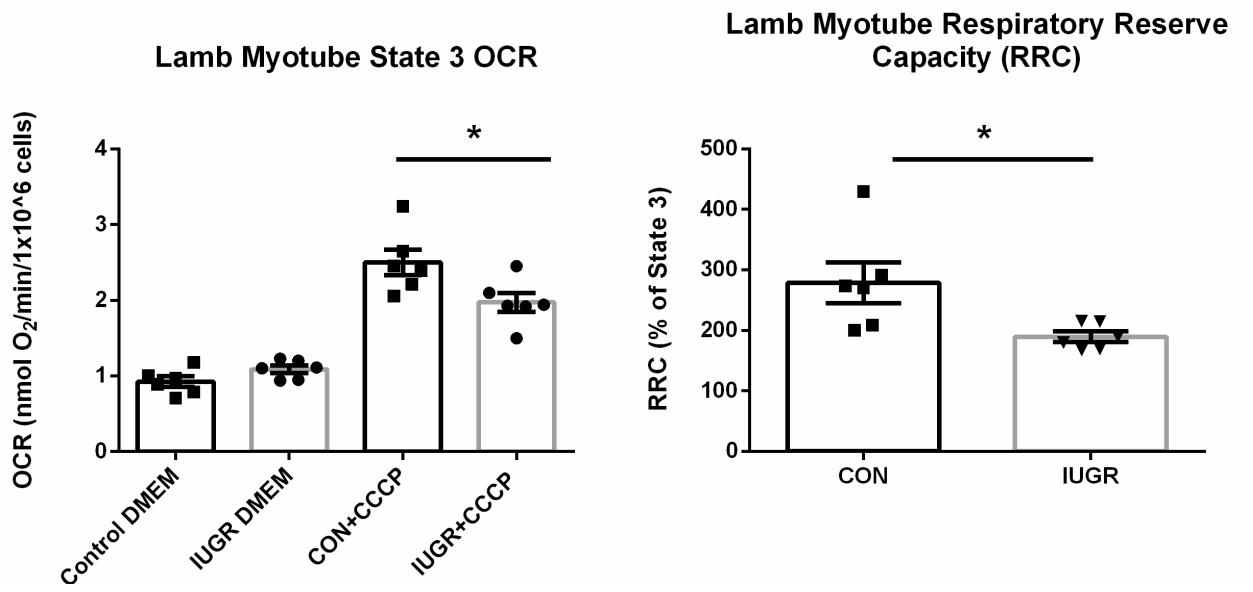

Figure 19. Lower maximal oxygen consumption rate (OCR) and respiratory reserve capacity (RRC) in IUGR myotubes. Oxygen consumption rates were measured in satellite cell-derived myotubes from control and IUGR lambs (n=6/group). A) State 3_{DMEM} OCR and uncoupled respiration (State 3_{CCCP}) rates were determined in DMEM media containing 10% FBS. B) The RRC was calculated by dividing State 3_{CCCP} by State 3_{DMEM}. Values for individual animals are presented for each condition. The data were analyzed using an unpaired t-test after testing for unequal variance, and the data are present as the mean ± SEM. Significant differences ($P<0.05$) between groups are indicated with *.

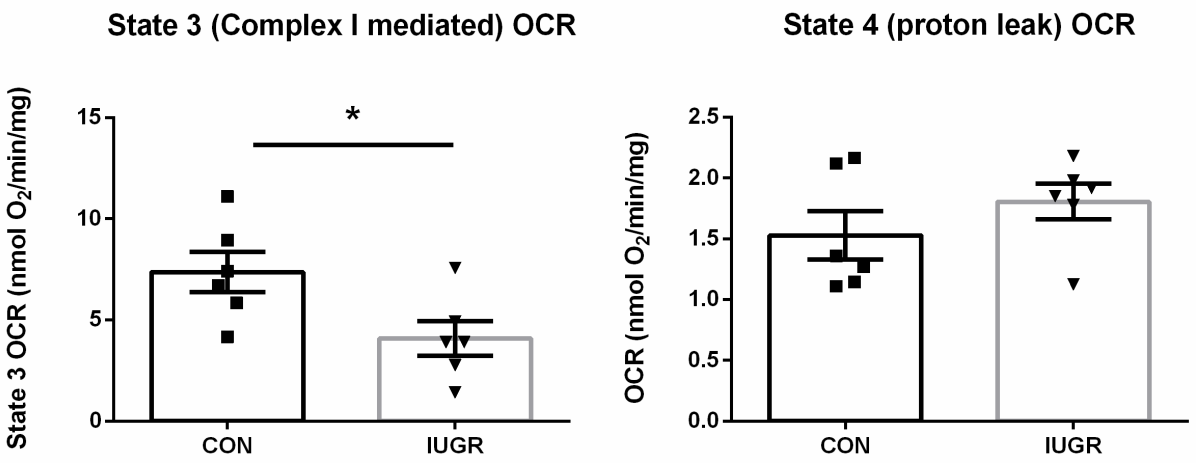

Figure 20. Lower oxygen consumption rate (OCR) in mitochondria isolated from IUGR myotubes. Mitochondria were isolated from satellite cell derived myotubes from control and IUGR lambs (n=6/group). A) OCR for mitochondria in State $3_{glutamate+malate}$ conditions that include 100 µmole/l ADP. B) OCR at State $4_{Oligomycin}$. Values for individual animals are presented for each condition. The data were analyzed using an unpaired t-test after testing for unequal variance, and the data are present as the mean ± SEM. Significant differences

5.4 Discussion

Prior reports have shown that skeletal muscle from IUGR lambs have defects in glucose oxidative metabolism that are associated with reduced muscle mass and mitochondrial dysfunction. Here, our experimental findings show that satellite cell-derived myotubes from IUGR lamb skeletal muscle have lower maximal respiration rates, and that mitochondria isolated from the IUGR myotubes have lower State $3_{glutamate+malate}$ OCR. IUGR mitochondria also have lower abundances of protein subunits comprising Complex III and Complex IV as well as lower abundances of Pyruvate Carboxylase (PC). Previous studies in fetal sheep show lower mitochondrial function in IUGR skeletal muscle due to lower Electron Transport Chain (ETC) function and lower Tricarboxylic Acid (TCA) Cycle abundances. These mitochondrial adaptations are directly associated with the placental restriction that lowers fetal oxygen and glucose concentrations. Notably, this experiment demonstrated that *in utero* complications to placental restriction permanently impair mitochondria performance by programming the satellite cells of IUGR lambs because satellite cells were isolated from 1-month old lambs and examined *in vitro* under identical culture conditions. The persistence of mitochondrial dysfunction in the skeletal muscle stem cells indicate that these cells were developmentally programmed. Moreover, skeletal muscle growth occurs through hypertrophy, which requires the differentiation and fusion of satellite cells to existing myofibers. Therefore, continued fusion of satellite cells with mitochondrial dysfunction into existing myofibers is expected to facilitate the progressive decline of metabolic function seen in individuals diagnosed with IUGR.

Under basal conditions, the mitochondrial bioenergetics produce ATP to meet the homeostatic energy demands of the cell. In adult skeletal muscle ~50% of the maximal respiratory capacity is used to maintain basal respiration (408,409). However, mitochondria possess the capacity to increase ATP synthesis under high energy demand, such as exercise, to meet the needs of the cell. This extended mitochondrial capacity is known as the RRC (410). Without the reserve respiratory capacity, basal mitochondrial ATP synthesis rates cannot respond to increases in ATP demand, ATP insufficiency ensues, and cellular function is compromised.

Mitochondrial metabolism is a dynamic process, and the range of the RRC is dependent upon multiple factors including ETC function and substrate oxidation. Briefly, the oxidation of NADH and $FADH_2$ produced through the oxidation of substrates, primarily in the tricarboxylic acid (TCA) cycle, produces a protonmotive force to synthesize ATP. To function efficiently, oxidative phosphorylation depends upon coupling between complexes to permit electron and proton flow. Because the ETC functions as a unit, inhibition of a single complex will lower the maximal activity or the RRC, but it will not necessarily a lower the basal respiration rate (411–414). This phenomenon explains the similar OCR in State 3_{DMEM}, but lower OCR in State 3_{CCCP}, observed in IUGR myotubes compared to control myotubes. Specifically, the lower abundance of subunits in Complex III (Cytochrome b5b, CYB5B) and Complex IV (MT-CO1) in IUGR mitochondria may be sufficient for basal rates of respiration but insufficient for maximal respiration rates. Isolated mitochondria from IUGR myotubes have lower State $3_{glutamate+malate}$ OCR compared to controls. Although this result is expected due to the lower abundances of Complexes III and IV subunits in IUGR

mitochondria, it conflicts with normal State 3_{DMEM} OCRs in intact myotubes from IUGR satellite cells. The normal State 3_{DMEM} OCRs in IUGR myotubes can result from higher non-mitochondrial oxygen consumption in IUGR myotubes (415–417). This prediction is supported by normal State 4 OCR (proton-leak) in isolated IUGR mitochondria. Alternatively, the discrepancy between normal State 3_{DMEM} OCR observed in IUGR myotubes and the lower State $3_{glutamate+malate}$ OCR observed in IUGR mitochondria may be explained by the ETC. Complex I, III and IV form a super complex which is responsible for the efficiency of the ETC(418). However, complex II is not involved in super complex formation, likely as a consequence of its substantial role in the TCA cycle (succinate dehydrogenase activity) (418). The lower State $3_{glutamate+malate}$ OCR in isolated IUGR myotube mitochondria can also represent reduced coupling between Complexes I and III/IV in the respiratory super complex in IUGR myotube mitochondria. Thus, the normal State 3_{DMEM} OCR in IUGR myotubes may be representative of an increased reliance upon Complex II mediated respiration to offset lower super complex coupling during basal respiration. However, maximal respiration rates cannot be maintained by Complex I or II mediated OCR due to lower Complex III and IV subunit abundances.

Upstream of the ETC, substrate oxidation can influence the range of RRC. The lower RRC in IUGR myotubes indicates that substrate oxidation is also unable to adequately supply the ETC with necessary NADH/FADH for maximal respiration. Glucose is a principle substrate for myotubes, and the oxidation of pyruvate, the metabolic end product of glycolysis, is critical for ATP synthesis. Pyruvate has one of two routes in the cytosol of muscle cells: oxidation in the mitochondria or conversion to lactate and transport into the blood. The conversion of pyruvate to lactate is energetically

less favorable, and typically occurs in the muscle under hypoxic conditions, but it can also occur if pyruvate oxidation is inhibited (236,419). Pyruvate is the primary oxidizable glycolytic substrate in the muscle, and pyruvate enters the mitochondrial matrix through the Mitochondrial Pyruvate Carrier (MPC). Within the mitochondrion, pyruvate is oxidized into acetyl-CoA by pyruvate dehydrogenase (PDH), and acetyl-CoA enters the TCA cycle. During energy stress conditions where additional ATP is needed, such as exercise, both glycolysis and mitochondrial pyruvate oxidation are enhanced, thereby allowing the cell to increase its ATP synthesis capacity. The inhibition of any step of pyruvate oxidation (glycolysis, pyruvate transport through the MPC, or PDH activity) can lower the reserve respiratory capacity (420–422). Alternatively, the oxidation of pyruvate in the mitochondrial matrix is dependent upon the condensation of acetyl-CoA to oxaloacetate. A sufficient supply of oxaloacetate is required for TCA cycle activity, which is regulated in part by the carboxylation of pyruvate from PC. The lower abundance of PC in IUGR mitochondria is predicted to be sufficient to supply the TCA cycle with oxaloacetate to maintain basal respiration, but limiting under energy stress conditions when greater anaplerotic backfill of oxaloacetate is required. Additionally, matched with lower abundances of subunits for Complex III and IV, the lower reserve respiratory capacity due to lower electron flux through the ETC begin to explain metabolic limitations in IUGR myotubes. Together, these results are likely causative of higher plasma lactate concentrations, and lower fractional glucose rates, in IUGR lambs where pyruvate oxidation is inhibited by low PC and low ETC abundance. Instead, pyruvate is shunted to lactate and excreted from the cells.

To date, no human study has investigated mitochondrial function of IUGR individuals from birth through adulthood. However, several studies with animal models of IUGR demonstrate that mitochondrial defects are induced during gestation and persists into neonatal life altering processes such as ETC enzyme abundances and substrate oxidation (351,423–426). In the present study, we show that satellite cell-derived myotubes from IUGR lambs have lower maximal respiration rates, as well as lower abundances of ETC subunits and PC. Moreover, isolated IUGR mitochondria have lower State $3_{glutamate+malate}$ OCR which indicates that there is lower ETC coupling. Because these myotubes are comprised of differentiated satellite cells that are derived from 1-month old lambs, these findings underscore the profound impact of fetal oxygen and nutrient restriction on mitochondrial function following the *in-utero* insult. The fusion of metabolically dysfunctional satellite cells due to fetal programming may be causative of, or continual to, early muscle fatigue and low athletic performance observed in SGA and IUGR individuals.

Chapter 6

Conclusions and Future Directions

IUGR is commonly caused by placental insufficiency, and is defined as a failure in fetal growth (189,427,428). Starting in mid-gestation, placental insufficiency results in progressive decline of oxygen and nutrient transfer from the maternal supply to the developing fetus (429). Unfortunately, the decline in nutrient availability to the fetus coincides with the phase of exponential fetal growth and high skeletal muscle protein accretion rates (185,430,431). Thus, fetal adaptations are needed to temper nutrient utilization to maintain the pregnancy (44,395). Skeletal muscle in IUGR fetuses is a potential site for mitigating whole-fetal nutrient usage at the expense of growth (77,213). In IUGR fetuses, this is accomplished, in part, by lowering substrate oxidation, and this is evidenced by lowering fractional glucose oxidation rates, amino acid oxygen quotients, and protein synthesis rates (76,196,197). Although nutrient and oxygen availability normalizes after birth, IUGR neonates still experience defects in lean mass, glucose homeostasis, and energy expenditure (43,141,201,349). As primary metabolic organelles, mitochondria are central to substrate oxidation. Therefore, understanding IUGR mitochondrial metabolism may give insight into the treatment of the metabolic pathophysiology of IUGR.

Glucose and amino acids serve as primary fuels for energy production in the fetus (53,432). Placental insufficiency lowers oxygen and glucose transfer between mother and fetus and results in lower fetal blood glucose and oxygen concentrations (366,433). Human studies and animal models measuring fetal amino acid concentrations are conflicting, but a consistent feature of both is the lower placental transfer of certain essential amino acids (366,368,433). Thus, fetal skeletal muscle must cope with lower nutrient and oxygen availability. To elucidate how IUGR impacts pyruvate flux into the

TCA cycle, as discussed in Chapter 2, pyruvate metabolism was investigated in the skeletal muscle of IUGR fetuses. Within the mitochondria, amino acids can also be oxidized to produce ATP. Because IUGR skeletal muscle is growth restricted, it is likely IUGR skeletal muscle mitochondria metabolism is adjusted to match lower energy needs. Therefore, in Chapter 3, we use proteomic approaches to define mitochondrial metabolic pathways and show defects in TCA enzyme abundances and ETC function. Skeletal muscle metabolism does not occur in a physiological vacuum; specifically, there is significant cross-talk with the liver for whole-body metabolic homeostasis. In Chapter 4, the differences and similarities between hepatic and skeletal muscle mitochondrial adaptations in IUGR fetuses in a variety of animal models of IUGR are presented. Finally, defects in metabolic homeostasis persists in IUGR individuals at birth, and adaptations made to low nutrient availability in utero lead to long-term metabolic consequences that increase the odds of developing type 2 diabetes and obesity(434,435). In Chapter 5, the persistence of mitochondrial metabolic adaptation in response to IUGR was investigated in satellite cells from1-month old lambs.

The findings from these studies are critical to defining metabolic aberrations in IUGR skeletal muscle. Specific mechanisms of mitochondrial dysfunction in fetal and lamb skeletal muscle tissue are discussed below.

6.1 Pyruvate Metabolism in IUGR fetuses. Defining the specific mechanism that lower glucose oxidation rates in IUGR fetuses can guide appropriate therapies to reduce metabolic maladaptations in IUGR fetuses and the long-term metabolic impact of being born IUGR. Previous studies have shown that IUGR fetuses have normal glucose

utilization rates, but lower fractional glucose oxidation rates, indicating glucose oxidation is deficient in the skeletal muscle (366,433).

Although PDH is likely not an inhibitory point for pyruvate oxidation in IUGR fetal skeletal muscle, lower pyruvate transport across the mitochondria can severely limit pyruvate oxidation. The majority of pyruvate transport into the mitochondrial matrix is believed to be performed by the oligomeric complex formed by MPC1 and MPC2, which are both mandatory components for mitochondrial transport (321,322,436). A key finding in Chapter 3 was lower MPC2 abundance in IUGR mitochondria compared to control. Defects in MPC2 abundance are associated with higher lactate production, lower pyruvate oxidation, and deficiencies in ETC function (437). Interestingly, the lower MPC 2 abundances in IUGR skeletal muscle are postulated to increase PDH activity as the concentration of pyruvate in the mitochondrial matrix is low due to inhibited pyruvate transport. Accordingly, involvement of additional regulatory mechanisms are expected to lower pyruvate oxidation in IUGR skeletal muscle, but pyruvate entry appears is a critical component.

Once inside the mitochondrial matrix, pyruvate can be metabolized into acetyl CoA or catalyzed into oxaloacetate via ATP-dependent carboxylation. The ATP-dependent carboxylation of pyruvate into oxaloacetate is performed by pyruvate carboxylase (PC), and the function of PC in non-gluconeogenic cells is to enhance pyruvate cycling through enhanced condensation of oxaloacetate and acetyl-CoA (58–60). Enhanced pyruvate cycling would lead to an increase in ATP production through oxidative phosphorylation. However, PC expression is lower in IUGR fetal skeletal muscle. Although deficiencies in PC result in lactic acidemia, due an inability to oxidize

pyruvate (reduced acetyl-CoA condensation), reduced PC abundance in IUGR skeletal muscle may be beneficial. If pyruvate transport into the mitochondrial matrix is reduced by lower MPC2 abundance, the lower PC abundance, combined with higher PDH activity, would preferentially shunt pyruvate into acetyl-CoA production. While oxaloacetate production is expected to be lower in IUGR skeletal muscle due to lower PC abundance, the lower PC abundance does not completely diminish oxaloacetate production; oxaloacetate production still occurs—albeit—at a lower rate. If pyruvate oxidation in IUGR skeletal muscle was lowered only through the inhibition of PDH alone, pyruvate flux driven through uninhibited PC would lead to a buildup of oxaloacetate and carbon efflux from the TCA cycle (in the form of malate) would ensue. This option is energetically inefficient as pyruvate would not be oxidized. Because IUGR skeletal muscle is slower growing, and has lower rates of protein synthesis, it is likely in a lower energy utilizing state(77). Therefore, the lower PC abundance in combination with lower MPC2 abundance will act to finely regulate pyruvate oxidation in proportion with energy needs. IUGR fetal skeletal muscle does this by:

1. Lowering pyruvate entry through MPC2, lowering the matrix pyruvate concentration
2. Preferentially shunting pyruvate to acetyl-CoA via lower PC abundance and higher PDH activity

This strategy is evidenced by similar glucose-oxygen quotients in IUGR skeletal muscle even though IUGR fetuses have lower hindlimb oxygen uptake (76).

Fetal skeletal muscle also oxidizes amino acids, in conjunction with pyruvate. Thus, alterations in mitochondrial ATP synthesis are needed to lower energy production from amino acids. These methods are discussed below.

6.2 Mitochondrial Function and Metabolism in IUGR Fetuses. IUGR fetuses develop in a low nutrient, low oxygen environment. Mitochondria are central to nutrient oxidation, and limiting mitochondrial bioenergetics is key to limiting energy production. A key finding in Chapter 3 is lower State 3 (Complex I mediated) OCR in IUGR mitochondria, but similar State 4 OCR between groups. The lower State 3 OCR represents an adaptation to low nutrient and low oxygen availability by limiting oxidative phosphorylation. While limiting energy production is necessary to match lower energy utilization rates, lower State 3 OCR also lowers ROS production.

Although not explicitly measured in this study, oxidative stress is confidently linked with IUGR likely as a result hypoxia (438–440). The definite source of fetal ROS production is unknown, but, within the mitochondria, complex I and III represent major sites of ROS production (441). ROS are involved in numerous pathologies including DNA damage and mutation, but also act as acute second messengers in a variety of homeostatic processes (442–444). Under acute hypoxic conditions, Complex I is deactivated, ROS is produced from Complex I, and ROS mediates downstream responses such as ion channel opening/closing (445,446). Alternatively, under chronic hypoxia, ROS production may be necessary to mediate long-term HIF1α activation(445,446). Despite upregulated HIF1α-mediated activity, IUGR fetuses have normal expression of HIF1α which may represent a hypoxia-driven “reprogramming” of the metabolic setpoint (242,244). NDUFA4L2, a HIF1α-mediated gene, has been shown to be protective against

ROS production(301,447). Thus, the increase in NDUFA4L2 in IUGR mitochondria may represent adaptation to attempt to lower ROS production and limit oxygen consumption by limiting Complex I activity. Downregulating ETC activity is a common strategy for mitigating the mismatch between normal ETC function and oxygen availability in hypoxic conditions (448,449). However, the lower OCR dictate lower substrate oxidation rates.

Fetal IUGR skeletal muscle mitochondria have lower abundances of IDH3B, OGDH, and SUCLA2. Both IDH and OGDH are rate limiting enzymes of the TCA cycle. Therefore, lowering the abundances of these key TCA cycle enzymes is necessary to reduce the production of reducing equivalents (and therefore OCR). Interestingly, OGDH also intersects with substrate oxidation and ROS production. Substrate oxidation by OGDH depends on 3 catalytic subunits to oxidize α-ketoglutarate and reduce NAD+. At the E1 subunit, α-ketoglutarate is oxidized and the electrons from α-ketoglutarate oxidation are eventually transferred to NAD+ at the E3 subunit. Additionally, the oxidation of α-ketoglutarate allows the E2 subunit to interact with CoA to produce Succinyl-CoA (450). The major electron transfer steps at E1 and E3 (α-ketoglutarate oxidation and NADH reduction) are naturally the ROS generating sites of OGDH due to incomplete electron transfer from the OGDH complex (leak) (450–452). However, the E2 subunit is sensitive to changes in ROS concentration, and its activity is lowered in response to increased ROS (450,451). Thus, similar to the increased abundance of NDUFA4L2 in IUGR mitochondria, lower OGDH may serve two purposes in response to nutrient restriction: to lower substrate oxidation and to lower ROS production.

Besides being critical components of the TCA cycle, OGDH and SUCLA2 also serve as the integration points for amino acid metabolism into the TCA cycle. The downregulation of these enzymes in IUGR skeletal muscle mitochondria, with other amino acid metabolism enzymes such as BCAT2, represents a lower reliance upon amino acids as oxidative fuels. This is evidenced by lower amino acid uptakes and lower amino acid oxygen quotients in the hindlimb of IUGR sheep fetuses (76,77). Interestingly, a chronic infusion of a mixed amino acid cocktail into IUGR sheep fetuses increases whole-body leucine oxidation rates, but does not impact fetal protein accretion rates (453). Amino acid oxidation in the mitochondrial matrix requires transporters on the mitochondrial membrane(s), and proteomic analysis indicates the abundances of amino acid transporters are not different between groups (454). Although functional capacity of these transporters was not investigated, it is likely that amino acid transport is unhindered in IUGR skeletal muscle mitochondria. Moreover, lower ETC and TCA cycle abundances in IUGR skeletal muscle mitochondria may be the root causes of lower amino acid oxidation rates in IUGR fetuses. On a deeper level, this is consistent with the concept that fetal growth is dictated by its oxygen, nutrient, and growth factor supply.

In IUGR fetuses, growth is limited by low oxygen and nutrient availability. Therefore, boosting carbon substrate availability, such as a chronic amino acid infusion, without increasing oxygen availability is futile because oxygen supply remains limited. Future directions should focus on IUGR treatments which boost the fetal supply nutrients *and* oxygen. Importantly, the findings in chapter 2 and chapter 3, such as ETC function or enzyme abundances, can be used as markers for successful treatments in ameliorating IUGR pathophysiology.

6.3 Skeletal Muscle Mitochondrial Function and Metabolism in IUGR neonates. Conditions affecting fetal development, such as nutrient or oxygen rarefaction, have been proposed to induce long-term impacts to health and overall metabolic homeostasis (435,455). Skeletal muscle is a major metabolic organ, and an adequate complement of skeletal muscle is needed in adulthood for physical function (locomotion) and energy balance (metabolic rate and nutrient disposal). However, IUGR fetuses are born with lower skeletal muscle masses (44,214,359). This adaptive growth restriction response by the skeletal muscle occurs during secondary myogenesis—a period where skeletal muscle mass is established through myoblast replication and fusion—which establishes myofiber number by the time of birth (33,456). Secondary myogenesis also establishes a complement of quiescent satellite cells within the myofiber network which are activated in postnatal life to grow skeletal muscle (33).

Proteomic results in Chapter 5 shows that mitochondria isolated from satellite cell-derived myotubes have lower abundances of enzymes involved in the ETC and pyruvate metabolism in IUGR lambs. Moreover, mitochondria isolated from IUGR lamb myotubes have lower State 3 (complex-I mediated) OCR. Both of these results mirror metabolic changes seen in IUGR fetal skeletal muscle mitochondria. However, there are two different adaptative responses that are responsible for lower State 3 OCR in the isolated mitochondria from lamb myotubes vs fetal skeletal muscle. In IUGR lamb myotube mitochondria, lower State 3 OCR is associated with lower abundances of subunits in Complex III and Complex IV. In IUGR fetal skeletal muscle mitochondria, higher NDUFA4L2 expression is associated with lower Complex I activity and a lower State 3 OCR. Curiously, at both ages, lower State 3 OCR also accompanies lower

abundances of enzymes associated with substrate oxidation. However, age-dependent differences are responsible for the potential reduction of nutrient oxidation. In IUGR lamb myotubes (AIM 3), TCA cycle rate is postulated to be lower due to lower PC abundance. Contrastingly, in IUGR fetal skeletal muscle (AIM 2), not only is PC abundance lower, but so are the abundances of metabolic enzymes in amino acid oxidation and the TCA cycle.

Lamb satellite cells experience the postnatal environment, including "normalized" nutrient and oxygen concentrations, and this may positively impact the abundances of key nutrient oxidizing enzymes. On the other hand, IUGR fetal skeletal muscle is developing under conditions of low nutrient availability. Therefore, comparing the mitochondria from pluripotent satellite cells in IUGR lambs to the mitochondria in "mature" IUGR fetal skeletal muscle may not be a fair "feature-for-feature" comparison. Instead, it is likely that fetal myoblasts isolated from IUGR fetuses more closely resemble IUGR skeletal muscle than lamb myoblasts. However, lamb satellite cells still retain similar defects associated with IUGR fetal skeletal muscle mitochondria. Because satellite cells contribute to the maintenance of adult muscle through activation and fusion events over the life course, this likely contributes to the progressive onset of adult metabolic disease associated with IUGR.

6.4 Summary. These studies define metabolic adaptation of skeletal muscle mitochondria in IUGR fetuses, and outline how these maladaptations persist into postnatal life. Mitochondrial adaptation is crucial for IUGR fetal adaptation to low nutrient and oxygen conditions because these organelles are central to energy production. Because nutrient/oxygen transfer is lowered in IUGR pregnancies, fetal skeletal muscle

mitochondria adaptations involve lowering substrate oxidation and energy production by lowering pyruvate entry, TCA cycle enzyme abundances, and ETC function. Moreover, these mechanisms may act supplementary to, or upstream of, skeletal muscle growth restriction. Lowering skeletal muscle growth and metabolic capacity in the IUGR fetus spares oxygen and nutrients for other vital tissues such as the brain and ensures that these vital organs are developed for life post parturition. However, metabolic adaptations acquired *in utero* may have lasting effects as defects in skeletal muscle mitochondria bioenergetics persist into postnatal life. Understanding these defects may be key in the development of treatments to treating fetal and postnatal consequences of IUGR.

References

1. Hughes MM, Black RE, Katz J. 2500-g Low Birth Weight Cutoff: History and Implications for Future Research and Policy. *Matern Child Health J* (2017) doi:10.1007/s10995-016-2131-9
2. Blencowe H, Krasevec J, de Onis M, Black RE, An X, Stevens GA, Borghi E, Hayashi C, Estevez D, Cegolon L, et al. National, regional, and worldwide estimates of low birthweight in 2015, with trends from 2000: a systematic analysis. *Lancet Glob Heal* (2019) doi:10.1016/S2214-109X(18)30565-5
3. Valdez R, Athens MA, Thompson GH, Bradshaw BS, Stern MP. Birthweight and adult health outcomes in a biethnic population in the USA. *Diabetologia* (1994) doi:10.1007/BF00403383
4. Barker DJP, Osmond C, Simmonds SJ, Wield GA. The relation of small head circumference and thinness at birth to death from cardiovascular disease in adult life. *Br Med J* (1993) doi:10.1136/bmj.306.6875.422
5. Hales CN, Barker DJP, Clark PMS, Cox LJ, Fall C, Osmond C, Winter PD. Fetal and infant growth and impaired glucose tolerance at age 64. *Br Med J* (1991) 303:1019–1022. doi:10.1136/bmj.303.6815.1474-b
6. Godfrey KM, Barker DJP. Fetal nutrition and adult disease. in *American Journal of Clinical Nutrition* doi:10.1111/j.1365-277x.2005.00612.x
7. Wollmann HA. Intrauterine growth restriction: Definition and etiology. *Horm Res* (1998) doi:10.1159/000053079
8. Cetin I, Mandò C, Calabrese S. Maternal predictors of intrauterine growth restriction. *Curr Opin Clin Nutr Metab Care* (2013)

doi:10.1097/MCO.0b013e32835e8d9c

9. De Onis M, Blössner M, Villar J. Levels and patterns of intrauterine growth retardation in developing countries. in *European Journal of Clinical Nutrition*

10. Tchirikov M, Rybakowski C, Huneke B, Schroder HJ. Blood flow through the ductus venosus in singleton and multifetal pregnancies and in fetuses with intrauterine growth retardation. *Am J Obstet Gynecol* (1998) doi:10.1016/S0002-9378(98)70528-9

11. Gluckman PD, Breier BH, Oliver M, Harding J, Bassett N. Fetal growth in late gestation - A constrained pattern of growth. in *Acta Paediatrica Scandinavica, Supplement* doi:10.1111/j.1651-2227.1990.tb11644.x

12. Platz E, Newman R. Diagnosis of IUGR: Traditional Biometry. *Semin Perinatol* (2008) doi:10.1053/j.semperi.2008.02.002

13. Molteni RA, Stys SJ, Battaglia FC. Relationship of fetal and placental weight in human beings: Fetal/placental weight ratios at various gestational ages and birth weight distributions. *J Reprod Med Obstet Gynecol* (1978)

14. Larciprete G, Valensise H, Di Pierro G, Vasapollo B, Casalino B, Arduini D, Jarvis S, Cirese E. Intrauterine growth restriction and fetal body composition. *Ultrasound Obstet Gynecol* (2005) 26:258–262. doi:10.1002/uog.1980

15. Beltrand J, Verkauskiene R, Nicolescu R, Sibony O, Gaucherand P, Chevenne D, Claris O, Lévy-Marchal C. Adaptive changes in neonatal hormonal and metabolic profiles induced by fetal growth restriction. *J Clin Endocrinol Metab* (2008) 93:4027–4032. doi:10.1210/jc.2008-0562

16. Rivas DA, Fielding RA. “Skeletal Muscle,” in *Encyclopedia of Human Nutrition*

doi:10.1016/B978-0-12-375083-9.00188-4

17. Janssen I, Heymsfield SB, Wang ZM, Ross R. Skeletal muscle mass and distribution in 468 men and women aged 18-88 yr. *J Appl Physiol* (2000) doi:10.1152/jappl.2000.89.1.81

18. Cortright RN, Muoio DM, Dohm GL. Skeletal muscle lipid metabolism: A frontier for new insights into fuel homeostasis. *J Nutr Biochem* (1997) doi:10.1016/S0955-2863(97)89660-X

19. Malherbe C, de Gasparo M, de Hertogh R, Hoem JJ. Circadian variations of blood sugar and plasma insulin levels in man. *Diabetologia* (1969) doi:10.1007/BF00427978

20. Bröer S, Bröer A. Amino acid homeostasis and signalling in mammalian cells and organisms. *Biochem J* (2017) doi:10.1042/BCJ20160822

21. DeFronzo RA, Ferrannini E, Sato Y, Felig P, Wahren J. Synergistic interaction between exercise and insulin on peripheral glucose uptake. *J Clin Invest* (1981) doi:10.1172/JCI110399

22. Baron AD, Brechtel G, Wallace P, Edelman S V. Rates and tissue sites of non-insulin- and insulin-mediated glucose uptake in humans. *Am J Physiol Metab* (1988) 255:E769–E774. doi:10.1152/ajpendo.1988.255.6.E769

23. Groen BBL, Horstman AM, Hamer HM, De Haan M, Van Kranenburg J, Bierau J, Poeze M, Wodzig WKWH, Rasmussen BB, Van Loon LJC. Post-prandial protein handling: You are what you just ate. *PLoS One* (2015) doi:10.1371/journal.pone.0141582

24. Ravikumar B, Carey PE, Snaar JEM, Deelchand DK, Cook DB, Neely RDG,

English PT, Firbank MJ, Morris PG, Taylor R. Real-time assessment of postprandial fat storage in liver and skeletal muscle in health and type 2 diabetes. *Am J Physiol - Endocrinol Metab* (2005) doi:10.1152/ajpendo.00557.2004

25. Berg J, Tymoczko J, Stryer L. *Biochemistry, 5th edition*. (2002).
26. Mifflin MD, St Jeor ST, Hill LA, Scott BJ, Daugherty SA, Koh YO. A new predictive equation for resting energy expenditure in healthy individuals. *Am J Clin Nutr* (1990) doi:10.1093/ajcn/51.2.241
27. Wolfe RR. The underappreciated role of muscle in health and disease. *Am J Clin Nutr* (2006) 84:475–482. doi:10.1093/ajcn/84.3.475
28. Hong S, Chang Y, Jung HS, Yun KE, Shin H, Ryu S. Relative muscle mass and the risk of incident type 2 diabetes: A cohort study. *PLoS One* (2017) doi:10.1371/journal.pone.0188650
29. Delezie J, Handschin C. Endocrine crosstalk between Skeletal muscle and the brain. *Front Neurol* (2018) doi:10.3389/fneur.2018.00698
30. Wigmore PM, Stickland NC. Muscle development in large and small pig fetuses. *J Anat* (1983)
31. Rowe RW, Goldspink G. Muscle fibre growth in five different muscles in both sexes of mice. *J Anat* (1969)
32. Tajbakhsh S, Cossu G. Establishing myogenic identity during somitogenesis. *Curr Opin Genet Dev* (1997) doi:10.1016/S0959-437X(97)80011-1
33. Draeger A, Weeds AG, Fitzsimons RB. Primary, secondary and tertiary myotubes in developing skeletal muscle: A new approach to the analysis of human myogenesis. *J Neurol Sci* (1987) 81:19–43. doi:10.1016/0022-510X(87)90181-X

34. Ecob-Prince M, Hill M, Brown W. Immunocytochemical demonstration of myosin heavy chain expression in human muscle. *J Neurol Sci* (1989) 91:71–78. doi:10.1016/0022-510X(89)90076-2

35. Moss FP, Leblond CP. Satellite cells as the source of nuclei in muscles of growing rats. *Anat Rec* (1971) doi:10.1002/ar.1091700405

36. Chal J, Pourquié O. Making muscle: Skeletal myogenesis in vivo and in vitro. *Dev* (2017) doi:10.1242/dev.151035

37. Enwere EK, LaCasse EC, Adam NJ, Korneluk RG. Role of the TWEAK-Fn14-cIAP1-NF-κB signaling axis in the regulation of myogenesis and muscle homeostasis. *Front Immunol* (2014) doi:10.3389/fimmu.2014.00034

38. Srikanthan P, Karlamangla AS. Relative muscle mass is inversely associated with insulin resistance and prediabetes. Findings from the Third National Health and Nutrition Examination Survey. *J Clin Endocrinol Metab* (2011) doi:10.1210/jc.2011-0435

39. Barker DJP. Fetal programming of coronary heart disease. *Trends Endocrinol Metab* (2002) 13:364–368. doi:10.1016/S1043-2760(02)00689-6

40. Atlantis E, Martin SA, Haren MT, Taylor AW, Wittert GA. Inverse associations between muscle mass, strength, and the metabolic syndrome. *Metabolism* (2009) doi:10.1016/j.metabol.2009.02.027

41. Tsou Yau KI, Chang MH. Growth and body composition of preterm, small-for-gestational-age infants at a postmenstrual age of 37-40 weeks. *Early Hum Dev* (1993) doi:10.1016/0378-3782(93)90207-b

42. Felicioni F, Pereira AD, Caldeira-Brant AL, Santos TG, Paula TMD, Magnabosco

D, Bortolozzo FP, Tsoi S, Dyck MK, Dixon W, et al. Postnatal development of skeletal muscle in pigs with intrauterine growth restriction: morphofunctional phenotype and molecular mechanisms. *J Anat* (2020) doi:10.1111/joa.13152

43. Yates DT, MacKo AR, Nearing M, Chen X, Rhoads RP, Limesand SW. Developmental programming in response to intrauterine growth restriction impairs myoblast function and skeletal muscle metabolism. *J Pregnancy* (2012) 2012:1–10. doi:10.1155/2012/631038

44. Năstase L, Cretoiu D, Stoicescu SM. "Skeletal muscle damage in intrauterine growth restriction," in *Advances in Experimental Medicine and Biology*, 93–106. doi:10.1007/978-981-13-1435-3_5

45. MacDonald TM, Hui L, Tong S, Robinson AJ, Dane KM, Middleton AL, Walker SP. Reduced growth velocity across the third trimester is associated with placental insufficiency in fetuses born at a normal birthweight: A prospective cohort study. *BMC Med* (2017) doi:10.1186/s12916-017-0928-z

46. Cosmi E, Fanelli T, Visentin S, Trevisanuto D, Zanardo V. Consequences in infants that were intrauterine growth restricted. *J Pregnancy* (2011) 2011:364381. doi:10.1155/2011/364381

47. Powell SE, Aberle ED. Effects of birth weight on growth and carcass composition of swine. *J Anim Sci* (1980) doi:10.2527/jas1980.505860x

48. Wilson SJ, Ross JJ, Harris AJ. A critical period for formation of secondary myotubes defined by prenatal undernourishment in rats. *Development* (1988)

49. Zhu MJ, Ford SP, Nathanielsz PW, Du M. Effect of maternal nutrient restriction in sheep on the development of fetal skeletal muscle. *Biol Reprod* (2004)

doi:10.1095/biolreprod.104.034561

50. Dwyer CM, Stickland NC, Fletcher JM. The influence of maternal nutrition on muscle fiber number development in the porcine fetus and on subsequent postnatal growth. *J Anim Sci* (1994) 72:911–917. doi:10.2527/1994.724911x

51. Ward SS, Stickland NC. Why are slow and fast muscles differentially affected during prenatal undernutrition? *Muscle Nerve* (1991) doi:10.1002/mus.880140310

52. Stouthamer AH. A theoretical study on the amount of ATP required for synthesis of microbial cell material. *Antonie Van Leeuwenhoek* (1973) doi:10.1007/BF02578899

53. Hay WW. Placental-fetal glucose exchange and fetal glucose metabolism. *Trans Am Clin Climatol Assoc* (2006) 117:

54. Makrides M, Anderson A, Gibson RA. Early influences of nutrition on fetal growth. in *Nestle Nutrition Institute Workshop Series* doi:10.1159/000342500

55. Hay WW. *Placental-fetal glucose exchange and fetal glucose metabolism.* 1st ed. , ed. J. Senterre Nestle Nutrition Services (1989).

56. Sugden MC, Orfali K a, Holness MJ. The pyruvate dehydrogenase complex: nutrient control and the pathogenesis of insulin resistance. *J Nutr* (1995) 125:1746S-1752S.

57. Wu CA, Chao Y, Shiah SG, Lin WW. Nutrient deprivation induces the Warburg effect through ROS/AMPK-dependent activation of pyruvate dehydrogenase kinase. *Biochim Biophys Acta - Mol Cell Res* (2013) 1833:1147–1156. doi:10.1016/j.bbamcr.2013.01.025

58. Liu YQ, Han J, Epstein PN, Long YS. Enhanced rat β-cell proliferation in 60%

pancreatectomized islets by increased glucose metabolic flux through pyruvate carboxylase pathway. *Am J Physiol - Endocrinol Metab* (2005) doi:10.1152/ajpendo.00427.2004

59. Elias CB, Carpentier E, Durocher Y, Bisson L, Wagner R, Kamen A. Improving glucose and glutamine metabolism of human HEK 293 and Trichoplusia ni insect cells engineered to express a cytosolic pyruvate carboxylase enzyme. in *Biotechnology Progress* doi:10.1021/bp025572x

60. Irani N, Wirth M, Van Den Heuvel J, Wagner R. Improvement of the primary metabolism of cell cultures by introducing a new cytoplasmic pyruvate carboxylase reaction. *Biotechnol Bioeng* (1999) doi:10.1002/(SICI)1097-0290(1999)66:4<238::AID-BIT5>3.0.CO;2-6

61. Slonim AE. Skeletal Muscle Metabolism In Exercise and Diabetes. *Am J Clin Nutr* (1999) doi:10.1093/ajcn/70.1.114a

62. Palmer S. Recommended dietary allowances, tenth edition. in *European Journal of Clinical Nutrition*

63. Watt PW, Corbett ME, Rennie MJ. Stimulation of protein synthesis in pig skeletal muscle by infusion of amino acids during constant insulin availability. *Am J Physiol - Endocrinol Metab* (1992) doi:10.1152/ajpendo.1992.263.3.e453

64. Carraro F, Stuart CA, Hartl WH, Rosenblatt J, Wolfe RR. Effect of exercise and recovery on muscle protein synthesis in human subjects. *Am J Physiol - Endocrinol Metab* (1990) doi:10.1152/ajpendo.1990.259.4.e470

65. Bennet WM, Connacher AA, Scrimgeour CM, Smith K, Rennie MJ. Increase in anterior tibialis muscle protein synthesis in healthy man during mixed amino acid

infusion: Studies of incorporation of [1-13C]leucine. *Clin Sci* (1989) doi:10.1042/cs0760447

66. Pacy PJ, Price GM, Halliday D, Quevedo MR, Millward DJ. Nitrogen homoeostasis in man: The diurnal responses of protein synthesis and degradation and amino acid oxidation to diets with increasing protein intakes. *Clin Sci* (1994) doi:10.1042/cs0860103
67. Cheng KN, Pacy PJ, Dworzak F, Ford GC, Halliday D. Influence of fasting on leucine and muscle protein metabolism across the human forearm determined using L-[1-13C,15N]leucine as the tracer. *Clin Sci* (1987) doi:10.1042/cs0730241
68. Chang TW, Goldberg AL. The origin of alanine produced in skeletal muscle. *J Biol Chem* (1978) 253:3677–3684.
69. Chang TW, Goldberg AL. The metabolic fates of amino acids and the formation of glutamine in skeletal muscle. *J Biol Chem* (1978) 253:3685–3693.
70. Ahlborg G, Felig P, Hagenfeldt L, Hendler R, Wahren J. Substrate turnover during prolonged exercise in man. Splanchnic and leg metabolism of glucose, free fatty acids, and amino acids. *J Clin Invest* (1974) doi:10.1172/JCI107645
71. Elia M, Folmer P, Schlatmann A, Goren A, Austin S. Amino acid metabolism in muscle and in the whole body of man before and after ingestion of a single mixed meal. *Am J Clin Nutr* (1989) 49:1203–1210. doi:10.1093/ajcn/49.6.1203
72. Eriksson LS, Broberg S, Björkman O, Wahren J. Ammonia metabolism during exercise in man. *Clin Physiol* (1985) doi:10.1111/j.1475-097X.1985.tb00753.x
73. Wagenmakers AJ. Muscle amino acid metabolism at rest and during exercise: role in human physiology and metabolism. *Exerc Sport Sci Rev* (1998)

74. Sung-Hee Cho Lee, Davis EJ. Amino acid catabolism by perfused rat hindquarter. The matabolic fates of valine. *Biochem J* (1986) doi:10.1042/bj2330621

75. Zhang S, Heng J, Song H, Zhang Y, Lin X, Tian M, Chen F, Guan W. Role of maternal dietary protein and amino acids on fetal programming, early neonatal development, and lactation in Swine. *Animals* (2019) doi:10.3390/ani9010019

76. Rozance PJ, Zastoupil L, Wesolowski SR, Goldstrohm DA, Strahan B, Cree-Green M, Sheffield-Moore M, Meschia G, Hay WW, Wilkening RB, et al. Skeletal muscle protein accretion rates and hindlimb growth are reduced in late gestation intrauterine growth-restricted fetal sheep. *J Physiol* (2018) 596:67–82. doi:10.1113/JP275230

77. Chang EI, Wesolowski SR, Gilje EA, Baker PR, Reisz JA, D'Alessandro A, Hay, Jr. WW, Rozance PJ, Brown LD. Skeletal muscle amino acid uptake is lower and alanine production is greater in late gestation intrauterine growth restricted fetal sheep hindlimb. *Am J Physiol Integr Comp Physiol* (2019) doi:10.1152/ajpregu.00115.2019

78. Yamada T, Kikuchi K, Sugi H. 31P nuclear magnetic resonance studies on the glycogenolysis regulation in resting and contracting frog skeletal muscle. *J Physiol* (1993) doi:10.1113/jphysiol.1993.sp019471

79. Blei ML, Conley KE, Odderson IR, Esselman PC, Kushmerick MJ. Individual variation in contractile cost and recovery in a human skeletal muscle. *Proc Natl Acad Sci U S A* (1993) doi:10.1073/pnas.90.15.7396

80. Brand M. Approximate yield of ATP from glucose, designed by Donald Nicholson: Commentary. *Biochem Mol Biol Educ* (2003)

doi:10.1002/bmb.2003.494031010178

81. Hänninen O, Atalay M. “Oxidative metabolism in skeletal muscle,” in *Oxidative Stress in Skeletal Muscle* doi:10.1007/978-3-0348-8958-2_2

82. Ortiz-Prado E, Dunn JF, Vasconez J, Castillo D, Viscor G. Partial pressure of oxygen in the human body: a general review. *Am J Blood Res* (2019)

83. Rolfe DFS, Brown GC. Cellular energy utilization and molecular origin of standard metabolic rate in mammals. *Physiol Rev* (1997) doi:10.1152/physrev.1997.77.3.731

84. Wieser W, Krumschnabel G. Hierarchies of ATP-consuming processes: Direct compared with indirect measurements, and comparative aspects. *Biochem J* (2001) doi:10.1042/0264-6021:3550389

85. Buttgereit F, Brand MD. A hierarchy of ATP-consuming processes in mammalian cells. *Biochem J* (1995) doi:10.1042/bj3120163

86. Davidson AM, Halestrap AP. Partial inhibition by cyclosporin A of the swelling of liver mitochondria in vivo and in vitro induced by sub-micromolar [Ca2+], but not by butyrate. Evidence for two distinct swelling mechanisms. *Biochem J* (1990) doi:10.1042/bj2680147

87. Hindle AG, Otis JP, Elaine Epperson L, Hornberger TA, Goodman CA, Carey H V., Martin SL. Prioritization of skeletal muscle growth for emergence from hibernation. *J Exp Biol* (2015) doi:10.1242/jeb.109512

88. Goropashnaya A V., Barnes BM, Fedorov VB. Transcriptional changes in muscle of hibernating arctic ground squirrels (Urocitellus parryii): implications for attenuation of disuse muscle atrophy. *Sci Rep* (2020) doi:10.1038/s41598-020-

66030-9

89. MacDonald JA, Storey KB. Regulation of ground squirrel Na+K+-ATPase activity by reversible phosphorylation during hibernation. *Biochem Biophys Res Commun* (1999) doi:10.1006/bbrc.1998.9960

90. Storey KB. Survival under stress: Molecular mechanisms of metabolic rate depression in animals. *South African J Zool* (1998) doi:10.1080/02541858.1998.11448454

91. Yan J, Barnes BM, Kohl F, Marr TG. Modulation of gene expression in hibernating arctic ground squirrels. *Physiol Genomics* (2008) doi:10.1152/physiolgenomics.00075.2007

92. Bell RAV, Storey KB. Purification and characterization of skeletal muscle pyruvate kinase from the hibernating ground squirrel, Urocitellus richardsonii: potential regulation by posttranslational modification during torpor. *Mol Cell Biochem* (2018) doi:10.1007/s11010-017-3192-9

93. Staples JF, Kajimura M, Wood CM, Patel M, Ip YK, McClelland GB. Enzymatic and mitochondrial responses to 5 months of aerial exposure in the slender lungfish Protopterus dolloi. *J Fish Biol* (2008) doi:10.1111/j.1095-8649.2008.01955.x

94. Bishop T, St-Pierre J, Brand MD. Primary causes of decreased mitochondrial oxygen consumption during metabolic depression in snail cells. *Am J Physiol - Regul Integr Comp Physiol* (2002) doi:10.1152/ajpregu.00401.2001

95. Economides DL, Nicolaides KH. Blood glucose and oxygen tension levels in small-for-gestational-age fetuses. *Am J Obstet Gynecol* (1989) 160:385–389. doi:10.1016/0002-9378(89)90453-5

96. Nicolaides KH, Economides DL, Soothill PW. Blood gases, pH, and lactate in appropriate- and small-for-gestational-age fetuses. *Am J Obstet Gynecol* (1989) 161:996–1001. doi:10.1016/0002-9378(89)90770-9

97. Marconi AM, Paolini CL. Nutrient Transport Across the Intrauterine Growth-Restricted Placenta. *Semin Perinatol* (2008) 32:178–181. doi:10.1053/j.semperi.2008.02.007

98. Okamura K, Watanabe T, Tanigawara S, Endo H, Iwamoto M, Murotsuki J, Yajima A. Catecholamine levels and their correlation to blood gases in umbilical venous blood obtained by cordocentesis. *Fetal Diagn Ther* (1990) doi:10.1159/000263584

99. Greenough A, Nicolaides KH, Lagercrantz H. Human fetal sympathoadrenal responsiveness. *Early Hum Dev* (1990) doi:10.1016/0378-3782(90)90124-2

100. Nicolini U, Hubinont C, Santolaya J, Fisk NM, Rodeck CH. Effects of fetal intravenous glucose challenge in normal and growth retarded fetuses. *Horm Metab Res* (1990) doi:10.1055/s-2007-1004939

101. Nieto-Díaz A, Villar J, Matorras-Weinig R, Valenzuela-Ruìz P. Intrauterine growth retardation at term: Association between anthropometric and endocrine parameters. *Acta Obstet Gynecol Scand* (1996) doi:10.3109/00016349609033303

102. Van Assche FA, Prins F De, Aerts L, Verjans M. THE ENDOCRINE PANCREAS IN SMALL-FOR-DATES INFANTS. *BJOG An Int J Obstet Gynaecol* (1977) doi:10.1111/j.1471-0528.1977.tb12486.x

103. Setia S, Sridhar MG, Bhat V, Chaturvedula L, Vinayagamoorti R, John M. Insulin sensitivity and insulin secretion at birth in intrauterine growth retarded infants.

Pathology (2006) doi:10.1080/00313020600696256

104. Thorn SR, Regnault TRH, Brown LD, Rozance PJ, Keng J, Roper M, Wilkening RB, Hay WW, Friedman JE. Intrauterine growth restriction increases fetal hepatic gluconeogenic capacity and reduces messenger ribonucleic acid translation initiation and nutrient sensing in fetal liver and skeletal muscle. *Endocrinology* (2009) 150:3021–3030. doi:10.1210/en.2008-1789

105. De Blasio MJ, Gatford KL, Harland ML, Robinson JS, Owens JA. Placental restriction reduces insulin sensitivity and expression of insulin signaling and glucose transporter genes in skeletal muscle, but not liver, in young sheep. *Endocrinology* (2012) 153:2142–2151. doi:10.1210/en.2011-1955

106. De Blasio MJ, Gatford KL, McMillen IC, Robinson JS, Owens JA. Placental restriction of fetal growth increases insulin action, growth, and adiposity in the young lamb. *Endocrinology* (2007) 148:1350–1358. doi:10.1210/en.2006-0653

107. Walther FJ. Growth and development of term disproportionate small-for-gestational age infants at the age of 7 years. *Early Hum Dev* (1988) 18:1–11. doi:10.1016/0378-3782(88)90038-2

108. Brandt I, Sticker EJ, Lentze MJ. Catch-up growth of head circumference of very low birth weight, small for gestational age preterm infants and mental development to adulthood. *J Pediatr* (2003) 142:463–470. doi:10.1067/mpd.2003.149

109. Papageorgiou APO. Intrauterine growth restriction: Short and long term implications. *J Matern Neonatal Med* (2012) 25:13.

110. Karlberg J, Albertsson-Wikland K. Growth in full-term small-for-gestational-age infants: From birth to final height. *Pediatr Res* (1995) 38:733–739.

doi:10.1203/00006450-199511000-00017

111. Villar J, Smeriglio V, Martorell R, Brown CH, Klein RE. Heterogeneous growth and mental development of intrauterine growth-retarded infants during the first 3 years of life. *Pediatrics* (1984) 74:783–791.

112. Villar J, Belizán JM, Spalding J, Klein RE. Postnatal growth of intrauterine growth retarded infants. *Early Hum Dev* (1982) 6:265–271. doi:10.1016/0378-3782(82)90120-7

113. Lane RH, Flozak AS, Ogata ES, Bell GI, Simmons RA. Altered hepatic gene expression of enzymes involved in energy metabolism in the growth-retarded fetal rat. *Pediatr Res* (1996) 39:390–394. doi:10.1203/00006450-199603000-00003

114. Ogata ES, Swanson SL, Collins JW, Finley SL. Intrauterine growth retardation: Altered hepatic energy and redox states in the fetal rat. *Pediatr Res* (1990) doi:10.1203/00006450-199001000-00017

115. Lane RH, Chandorkar AK, Flozak AS, Simmons RA. Intrauterine growth retardation alters mitochondrial gene expression and function in fetal and juvenile rat skeletal muscle. *Pediatr Res* (1998) 43:563–570. doi:10.1203/00006450-199805000-00001

116. Chessex P, Reichman B, Verellen G, Putet G, Smith JM, Heim T, Swyer PR. Metabolic consequences of intrauterine growth retardation in very low birthweight infants. *Pediatr Res* (1984) 18:709–713. doi:10.1203/00006450-198408000-00006

117. Davies PSW. Total energy expenditure in small for gestational age infants. *Arch Dis Child Fetal Neonatal Ed* (1996) 74: doi:10.1136/fn.74.3.F208

118. Sinclair JC, Silverman WA. Intrauterine growth in active tissue mass of the human

fetus, with particular reference to the undergrown baby. *Pediatrics* (1966) 38:48–62.

119. Seppet E, Gruno M, Peetsalu A, Gizatullina Z, Nguyen HP, Vielhaber S, Wussling MHP, Trumbeckaite S, Arandarcikaite O, Jerzembeck D, et al. Mitochondria and energetic depression in cell pathophysiology. *Int J Mol Sci* (2009) 10:2252–2303. doi:10.3390/ijms10052252

120. Krebs HA. Rate control of the tricarboxylic acid cycle. *Adv Enzyme Regul* (1970) 8:335–353. doi:10.1016/0065-2571(70)90028-2

121. Selak MA, Storey BT, Peterside I, Simmons RA. Impaired oxidative phosphorylation in skeletal muscle of intrauterine growth-retarded rats. *Am J Physiol - Endocrinol Metab* (2003) 285: doi:10.1152/ajpendo.00322.2002

122. Chance B, Lees H, Postgate JR. The meaning of “reversed electron flow” and “high energy electron” in biochemistry. *Nature* (1972) 238:330–331. doi:10.1038/238330a0

123. Chance B, Hess B. Spectroscopic evidence of metabolic control. *Science (80-)* (1959) 129:700–708. doi:10.1126/science.129.3350.700

124. Klingenberg M. The ADP,ATP shuttle of the mitochondrion. *Trends Biochem Sci* (1979) 4:249–252. doi:10.1016/0968-0004(79)90215-9

125. Reynolds CM, Vickers MH. The role of adipokines in developmental programming: Evidence from animal models. *J Endocrinol* (2019) 242:T81–T94. doi:10.1530/JOE-18-0686

126. Malhotra A, Allison BJ, Castillo-Melendez M, Jenkin G, Polglase GR, Miller SL. Neonatal morbidities of fetal growth restriction: Pathophysiology and impact.

Front Endocrinol (Lausanne) (2019) doi:10.3389/fendo.2019.00055

127. Sharma D, Shastri S, Sharma P. Intrauterine Growth Restriction: Antenatal and Postnatal Aspects. *Clin Med Insights Pediatr* (2016) 10:CMPed.S40070. doi:10.4137/cmped.s40070

128. Garg M, Thamotharan M, Dai Y, Thamotharan S, Shin BC, Stout D, Devaskar SU. Early postnatal caloric restriction protects adult male intrauterine growth-restricted offspring from obesity. *Diabetes* (2012) 61:1391–1398. doi:10.2337/db11-1347

129. Yamada M, Wolfe D, Han G, French SW, Ross MG, Desai M. Early onset of fatty liver in growth-restricted rat fetuses and newborns. *Congenit Anom (Kyoto)* (2011) 51:167–173. doi:10.1111/j.1741-4520.2011.00336.x

130. Garofano A, Czernichow P, Bréant B. In utero undernutrition impairs rat beta-cell development. *Diabetologia* (1997) doi:10.1007/s001250050812

131. Park KS, Kim SK, Kim MS, Cho EY, Lee JH, Lee K-U, Pak YK, Lee HK. Fetal and Early Postnatal Protein Malnutrition Cause Long-Term Changes in Rat Liver and Muscle Mitochondria. *J Nutr* (2003) 133:3085–3090. doi:10.1093/jn/133.10.3085

132. Xing Y, Zhang J, Wei H, Zhang H, Guan Y, Wang X, Tong X. Reduction of the PI3K/Akt related signaling activities in skeletal muscle tissues involves insulin resistance in intrauterine growth restriction rats with catch-up growth. *PLoS One* (2019) 14: doi:10.1371/journal.pone.0216665

133. Kloesz JL, Serdikoff CM, Maclennan NK, Adibi SA, Lane RH. Uteroplacental insufficiency alters liver and skeletal muscle branched-chain amino acid metabolism in intrauterine growth-restricted fetal rats. *Pediatr Res* (2001) 50:604–

610. doi:10.1203/00006450-200111000-00012

134. Choi GY, Tosh DN, Garg A, Mansano R, Ross MG, Desai M. Gender-specific programmed hepatic lipid dysregulation in intrauterine growth-restricted offspring. *Am J Obstet Gynecol* (2007) 196:477.e1-477.e7. doi:10.1016/j.ajog.2007.02.024

135. Zeng Y, Gu P, Liu K, Huang P. Maternal protein restriction in rats leads to reduced PGC-1α expression via altered DNA methylation in skeletal muscle. *Mol Med Rep* (2013) 7:306–312. doi:10.3892/mmr.2012.1134

136. Zinkhan EK, Zalla JM, Carpenter JR, Yu B, Yu X, Chan G, Joss-Moore L, Lane RH. Intrauterine growth restriction combined with a maternal high-fat diet increases hepatic cholesterol and low-density lipoprotein receptor activity in rats. *Physiol Rep* (2016) 4: doi:10.14814/phy2.12862

137. Garg M, Thamotharan M, Pan G, Lee PWN, Devaskar SU. Early exposure of the pregestational intrauterine and postnatal growth-restricted female offspring to a peroxisome proliferator-activated receptor-γ agonist. *Am J Physiol - Endocrinol Metab* (2010) 298: doi:10.1152/ajpendo.00361.2009

138. Ogata ES, Bussey ME, Finley S. Altered gas exchange, limited glucose and branched chain amino acids, and hypoinsulinism retard fetal growth in the rat. *Metabolism* (1986) 35:970–977. doi:10.1016/0026-0495(86)90064-8

139. Germani D, Puglianiello A, Cianfarani S. Uteroplacental insufficiency down regulates insulin receptor and affects expression of key enzymes of long-chain fatty acid (LCFA) metabolism in skeletal muscle at birth. *Cardiovasc Diabetol* (2008) 7: doi:10.1186/1475-2840-7-14

140. Sohi G, Barry EJ, Velenosi TJ, Urquhart BL, Hardy DB. Protein restoration in

low-birth-weight rat offspring derived from maternal low-protein diet leads to elevated hepatic CYP3A and CYP2C11 activity in adulthood. *Drug Metab Dispos* (2014) 42:221–228. doi:10.1124/dmd.113.053538

141. Lane RH, Maclennan NK, Daood MJ, Hsu JL, Janke SM, Pham TD, Puri AR, Watchko JF. IUGR alters postnatal rat skeletal muscle peroxisome proliferator-activated receptor-γ coactivator-1 gene expression in a fiber specific manner. *Pediatr Res* (2003) 53:994–1000. doi:10.1203/01.PDR.0000064583.40495.51

142. Lane RH, Kelley DE, Ritov VH, Tsirka AE, Gruetzmacher EM. Altered expression and function of mitochondrial β-oxidation enzymes in juvenile intrauterine-growth-retarded rat skeletal muscle. *Pediatr Res* (2001) 50:83–90. doi:10.1203/00006450-200107000-00016

143. Langley-Evans SC, Gardner DS, Jackson AA. Maternal protein restriction influences the programming of the rat hypothalamic-pituitary-adrenal axis. *J Nutr* (1996) 126:1578–1585. doi:10.1093/jn/126.6.1578

144. Simmons RA, Templeton LJ, Gertz SJ. Intrauterine Growth Retardation Leads to the Development of Type 2 Diabetes in the Rat. *Diabetes* (2001) 50:2279–2286. doi:10.2337/diabetes.50.10.2279

145. Suenderhauf C, Parrott N. A physiologically based pharmacokinetic model of the minipig: data compilation and model implementation. *Pharm Res* (2013) 30:1–15. doi:10.1007/s11095-012-0911-5

146. Deglaire A, Moughan PJ. Animal models for determining amino acid digestibility in humans - A review. *Br J Nutr* (2012) 108: doi:10.1017/S0007114512002346

147. Rothkötter HJ. Anatomical particularities of the porcine immune system-A

physician's view. *Dev Comp Immunol* (2009) 33:267–272. doi:10.1016/j.dci.2008.06.016

148. Wu G, Bazer FW, Cudd TA, Meininger CJ, Spencer TE. Maternal Nutrition and Fetal Development. *J Nutr* (2004) 134:2169–2172. doi:10.1093/jn/134.9.2169

149. Shen L, Gan M, Zhang S, Ma J, Tang G, Jiang Y, Li M, Wang J, Li X, Che L, et al. Transcriptome analyses reveal adult metabolic syndrome with intrauterine growth restriction in pig models. *Front Genet* (2018) 9: doi:10.3389/fgene.2018.00291

150. Bauer R, Walter B, Brust P, Füchtner F, Zwiener U. Impact of asymmetric intrauterine growth restriction on organ function in newborn piglets. in *European Journal of Obstetrics and Gynecology and Reproductive Biology* doi:10.1016/S0301-2115(03)00171-4

151. Bauer R, Walter B, Hoppe A, Gaser E, Lampe V, Kauf E, Zwiener U. Body weight distribution and organ size in newborn swine (sus scrofa domestica) - A study describing an animal model for asymmetrical intrauterine growth retardation. *Exp Toxicol Pathol* (1998) 50:59–65. doi:10.1016/S0940-2993(98)80071-7

152. Mellor DJ, Cockburn F. a Comparison of Energy Metabolism in the New-Born Infant, Piglet and Lamb. *Q J Exp Physiol* (1986) 71:361–379. doi:10.1113/expphysiol.1986.sp002995

153. Handel SE, Stickland NC. The growth and differentiation of porcine skeletal muscle fibre types and the influence of birthweight. *J Anat* (1987) Vol. 152:107–119.

154. Bérard J, Pardo CE, Béthaz S, Kreuzer M, Bee G. Intrauterine crowding decreases

average birth weight and affects muscle fiber hyperplasia in piglets. *J Anim Sci* (2010) 88:3242–3250. doi:10.2527/jas.2010-2867

155. Wang J, Chen L, Li D, Yin Y, Wang X, Li P, Dangott LJ, Hu W, Wu G. Intrauterine Growth Restriction Affects the Proteomes of the Small Intestine, Liver, and Skeletal Muscle in Newborn Pigs. *J Nutr* (2008) 138:60–66. doi:10.1093/jn/138.1.60

156. Wu G, Bazer FW, Burghardt RC, Johnson GA, Kim SW, Li XL, Satterfield MC, Spencer TE. Impacts of amino acid nutrition on pregnancy outcome in pigs: mechanisms and implications for swine production. *J Anim Sci* (2010) 88: doi:10.2527/jas.2009-2446

157. Liu J, Chen D, Yao Y, Yu B, Mao X, He J, Huang Z, Zheng P. Intrauterine growth retardation increases the susceptibility of pigs to high-fat diet-induced mitochondrial dysfunction in skeletal muscle. *PLoS One* (2012) 7: doi:10.1371/journal.pone.0034835

158. Jamin A, D'Inca R, Le Floc'H N, Kuster A, Orsonneau JL, Darmaun D, Boudry G, Le Huërou-Luron I, Sève B, Gras-Le Guen C. Fatal effects of a neonatal high-protein diet in low-birth-weight piglets used as a model of intrauterine growth restriction. *Neonatology* (2010) 97:321–328. doi:10.1159/000260135

159. Engelsmann MN, Hansen CF, Nielsen MN, Kristensen AR, Amdi C. Glucose injections at birth, warmth and placing at a nurse sow improve the growth of IUGR piglets. *Animals* (2019) 9: doi:10.3390/ani9080519

160. Lynegaard JC, Hansen CF, Kristensen AR, Amdi C. Body composition and organ development of intra-uterine growth restricted pigs at weaning. *Animal* (2020)

14:322–329. doi:10.1017/S175173111900171X

161. Pond WG, Maurer RR, Klindt J. Fetal organ response to maternal protein deprivation during pregnancy in swine. *J Nutr* (1991) 121:504–509. doi:10.1093/jn/121.4.504

162. Poore KR, Fowden AL. The effects of birth weight and postnatal growth patterns on fat depth and plasma leptin concentrations in juvenile and adult pigs. *J Physiol* (2004) 558:295–304. doi:10.1113/jphysiol.2004.061390

163. Poore K, Fowden A. The effect of birth weight on glucose tolerance in pigs at 3 and 12 months of age. *Diabetologia* (2002) 45:1247–1254. doi:10.1007/s00125-002-0849-y

164. Poore KR, Forhead AJ, Gardner DS, Giussani DA, Fowden AL. The effects of birth weight on basal cardiovascular function in pigs at 3 months of age. *J Physiol* (2002) 539:969–978. doi:10.1113/jphysiol.2001.012926

165. Poore KR, Fowden AL. The effect of birth weight on hypothalamo-pituitary-adrenal axis function in juvenile and adult pigs. *J Physiol* (2003) 547:107–116. doi:10.1113/jphysiol.2002.024349

166. Bhide A, Vuolteenaho O, Haapsamo M, Erkinaro T, Rasanen J, Acharya G. Effect of Hypoxemia with or without Increased Placental Vascular Resistance on Fetal Left and Right Ventricular Myocardial Performance Index in Chronically Instrumented Sheep. *Ultrasound Med Biol* (2016) 42:2589–2598. doi:10.1016/j.ultrasmedbio.2016.07.006

167. Supramaniam VG, Jenkin G, Loose J, Wallace EM, Miller SL. Chronic fetal hypoxia increases activin A concentrations in the late-pregnant sheep. *BJOG An*

Int J Obstet Gynaecol (2006) 113:102–109. doi:10.1111/j.1471-0528.2005.00791.x

168. Zhang S, Barker P, Botting KJ, Roberts CT, McMillan CM, McMillen IC, Morrison JL. Early restriction of placental growth results in placental structural and gene expression changes in late gestation independent of fetal hypoxemia. *Physiol Rep* (2016) 4: doi:10.14814/phy2.13049

169. Carr DJ, Aitken RP, Milne JS, David AL, Wallace JM. Fetoplacental biometry and umbilical artery Doppler velocimetry in the overnourished adolescent model of fetal growth restriction. *Am J Obstet Gynecol* (2012) 207:141.e6-141.e15. doi:10.1016/j.ajog.2012.05.008

170. A.L. P, M.A. D, A.C. K, L.E. C, M.J. A. 2019 | Scientific Abstracts. *Reprod Sci* (2019) 26:62A-390A. doi:10.1177/1933719119834079

171. Wallace JM. Competition for nutrients in pregnant adolescents: Consequences for maternal, conceptus and offspring endocrine systems. *J Endocrinol* (2019) 242:T1–T19. doi:10.1530/JOE-18-0670

172. Macko AR, Yates DT, Chen X, Shelton LA, Kelly AC, Davis MA, Camacho LE, Anderson MJ, Limesand SW. Adrenal demedullation and oxygen supplementation independently increase glucose-stimulated insulin concentrations in fetal sheep with intrauterine growth restriction. *Endocrinology* (2016) 157:2104–2115. doi:10.1210/en.2015-1850

173. McMillen IC, Adams MB, Ross JT, Coulter CL, Simonetta G, Owens JA, Robinson JS, Edwards LJ. Fetal growth restriction: Adaptations and consequences. *Reproduction* (2001) doi:10.1530/rep.0.1220195

174. Simonetta G, Rourke AK, Owens JA, Robinson JS, McMillen IC. Impact of placental restriction on the development of the sympathoadrenal system. *Pediatr Res* (1997) doi:10.1203/00006450-199712000-00015

175. Owens JA, Falconer J, Robinson JS. Glucose metabolism in pregnant sheep when placental growth is restricted. *Am J Physiol - Regul Integr Comp Physiol* (1989) doi:10.1152/ajpregu.1989.257.2.r350

176. Kind KL, Owens JA, Robinson JS, Quinn KJ, Grant PA, Walton PE, Gilmour RS, Owens PC. Effect of restriction of placental growth on expression of IGFs in fetal sheep: Relationship to fetal growth, circulating IGFs and binding proteins. *J Endocrinol* (1995) doi:10.1677/joe.0.1460023

177. Danielson L, McMillen IC, Dyer JL, Morrison JL. Restriction of placental growth results in greater hypotensive response to α-adrenergic blockade in fetal sheep during late gestation. *J Physiol* (2005) doi:10.1113/jphysiol.2004.080523

178. Clapp JF, Szeto HH, Larrow R, Hewitt J, Mann LI. Umbilical blood flow response to embolization of the uterine circulation. *Am J Obstet Gynecol* (1980) doi:10.1016/0002-9378(80)90011-3

179. Gagnon R, Johnston L, Murotsuki J. Fetal placental embolization in the late-gestation ovine fetus: Alterations in umbilical blood flow and fetal heart rate patterns. *Am J Obstet Gynecol* (1996) doi:10.1016/S0002-9378(96)70252-1

180. Cheung CY, Bogic L, Gagnon R, Harding R, Brace RA. Morphologic alterations in ovine placenta and fetal liver following induced severe placental insufficiency. *J Soc Gynecol Investig* (2004) doi:10.1016/j.jsgi.2004.06.010

181. Murotsuki J, Challis JRG, Han VKM, Fraher LJ, Gagnon R. Chronic fetal

placental embolization and hypoxemia cause hypertension and myocardial hypertrophy in fetal sheep. *Am J Physiol - Regul Integr Comp Physiol* (1997) doi:10.1152/ajpregu.1997.272.1.r201

182. Cock ML, Albuquerque CA, Joyce BJ, Hooper SB, Harding R. Effects of intrauterine growth restriction on lung liquid dynamics and lung development in fetal sheep. *Am J Obstet Gynecol* (2001) doi:10.1067/mob.2001.108858

183. Emmanouilides GC, Townsend DE, Bauer RA. Effects of single umbilical artery ligation in the lamb fetus. *Pediatrics* (1968) doi:10.1097/00006254-196908000-00003

184. Oh W, Omori K, Hobel CJ, Erenberg A, Emmanouilides GC. Umbilical blood flow and glucose uptake in lamb fetus following single umbilical artery ligation. *Biol Neonate - Foetal Neonatal Res* (1975) doi:10.1159/000240741

185. Limesand SW, Camacho LE, Kelly AC, Antolic AT. Impact of thermal stress on placental function and fetal physiology. *Anim Reprod* (2018) 15:886–898. doi:10.21451/1984-3143-AR2018-0056

186. Brown LD, Rozance PJ, Thorn SR, Friedman JE, Hay WW. Acute supplementation of amino acids increases net protein accretion in IUGR fetal sheep. *Am J Physiol Metab* (2012) 303:E352–E364. doi:10.1152/ajpendo.00059.2012

187. Limesand SW, Rozance PJ, Brown LD, Hay WW. Effects of chronic hypoglycemia and euglycemic correction on lysine metabolism in fetal sheep. *Am J Physiol Endocrinol Metab* (2009) 296:E879-87. doi:10.1152/ajpendo.90832.2008

188. Pardi G, Marconi AM, Cetin I. Placental-fetal interrelationship in IUGR fetuses - A review. *Placenta* (2002) 23: doi:10.1053/plac.2002.0802

189. Gagnon R. Placental insufficiency and its consequences. in *European Journal of Obstetrics and Gynecology and Reproductive Biology* doi:10.1016/S0301-2115(03)00179-9

190. Miller J, Turan S, Baschat AA. Fetal Growth Restriction. *Semin Perinatol* (2008) 32:274–280. doi:10.1053/j.semperi.2008.04.010

191. Ananth C V., Peltier MR, Chavez MR, Kirby RS, Getahun D, Vintzileos AM. Recurrence of ischemic placental disease. *Obstet Gynecol* (2007) 110:128–133. doi:10.1097/01.AOG.0000266983.77458.71

192. Anthony R V., Scheaffer AN, Wright CD, Regnault TR. Ruminant models of prenatal growth restriction. *Reprod Suppl* (2003) 61:183–194. doi:10.1530/biosciprocs.5.014

193. Wilson SJ, McEwan JC, Sheard PW, Harris AJ. Early stages of myogenesis in a large mammal: Formation of successive generations of myotubes in sheep tibialis cranialis muscle. *J Muscle Res Cell Motil* (1992) 13:534–550. doi:10.1007/BF01737996

194. Kennaugh JM, Bell AW, Teng C, Meschia G, Battaglia F. Ontogenetic changes in the rates of protein synthesis and leucine oxidation during fetal life. *Pediatr Res* (1987) 22:688–692. doi:10.1203/00006450-198712000-00015

195. Garlick PJ, Burk TL, Swick RW. Protein synthesis and RNA in tissues of the pig. *Am J Physiol* (1976) 230:1108–1112. doi:10.1152/ajplegacy.1976.230.4.1108

196. Limesand SW, Rozance PJ, Smith D, Hay WW. Increased insulin sensitivity and

maintenance of glucose utilization rates in fetal sheep with placental insufficiency and intrauterine growth restriction. *Am J Physiol Metab* (2007) 293:E1716–E1725. doi:10.1152/ajpendo.00459.2007

197. Brown LD, Rozance PJ, Bruce JL, Friedman JE, Hay WW, Wesolowski SR. Limited capacity for glucose oxidation in fetal sheep with intrauterine growth restriction. *Am J Physiol Integr Comp Physiol* (2015) 309:R920–R928. doi:10.1152/ajpregu.00197.2015

198. Regnault TRH, Friedmann JE, Wilkening RB, Anthony R V., Hay WW. Fetoplacental transport and utilization of amino acids in IUGR - A review. *Placenta* (2005) 26: doi:10.1016/j.placenta.2005.01.003

199. Brown LD, Rozance PJ, Thorn SR, Friedman JE, Hay WW. Acute supplementation of amino acids increases net protein accretion in IUGR fetal sheep. *Am J Physiol - Endocrinol Metab* (2012) 303: doi:10.1152/ajpendo.00059.2012

200. Wesolowski SR, Hay WW. Role of placental insufficiency and intrauterine growth restriction on the activation of fetal hepatic glucose production. *Mol Cell Endocrinol* (2016) 435:61–68. doi:10.1016/j.mce.2015.12.016

201. Camacho LE, Chen X, Hay WW, Limesand SW. Enhanced insulin secretion and insulin sensitivity in young lambs with placental insufficiency-induced intrauterine growth restriction. *Am J Physiol Integr Comp Physiol* (2017) 313:R101–R109. doi:10.1152/ajpregu.00068.2017

202. Greenwood PL, Hunt AS, Hermanson JW, Bell AW. Effects of birth weight and postnatal nutrition on neonatal sheep: II. Skeletal muscle growth and development.

J Anim Sci (2000) 78:50–61. doi:10.2527/2000.78150x

203. Greenwood PL, Slepetis RM, Hermanson JW, Bell AW. Intrauterine growth retardation is associated with reduced cell cycle activity, but not myofibre number, in ovine fetal muscle. *Reprod Fertil Dev* (1999) 11:281–291. doi:10.1071/rd99054

204. George LA, Zhang L, Tuersunjiang N, Ma Y, Long NM, Uthlaut AB, Smith DT, Nathanielsz PW, Ford SP. Early maternal undernutrition programs increased feed intake, altered glucose metabolism and insulin secretion, and liver function in aged female offspring. *Am J Physiol - Regul Integr Comp Physiol* (2012) 302: doi:10.1152/ajpregu.00241.2011

205. Barry JS, Davidsen ML, Limesand SW, Galan HL, Friedman JE, Regnault TRH, Hay WW. Developmental changes in ovine myocardial glucose transporters and insulin signaling following hyperthermia-induced intrauterine fetal growth restriction. *Exp Biol Med* (2006) 231:566–575. doi:10.1177/153537020623100511

206. Thorn SR, Rozance PJ, Friedman JE, Hay WW, Brown LD. Evidence for increased Cori cycle activity in IUGR fetus. *Pediatr Res* (2013) 74:481.

207. Hay WW. *Intrauterine Growth Retardation (Nestle Nutrition Workshop Series 18)*. 1st ed. , ed. J. Senterre New York: Nestle Nutrition Services (1989).

208. Krishna U, Bhalerao S. Placental insufficiency and fetal growth restriction. *J Obstet Gynecol India* (2011) 61:505–511. doi:10.1007/s13224-011-0092-x

209. BARKER DJP. In utero programming of chronic disease. *Clin Sci* (1998) 95:115. doi:10.1042/cs19980019

210. Roseboom TJ, Van der Meulen JHP, Osmond C, Barker DJP, Ravelli ACJ, Schroeder-Tanka JM, Van Montfrans GA, Michels RPJ, Bleker OP. Coronary

heart disease after prenatal exposure to the Dutch famine, 1944-45. *Heart* (2000) 84:595–598. doi:10.1136/heart.84.6.595

211. Nicholas LM, Rattanatray L, MacLaughlin SM, Ozanne SE, Kleemann DO, Walker SK, Morrison JL, Zhang S, Muhlhäusler BS, Martin-Gronert MS, et al. Differential effects of maternal obesity and weight loss in the periconceptional period on the epigenetic regulation of hepatic insulin-signaling pathways in the offspring. *FASEB J* (2013) 27:3786–3796. doi:10.1096/fj.13-227918

212. Soto SM, Blake AC, Wesolowski SR, Rozance PJ, Barthel KB, Gao B, Hetrick B, McCurdy CE, Garza NG, Hay WW, et al. Myoblast replication is reduced in the IUGR fetus despite maintained proliferative capacity in vitro. *J Endocrinol* (2017) 232:475–491. doi:10.1530/joe-16-0123

213. Brown LD. Endocrine regulation of fetal skeletal muscle growth: impact on future metabolic health. *J Endocrinol* (2014) 221:R13–R29. doi:10.1530/joe-13-0567

214. Yates DT, Clarke DS, Macko AR, Anderson MJ, Shelton LA, Nearing M, Allen RE, Rhoads RP, Limesand SW. Myoblasts from intrauterine growth-restricted sheep fetuses exhibit intrinsic deficiencies in proliferation that contribute to smaller semitendinosus myofibres. *J Physiol* (2014) 592:3113–3125. doi:10.1113/jphysiol.2014.272591

215. Yates DT, Cadaret CN, Beede KA, Riley HE, Macko AR, Anderson MJ, Camacho LE, Limesand SW. Intrauterine growth-restricted sheep fetuses exhibit smaller hindlimb muscle fibers and lower proportions of insulin-sensitive Type I fibers near term. *Am J Physiol Integr Comp Physiol* (2016) 310:R1020–R1029. doi:10.1152/ajpregu.00528.2015

216. Owens JA, Gatford KL, De Blasio MJ, Edwards LJ, McMillen IC, Fowden AL. Restriction of placental growth in sheep impairs insulin secretion but not sensitivity before birth. *J Physiol* (2007) 584:935–949. doi:10.1113/jphysiol.2007.142141

217. Owens JA, Falconer J, Robinson JS. Glucose metabolism in pregnant sheep when placental growth is restricted. *Am J Physiol Integr Comp Physiol* (2017) 257:R350–R357. doi:10.1152/ajpregu.1989.257.2.r350

218. Hay WW, Myers SA, Sparks JW, Wilkening RB, Meschia G, Battaglia FC. Glucose and Lactate Oxidation Rates in the Fetal Lamb. *Exp Biol Med* (2013) 173:553–563. doi:10.3181/00379727-173-41686

219. Regnault TRH, de Vrijer B, Galan HL, Davidsen ML, Trembler KA, Battaglia FC, Wilkening RB, Anthony R V. The relationship between transplacental O2 diffusion and placental expression of PIGF, VEGF and their receptors in a placental insufficiency model of fetal growth restriction. *J Physiol* (2003) 550:641–656. doi:10.1113/jphysiol.2003.039511

220. Regnault TRH, de Vrijer B, Galan HL, Wilkening RB, Battaglia FC, Meschia G. Development and Mechanisms of Fetal Hypoxia in Severe Fetal Growth Restriction. *Placenta* (2007) 28:714–723. doi:10.1016/j.placenta.2006.06.007

221. Thorn SR, Brown LD, Rozance PJ, Hay WW, Friedman JE. Increased hepatic glucose production in fetal sheep with intrauterine growth restriction is not suppressed by insulin. *Diabetes* (2013) 62:65–73. doi:10.2337/db11-1727

222. Barry JS, Rozance PJ, Brown LD, Anthony R V., Thornburg KL, Hay WW. Increased fetal myocardial sensitivity to insulin-stimulated glucose metabolism

during ovine fetal growth restriction. *Exp Biol Med* (2016) 241:839–847. doi:10.1177/1535370216632621

223. Muhlhausler BS, Duffield JA, Ozanne SE, Pilgrim C, Turner N, Morrison JL, McMillen IC. The transition from fetal growth restriction to accelerated postnatal growth: A potential role for insulin signalling in skeletal muscle. *J Physiol* (2009) 587:4199–4211. doi:10.1113/jphysiol.2009.173161

224. Patel MS, Korotchkina LG. Regulation of mammalian pyruvate dehydrogenase complex by phosphorylation: complexity of multiple phosphorylation sites and kinases. *Exp Mol Med* (2013) 33:191–197. doi:10.1038/emm.2001.32

225. Sun W, Xie Z, Liu Y, Zhao D, Wu Z, Zhang D, Lv H, Tang S, Jin N, Jiang H, et al. JX06 selectively inhibits pyruvate dehydrogenase kinase PDK1 by a covalent cysteine modification. *Cancer Res* (2015) 75:4923–4936. doi:10.1158/0008-5472.CAN-15-1023

226. Rardin MJ, Wiley SE, Naviaux RK, Murphy AN, Dixon JE. Monitoring phosphorylation of the pyruvate dehydrogenase complex. *Anal Biochem* (2009) 389:157–164. doi:10.1016/j.ab.2009.03.040

227. Yeaman SJ, Hutcheson ET, Roch TE, Pettit FH, Brown JR, Reed LJ, Watson DC, Dixon GH. Sites of Phosphorylation on Pyruvate Dehydrogenase from Bovine Kidney and Heart. *Biochemistry* (1978) 17:2364–2370. doi:10.1021/bi00605a017

228. Kelly AC, Bidwell CA, Chen X, MacKo AR, Anderson MJ, Limesand SW. Chronic Adrenergic Signaling Causes Abnormal RNA Expression of Proliferative Genes in Fetal Sheep Islets. *Endocrinology* (2018) 159:3565–3578. doi:10.1210/en.2018-00540

229. Livak KJ, Schmittgen TD. Analysis of relative gene expression data using real-time quantitative PCR and the 2-ΔΔCT method. *Methods* (2001) 25:402–408. doi:10.1006/meth.2001.1262

230. Bustin SA, Benes V, Garson JA, Hellemans J, Huggett J, Kubista M, Mueller R, Nolan T, Pfaffl MW, Shipley GL, et al. The MIQE guidelines: Minimum information for publication of quantitative real-time PCR experiments. *Clin Chem* (2009) 55:611–622. doi:10.1373/clinchem.2008.112797

231. Lee JH, Kim EJ, Kim DK, Lee JM, Park SB, Lee IK, Harris RA, Lee MO, Choi HS. Hypoxia Induces PDK4 Gene Expression through Induction of the Orphan Nuclear Receptor ERRγ. *PLoS One* (2012) 7: doi:10.1371/journal.pone.0046324

232. Connaughton S, Chowdhury F, Attia RR, Song S, Zhang Y, Elam MB, Cook GA, Park EA. Regulation of pyruvate dehydrogenase kinase isoform 4 (PDK4) gene expression by glucocorticoids and insulin. *Mol Cell Endocrinol* (2010) 315:159–167. doi:10.1016/j.mce.2009.08.011

233. Cairns RA, Papandreou I, Sutphin PD, Denko NC. Metabolic targeting of hypoxia and HIF1 in solid tumors can enhance cytotoxic chemotherapy. *Proc Natl Acad Sci* (2007) 104:9445–9450. doi:10.1073/pnas.0611662104

234. Dupuy F, Tabariès S, Andrzejewski S, Dong Z, Blagih J, Annis MG, Omeroglu A, Gao D, Leung S, Amir E, et al. PDK1-dependent metabolic reprogramming dictates metastatic potential in breast cancer. *Cell Metab* (2015) 22:577–589. doi:10.1016/j.cmet.2015.08.007

235. Semenza GL. Oxygen-dependent regulation of mitochondrial respiration by hypoxia-inducible factor 1. *Biochem J* (2007) 405:1–9. doi:10.1042/BJ20070389

236. Kim JW, Tchernyshyov I, Semenza GL, Dang C V. HIF-1-mediated expression of pyruvate dehydrogenase kinase: A metabolic switch required for cellular adaptation to hypoxia. *Cell Metab* (2006) 3:177–185. doi:10.1016/j.cmet.2006.02.002

237. Balaban RS, Nemoto S, Finkel T. Mitochondria, oxidants, and aging. *Cell* (2005) 120:483–495. doi:10.1016/j.cell.2005.02.001

238. Yankovskaya V, Horsefield R, Törnroth S, Luna-Chavez C, Miyoshi H, Léger C, Byrne B, Cecchini G, Iwata S. Architecture of succinate dehydrogenase and reactive oxygen species generation. *Science (80-)* (2003) 299:700–704. doi:10.1126/science.1079605

239. Papandreou I, Cairns RA, Fontana L, Lim AL, Denko NC. HIF-1 mediates adaptation to hypoxia by actively downregulating mitochondrial oxygen consumption. *Cell Metab* (2006) 3:187–197. doi:10.1016/j.cmet.2006.01.012

240. Orgeig S, McGillick E V., Botting KJ, Zhang S, McMillen IC, Morrison JL. Increased lung prolyl hydroxylase and decreased glucocorticoid receptor are related to decreased surfactant protein in the growth-restricted sheep fetus. *Am J Physiol Cell Mol Physiol* (2015) 309:L84–L97. doi:10.1152/ajplung.00275.2014

241. McGillick E V., Orgeig S, Morrison JL. Regulation of lung maturation by prolyl hydroxylase domain inhibition in the lung of the normally grown and placentally restricted fetus in late gestation. *Am J Physiol Integr Comp Physiol* (2016) 310:R1226–R1243. doi:10.1152/ajpregu.00469.2015

242. Mcgillick E V., Orgeig S, Morrison JL. Structural and molecular regulation of lung maturation by intratracheal vascular endothelial growth factor administration in the

normally grown and placentally restricted fetus. *J Physiol* (2016) 594:1399–1420. doi:10.1113/JP271113

243. Botting KJ, Caroline McMillen I, Forbes H, Nyengaard JR, Morrison JL. Chronic hypoxemia in late gestation decreases cardiomyocyte number but does not change expression of hypoxia-responsive genes. *J Am Heart Assoc* (2014) 3: doi:10.1161/JAHA.113.000531

244. Ginouves A, Ilc K, Macias N, Pouyssegur J, Berra E. PHDs overactivation during chronic hypoxia "desensitizes" HIF and protects cells from necrosis. *Proc Natl Acad Sci* (2008) 105:4745–4750. doi:10.1073/pnas.0705680105

245. Jeoung NH. Pyruvate dehydrogenase kinases: Therapeutic targets for diabetes and cancers. *Diabetes Metab J* (2015) 39:188–197. doi:10.4093/dmj.2015.39.3.188

246. Jeong JY, Jeoung NH, Park KG, Lee IK. Transcriptional regulation of pyruvate dehydrogenase kinase. *Diabetes Metab J* (2012) 36:328–335. doi:10.4093/dmj.2012.36.5.328

247. Huang B, Wu P, Bowker-Kinley MM, Harris RA. Regulation of pyruvate dehydrogenase kinase expression by peroxisome proliferator-activated receptor-α ligands, glucocorticoids, and insulin. *Diabetes* (2002) 51:276–283. doi:10.2337/diabetes.51.2.276

248. Wu P, Inskeep K, Bowker-Kinley MM, Popov KM, Harris RA. Mechanism responsible for inactivation of skeletal muscle pyruvate dehydrogenase complex in starvation and diabetes. *Diabetes* (1999) 48:1593–1599. doi:10.2337/diabetes.48.8.1593

249. Pilegaard H, Darrell Neufer P. Transcriptional regulation of pyruvate

dehydrogenase kinase 4 in skeletal muscle during and after exercise. *Proc Nutr Soc* (2004) 63:221–226. doi:10.1079/pns2004345

250. Tao R, Xiong X, Harris RA, White MF, Dong XC. Genetic Inactivation of Pyruvate Dehydrogenase Kinases Improves Hepatic Insulin Resistance Induced Diabetes. *PLoS One* (2013) 8: doi:10.1371/journal.pone.0071997

251. Pilegaard H, Saltin B, Neufer PD. Effect of short-term fasting and refeeding on transcriptional regulation of metabolic genes in human skeletal muscle. *Diabetes* (2003) 52:657–662. doi:10.2337/diabetes.52.3.657

252. Pilegaard H, Birk JB, Sacchetti M, Mourtzakis M, Hardie DG, Stewart G, Neufer PD, Saltin B, Van Hall G, Wojtaszewski JFP. PDH-E1α dephosphorylation and activation in human skeletal muscle during exercise: Effect of intralipid infusion. *Diabetes* (2006) 55:3020–3027. doi:10.2337/db06-0152

253. Park S, Jeon JH, Min BK, Ha CM, Thoudam T, Park BY, Lee IK. Role of the pyruvate dehydrogenase complex in metabolic remodeling: Differential pyruvate dehydrogenase complex functions in metabolism. *Diabetes Metab J* (2018) 42:270–281. doi:10.4093/dmj.2018.0101

254. Caruso M, Maitan MA, Bifulco G, Miele C, Vigliotta G, Oriente F, Formisano P, Beguinot F. Activation and Mitochondrial Translocation of Protein Kinase Cδ Are Necessary for Insulin Stimulation of Pyruvate Dehydrogenase Complex Activity in Muscle and Liver Cells. *J Biol Chem* (2001) 276:45088–45097. doi:10.1074/jbc.M105451200

255. García-Cazorla A, Rabier D, Touati G, Chadefaux-Vekemans B, Marsac C, De Lonlay P, Saudubray JM. Pyruvate carboxylase deficiency: Metabolic

characteristics and new neurological aspects. *Ann Neurol* (2006) 59:121–127. doi:10.1002/ana.20709

256. Waterhouse C, Keilson J. Cori cycle activity in man. *J Clin Invest* (1969) 48:2359–2366. doi:10.1172/JCI106202

257. Wang YX, Zhang CL, Yu RT, Cho HK, Nelson MC, Bayuga-Ocampo CR, Ham J, Kang H, Evans RM. Regulation of muscle fiber type and running endurance by PPARδ. *PLoS Biol* (2004) 2: doi:10.1371/journal.pbio.0020294

258. Venhoff N, Lebrecht D, Pfeifer D, Venhoff AC, Bissé E, Kirschner J, Walker UA. Muscle-fiber transdifferentiation in an experimental model of respiratory chain myopathy. *Arthritis Res Ther* (2012) 14: doi:10.1186/ar4076

259. SUGDEN MC, KRAUS A, HARRIS RA, HOLNESS MJ. Fibre-type specific modification of the activity and regulation of skeletal muscle pyruvate dehydrogenase kinase (PDK) by prolonged starvation and refeeding is associated with targeted regulation of PDK isoenzyme 4 expression. *Biochem J* (2015) 346:651–657. doi:10.1042/bj3460651

260. Peters SJ, Harris RA, Heigenhauser GJF, Spriet LL. Muscle fiber type comparison of PDH kinase activity and isoform expression in fed and fasted rats. *Am J Physiol Integr Comp Physiol* (2017) 280:R661–R668. doi:10.1152/ajpregu.2001.280.3.r661

261. Warner MJ, Ozanne SE. Mechanisms involved in the developmental programming of adulthood disease. *Biochem J* (2010) 427:333–347. doi:10.1042/BJ20091861

262. Soothill PW, Nicolaides KH, Campbell S. Prenatal asphyxia, hyperlacticaemia, hypoglycaemia, and erythroblastosis in growth retarded fetuses. *Br Med J (Clin*

Res Ed) (1987) 294:1051–1053. doi:10.1136/bmj.294.6579.1051

263. Pardi G, Cetin I, Marconi AM, Lanfranchi A, Bozzetti P, Ferrazzi E, Buscaglia M, Battaglia FC. Diagnostic value of blood sampling in fetuses with growth retardation. *Obstet Gynecol Surv* (1993) 48:601–602. doi:10.1097/00006254-199309000-00008

264. Osmond C, Barker DJP. Fetal, infant, and childhood growth are predictors of coronary heart disease, diabetes, and hypertension in adult men and women. *Environ Health Perspect* (2000) 108:545–553. doi:10.2307/3454545

265. Barker DJP, Eriksson JG, Forsén T, Osmond C. Fetal origins of adult disease: Strength of effects and biological basis. *Int J Epidemiol* (2002) 31:1235–1239. doi:10.1093/ije/31.6.1235

266. Roseboom TJ. Epidemiological evidence for the developmental origins of health and disease: Effects of prenatal undernutrition in humans. *J Endocrinol* (2019) 242:T135–T144. doi:10.1530/JOE-18-0683

267. Padoan A, Rigano S, Ferrazzi E, Beaty BL, Battaglia FC, Galan HL. Differences in fat and lean mass proportions in normal and growth-restricted fetuses. in *American Journal of Obstetrics and Gynecology*, 1459–1464. doi:10.1016/j.ajog.2004.06.045

268. Yates DT, Camacho LE, Kelly AC, Steyn L V., Davis MA, Antolic AT, Anderson MJ, Goyal R, Allen RE, Papas KK, et al. Postnatal β2 adrenergic treatment improves insulin sensitivity in lambs with IUGR but not persistent defects in pancreatic islets or skeletal muscle. *J Physiol* (2019) 597:5835–5858. doi:10.1113/JP278726

269. Pendleton AL, Humphreys LR, Davis MA, Camacho LE, Anderson MJ, Limesand SW. Increased pyruvate dehydrogenase activity in skeletal muscle of growth-restricted ovine fetuses. *Am J Physiol Integr Comp Physiol* (2019) 317:R513–R520. doi:10.1152/ajpregu.00106.2019

270. Owen OE, Kalhan SC, Hanson RW. The key role of anaplerosis and cataplerosis for citric acid cycle function. *J Biol Chem* (2002) 277:30409–30412. doi:10.1074/jbc.R200006200

271. Akram M. Citric Acid Cycle and Role of its Intermediates in Metabolism. *Cell Biochem Biophys* (2014) 68:475–478. doi:10.1007/s12013-013-9750-1

272. Kamzolova S V., Shishkanova N V., Morgunov IG, Finogenova T V. Oxygen requirements for growth and citric acid production of Yarrowia lipolytica. *FEMS Yeast Res* (2003) 3:217–222. doi:10.1016/S1567-1356(02)00188-5

273. Zhang Y, Marcillat O, Giulivi C, Ernster L, Davies KJA. The oxidative inactivation of mitochondrial electron transport chain components and ATPase. *J Biol Chem* (1990) 265:16330–16336.

274. Mason HS. Mechanisms of oxygen metabolism. *Science (80-)* (1957) 125:1185–1188. doi:10.1126/science.125.3259.1185

275. Cerretelli P, Gelfi C. Energy metabolism in hypoxia: Reinterpreting some features of muscle physiology on molecular grounds. *Eur J Appl Physiol* (2011) 111:421–432. doi:10.1007/s00421-010-1399-5

276. Senthilnathan P, Padmavathi R, Magesh V, Sakthisekaran D. Modulation of TCA cycle enzymes and electron transport chain systems in experimental lung cancer. *Life Sci* (2006) 78:1010–1014. doi:10.1016/j.lfs.2005.06.005

277. Bubber P, Hartounian V, Gibson GE, Blass JP. Abnormalities in the tricarboxylic acid (TCA) cycle in the brains of schizophrenia patients. *Eur Neuropsychopharmacol* (2011) 21:254–260. doi:10.1016/j.euroneuro.2010.10.007

278. Fernie AR, Carrari F, Sweetlove LJ. Respiratory metabolism: Glycolysis, the TCA cycle and mitochondrial electron transport. *Curr Opin Plant Biol* (2004) 7:254–261. doi:10.1016/j.pbi.2004.03.007

279. Capitanio D, Fania C, Torretta E, Viganò A, Moriggi M, Bravatà V, Caretti A, Levett DZH, Grocott MPW, Samaja M, et al. TCA cycle rewiring fosters metabolic adaptation to oxygen restriction in skeletal muscle from rodents and humans. *Sci Rep* (2017) 7: doi:10.1038/s41598-017-10097-4

280. Aretz I, Hardt C, Wittig I, Meierhofer D. An impaired respiratory electron chain triggers down-regulation of the energy metabolism and de-ubiquitination of solute carrier amino acid transporters. *Mol Cell Proteomics* (2016) 15:1526–1538. doi:10.1074/mcp.M115.053181

281. Kilkenny C, Browne WJ, Cuthill IC, Emerson M, Altman DG. Improving bioscience research reporting: The arrive guidelines for reporting animal research. *PLoS Biol* (2010) 8: doi:10.1371/journal.pbio.1000412

282. Johnson MA, Polgar J, Weightman D, Appleton D. Data on the distribution of fibre types in thirty-six human muscles. An autopsy study. *J Neurol Sci* (1973) 18:111–129. doi:10.1016/0022-510X(73)90023-3

283. Dahmane R, Djordjevič S, Smerdu V. Adaptive potential of human biceps femoris muscle demonstrated by histochemical, immunohistochemical and mechanomyographical methods. *Med Biol Eng Comput* (2006) 44:999–1006.

doi:10.1007/s11517-006-0114-5

284. Gouzi F, Maury J, Molinari N, Pomiès P, Mercier J, Préfaut C, Hayot M. Reference values for vastus lateralis fiber size and type in healthy subjects over 40 years old: A systematic review and metaanalysis. *J Appl Physiol* (2013) 115:346–354. doi:10.1152/japplphysiol.01352.2012

285. Frezza C, Cipolat S, Scorrano L. Organelle isolation: Functional mitochondria from mouse liver, muscle and cultured filroblasts. *Nat Protoc* (2007) 2:287–295. doi:10.1038/nprot.2006.478

286. Papas KK, Pisania A, Wu H, Weir GC, Colton CK. A stirred microchamber for oxygen consumption rate measurements with pancreatic islets. *Biotechnol Bioeng* (2007) 98:1071–1082. doi:10.1002/bit.21486

287. Brand MD, Nicholls DG. Assessing mitochondrial dysfunction in cells. *Biochem J* (2011) 435:297–312. doi:10.1042/BJ20110162

288. Parker SS, Krantz J, Kwak EA, Barker NK, Deer CG, Lee NY, Mouneimne G, Langlais PR. Insulin induces microtubule stabilization and regulates the microtubule plus-end tracking protein network in adipocytes. *Mol Cell Proteomics* (2019) 18:1363–1381. doi:10.1074/mcp.RA119.001450

289. Binder JX, Pletscher-Frankild S, Tsafou K, Stolte C, O'Donoghue SI, Schneider R, Jensen LJ. COMPARTMENTS: Unification and visualization of protein subcellular localization evidence. *Database* (2014) 2014: doi:10.1093/database/bau012

290. Tyanova S, Temu T, Sinitcyn P, Carlson A, Hein MY, Geiger T, Mann M, Cox J. The Perseus computational platform for comprehensive analysis of (prote)omics

data. *Nat Methods* (2016) 13:731–740. doi:10.1038/nmeth.3901

291. Ashburner M, Ball CA, Blake JA, Botstein D, Butler H, Cherry JM, Davis AP, Dolinski K, Dwight SS, Eppig JT, et al. Gene ontology: Tool for the unification of biology. *Nat Genet* (2000) 25:25–29. doi:10.1038/75556

292. Carbon S, Douglass E, Dunn N, Good B, Harris NL, Lewis SE, Mungall CJ, Basu S, Chisholm RL, Dodson RJ, et al. The Gene Ontology Resource: 20 years and still GOing strong. *Nucleic Acids Res* (2019) 47:D330–D338. doi:10.1093/nar/gky1055

293. Huang DW, Sherman BT, Lempicki RA. Systematic and integrative analysis of large gene lists using DAVID bioinformatics resources. *Nat Protoc* (2009) 4:44–57. doi:10.1038/nprot.2008.211

294. Huang DW, Sherman BT, Lempicki RA. Bioinformatics enrichment tools: Paths toward the comprehensive functional analysis of large gene lists. *Nucleic Acids Res* (2009) 37:1–13. doi:10.1093/nar/gkn923

295. Kanehisa M. KEGG: Kyoto Encyclopedia of Genes and Genomes. *Nucleic Acids Res* (2000) 28:27–30. doi:10.1093/nar/28.1.27

296. Kanehisa M, Goto S, Sato Y, Kawashima M, Furumichi M, Tanabe M. Data, information, knowledge and principle: Back to metabolism in KEGG. *Nucleic Acids Res* (2014) 42: doi:10.1093/nar/gkt1076

297. Kanehisa M, Goto S, Sato Y, Furumichi M, Tanabe M. KEGG for integration and interpretation of large-scale molecular data sets. *Nucleic Acids Res* (2012) 40: doi:10.1093/nar/gkr988

298. Darby JRT, Sorvina A, Bader CA, Lock MC, Soo JY, Holman SL, Seed M, Kuchel T, Brooks DA, Plush SE, et al. Detecting metabolic differences in fetal and

adult sheep adipose and skeletal muscle tissues. *J Biophotonics* (2020) 13: doi:10.1002/jbio.201960085

299. Morrison JL. Sheep models of intrauterine growth restriction: Fetal adaptations and consequences. *Clin Exp Pharmacol Physiol* (2008) 35:730–743. doi:10.1111/j.1440-1681.2008.04975.x

300. Tello D, Balsa E, Acosta-Iborra B, Fuertes-Yebra E, Elorza A, Ordóñez Á, Corral-Escariz M, Soro I, López-Bernardo E, Perales-Clemente E, et al. Induction of the mitochondrial NDUFA4L2 protein by HIF-1α decreases oxygen consumption by inhibiting complex i activity. *Cell Metab* (2011) 14:768–779. doi:10.1016/j.cmet.2011.10.008

301. Lai RKH, Xu IMJ, Chiu DKC, Tse APW, Wei LL, Law CT, Lee D, Wong CM, Wong MP, Ng IOL, et al. NDUFA4L2 fine-tunes oxidative stress in hepatocellular carcinoma. *Clin Cancer Res* (2016) 22:3105–3117. doi:10.1158/1078-0432.CCR-15-1987

302. Chaillou T, Hynynen H, Ferreira D, Pironti G, Kenne E, Andersson DC, Ruas JL, Tavi P, Lanner JT. NDUFA4L2 – Connecting Metabolic Signals and Mitochondrial Function in Cardiac and Skeletal Muscle. *Free Radic Biol Med* (2016) 100:S186. doi:10.1016/j.freeradbiomed.2016.10.511

303. Vacanti NM, Divakaruni AS, Green CR, Parker SJ, Henry RR, Ciaraldi TP, Murphy AN, Metallo CM. Regulation of substrate utilization by the mitochondrial pyruvate carrier. *Mol Cell* (2014) 56:425–435. doi:10.1016/j.molcel.2014.09.024

304. Cetin I, Radaelli T, Taricco E, Giovannini N, Alvino G, Pardi G. The endocrine and metabolic profile of the growth-retarded fetus. *J Pediatr Endocrinol Metab*

(2001) 14:1497–1505.

305. Nicolini U, Hubinont C, Santolaya J, Fisk NM, Coe AM, Rodeck CH. Maternal-fetal glucose gradient in normal pregnancies and in pregnancies complicated by alloimmunization and fetal growth retardation. *Am J Obstet Gynecol* (1989) 161:924–927. doi:10.1016/0002-9378(89)90753-9

306. Sharma L, Lu J, Bai Y. Mitochondrial Respiratory Complex I: Structure, Function and Implication in Human Diseases. *Curr Med Chem* (2009) 16:1266–1277. doi:10.2174/092986709787846578

307. Fuhrmann DC, Brüne B. Mitochondrial composition and function under the control of hypoxia. *Redox Biol* (2017) 12:208–215. doi:10.1016/j.redox.2017.02.012

308. Kotlyar AB, Vinogradov AD. Slow active/inactive transition of the mitochondrial NADH-ubiquinone reductase. *BBA - Bioenerg* (1990) 1019:151–158. doi:10.1016/0005-2728(90)90137-S

309. Babot M, Birch A, Labarbuta P, Galkin A. Characterisation of the active/de-active transition of mitochondrial complex i. *Biochim Biophys Acta - Bioenerg* (2014) 1837:1083–1092. doi:10.1016/j.bbabio.2014.02.018

310. Galkin A, Moncada S. Modulation of the conformational state of mitochondrial complex I as a target for therapeutic intervention. *Interface Focus* (2017) 7: doi:10.1098/rsfs.2016.0104

311. Zickermann V, Kerscher S, Zwicker K, Tocilescu MA, Radermacher M, Brandt U. Architecture of complex I and its implications for electron transfer and proton pumping. *Biochim Biophys Acta - Bioenerg* (2009) 1787:574–583.

doi:10.1016/j.bbabio.2009.01.012

312. Karamanlidis G, Lee CF, Garcia-Menendez L, Kolwicz SC, Suthammarak W, Gong G, Sedensky MM, Morgan PG, Wang W, Tian R. Mitochondrial complex i deficiency increases protein acetylation and accelerates heart failure. *Cell Metab* (2013) 18:239–250. doi:10.1016/j.cmet.2013.07.002

313. Kammermeier H. Phosphorylation Potential and Free Energy of ATP. *Adv Organ Biol* (1998) 4:159–169. doi:10.1016/S1569-2590(08)60085-3

314. Korzeniewski B. What regulates respiration in mitochondria? *Biochem Mol Biol Int* (1996) 39:415–419. doi:10.1080/15216549600201451

315. Giesen J, Kammermeier H. Relationship of phosphorylation potential and oxygen consumption in isolated perfused rat hearts. *J Mol Cell Cardiol* (1980) 12:891–907. doi:10.1016/0022-2828(80)90058-9

316. Berg JM, Tymoczko JL, Stryer L. *The Regulation of Cellular Respiration Is Governed Primarily by the Need for ATP*. (2002).

317. Kien CL, Rohrbaugh DK, Burke JF, Young VR. Whole body protein synthesis in relation to basal energy expenditure in healthy children and in children recovering from burn injury. *Pediatr Res* (1978) 12:211–216. doi:10.1203/00006450-197803000-00010

318. Lindqvist LM, Tandoc K, Topisirovic I, Furic L. Cross-talk between protein synthesis, energy metabolism and autophagy in cancer. *Curr Opin Genet Dev* (2018) 48:104–111. doi:10.1016/j.gde.2017.11.003

319. Bier D. *The Role of Protein and Amino Acids in Sustaining and Enhancing Performance*. Washington D.C.: National Academies Press (1999).

doi:10.17226/9620

320. BURTON K, KREBS HA. The free-energy changes associated with the individual steps of the tricarboxylic acid cycle, glycolysis and alcoholic fermentation and with the hydrolysis of the pyrophosphate groups of adenosinetriphosphate. *Biochem J* (1953) 54:94–107. doi:10.1042/bj0540094

321. Herzig S, Raemy E, Montessuit S, Veuthey JL, Zamboni N, Westermann B, Kunji ERS, Martinou JC. Identification and functional expression of the mitochondrial pyruvate carrier. *Science (80-)* (2012) 336:93–96. doi:10.1126/science.1218530

322. Bricker DK, Taylor EB, Schell JC, Orsak T, Boutron A, Chen YC, Cox JE, Cardon CM, Van Vranken JG, Dephoure N, et al. A mitochondrial pyruvate carrier required for pyruvate uptake in yeast, Drosophila, and humans. *Science (80-)* (2012) 336:96–100. doi:10.1126/science.1218099

323. Nagampalli RSK, Quesnãy JEN, Adamoski D, Islam Z, Birch J, Sebinelli HG, Girard RMBM, Ascencõ CFR, Fala AM, Pauletti BA, et al. Human mitochondrial pyruvate carrier 2 as an autonomous membrane transporter. *Sci Rep* (2018) 8: doi:10.1038/s41598-018-21740-z

324. Abd El-Wahed MA, El-Farghali OG, ElAbd HSA, El-Desouky ED, Hassan SM. Metabolic derangements in IUGR neonates detected at birth using UPLC-MS. *Egypt J Med Hum Genet* (2017) 18:281–287. doi:10.1016/j.ejmhg.2016.12.002

325. Hales CN, Barker DJP. Type 2 (non-insulin-dependent) diabetes mellitus: the thrifty phenotype hypothesis. *Int J Epidemiol* (2013) 42:1215–1222. doi:10.1093/ije/dyt133

326. Ylihärsilä H, Kajantie E, Osmond C, Forsén T, Barker DJP, Eriksson JG. Birth

size, adult body composition and muscle strength in later life. *Int J Obes* (2007) 31:1392–1399. doi:10.1038/sj.ijo.0803612

327. GRAUAUG A. Neonatal Hypoglycaemia. *Med J Aust* (1965) 1:455–459. doi:10.5694/j.1326-5377.1965.tb71817.x

328. SANN L, RUITTON A, MATHIEU M, LASNE Y. Effect of Intravenous Hydrocortisone Administration on Glucose Homeostasis in Small for Gestational Age Infants. *Acta Pædiatrica* (1979) 68:113–118. doi:10.1111/j.1651-2227.1979.tb04970.x

329. Haymond MW, Karl IE, Pagliara AS. Increased Gluconeogenic Substrates in the Small-for-Gestational-Age Infant. *N Engl J Med* (1974) 291:322–328. doi:10.1056/NEJM197408152910702

330. Williams PR, Fiser RH, Sperling MA, oh W. Effects of Oral Alanine Feeding on Blood Glucose, Plasma Glucagon and Insulin Concentrations in Small-for-Gestational-Age Infants. *N Engl J Med* (1975) 292:612–614. doi:10.1056/NEJM197503202921204

331. Khouzami VA, Ginsburg DS, Daikoku NH, Johnson JWC. The glucose tolerance test as a means of identifying intrauterine growth retardation. *Am J Obstet Gynecol* (1981) 139:423–426. doi:10.1016/0002-9378(81)90319-7

332. Battaglia FC, Meschia G. Principal substrates of fetal metabolism. *Physiol Rev* (1978) 58:499–527. doi:10.1152/physrev.1978.58.2.499

333. Regnault TRH, Galan HL, Parker TA, Anthony R V. Placental development in normal and compromised pregnancies - A review. *Placenta* (2002) 23: doi:10.1053/plac.2002.0792

334. Carlyle A. An integration of the total oxygen consumption of the sheep foetus from that of the tissues. *J Physiol* (1948) 107:355–364. doi:10.1113/jphysiol.1948.sp004280

335. McCoard SA, McNabb WC, Peterson SW, McCutcheon SN, Harris PM. Muscle growth, cell number, type and morphometry in single and twin fetal lambs during mid to late gestation. *Reprod Fertil Dev* (2000) 12:319–327. doi:10.1071/rd99059

336. Gimondo P, Mirk P, La Bella A, Messina G, Pizzi C. Sonographic estimation of fetal liver weight: An additional biometric parameter for assessment of fetal growth. *J Ultrasound Med* (1995) 14:327–333. doi:10.7863/jum.1995.14.5.327

337. MITROPOULOS G, SCURRY J, CUSSEN L. Organ weight/bodyweight ratios: Growth rates of fetal organs in the latter half of pregnancy with a simple method for calculating mean organ weights. *J Paediatr Child Health* (1992) 28:236–239. doi:10.1111/j.1440-1754.1992.tb02653.x

338. Houin SS, Rozance PJ, Brown LD, Hay WW, Wilkening RB, Thorn SR. Coordinated changes in hepatic amino acid metabolism and endocrine signals support hepatic glucose production during fetal hypoglycemia. *Am J Physiol - Endocrinol Metab* (2015) 308:E306–E314. doi:10.1152/ajpendo.00396.2014

339. Peleg D, Kennedy CM, Hunter SK. Intrauterine growth restriction: Identification and management. *Am Fam Physician* (1998) 58:453–460.

340. Vasu V, Thomas EL, Durighel G, Hyde MJ, Bell JD, Modi N. Early nutritional determinants of intrahepatocellular lipid deposition in preterm infants at term age. *Int J Obes* (2013) 37:500–504. doi:10.1038/ijo.2012.213

341. Thomas EL, Parkinson JR, Hyde MJ, Yap IKS, Holmes E, Doré CJ, Bell JD, Modi

N. Aberrant adiposity and ectopic lipid deposition characterize the adult phenotype of the preterm infant. *Pediatr Res* (2011) 70:507–512. doi:10.1203/PDR.0b013e31822d7860

342. Cho WK, Suh BK. Catch-up growth and catch-up fat in children born small for gestational age. *Korean J Pediatr* (2016) 59:1–7. doi:10.3345/kjp.2016.59.1.1

343. Barker DJP, Martyn CN, Osmond C, Hales CN, Fall CHD. Growth in utero and serum cholesterol concentrations in adult life. *Br Med J* (1993) 307:1524–1527. doi:10.1136/bmj.307.6918.1524

344. Labayen I, Moreno LA, Ruiz JR, González-Gross M, Wärnberg J, Breidenassel C, Ortega FB, Marcos A, Bueno M, Marcos A, et al. Small birth weight and later body composition and fat distribution in adolescents: The AVENA study. *Obesity* (2008) 16:1680–1686. doi:10.1038/oby.2008.258

345. Brown LD, Kohn JR, Rozance PJ, Hay WW, Wesolowski SR. Exogenous amino acids suppress glucose oxidation and potentiate hepatic glucose production in late gestation fetal sheep. *Am J Physiol - Regul Integr Comp Physiol* (2017) 312:R654–R663. doi:10.1152/ajpregu.00502.2016

346. Reynafarje BD, Ferreira J. Oxidative phosphorylation: Kinetic and thermodynamic correlation between electron flow, proton translocation, oxygen consumption and ATP synthesis under close to in vivo concentrations of oxygen. *Int J Med Sci* (2008) 5:143–151. doi:10.7150/ijms.5.143

347. Wheaton WW, Chandel NS. Hypoxia. 2. Hypoxia regulates cellular metabolism. *Am J Physiol - Cell Physiol* (2011) 300: doi:10.1152/ajpcell.00485.2010

348. García-Ruiz C, Baulies A, Mari M, García-Rovés PM, Fernandez-Checa JC.

Mitochondrial dysfunction in non-alcoholic fatty liver disease and insulin resistance: Cause or consequence? *Free Radic Res* (2013) 47:854–868. doi:10.3109/10715762.2013.830717

349. Salam RA, Das JK, Bhutta ZA. Impact of intrauterine growth restriction on long-term health. *Curr Opin Clin Nutr Metab Care* (2014) 17:249–254. doi:10.1097/MCO.0000000000000051

350. Gatford KL, Simmons RA, De Blasio MJ, Robinson JS, Owens JA. Review: Placental Programming of Postnatal Diabetes and Impaired Insulin Action after IUGR. *Placenta* (2010) 31: doi:10.1016/j.placenta.2009.12.015

351. Peterside IE, Selak MA, Simmons RA. Impaired oxidative phosphorylation in hepatic mitochondria in growth-retarded rats. *Am J Physiol - Endocrinol Metab* (2003) 285: doi:10.1152/ajpendo.00437.2002

352. Pendleton AL, Humphreys LR, Davis MA, Camacho LE, Anderson MJ, Limesand SW. Increased pyruvate dehydrogenase activity in skeletal muscle of growth-restricted ovine fetuses. *Am J Physiol Integr Comp Physiol* (2019) doi:10.1152/ajpregu.00106.2019

353. Pendleton AL, Antolic AT, Kelly AC, Davis MA, Camacho LE, Doubleday K, Anderson MJ, Langlais PR, Lynch RM, Limesand SW. Lower Oxygen Consumption and Complex I Activity in Mitochondria Isolated from Skeletal Muscle of Fetal Sheep with Intrauterine Growth Restriction. *Am J Physiol Metab* (2020) doi:10.1152/ajpendo.00057.2020

354. Kushnareva Y, Murphy AN, Andreyev A. Complex I-mediated reactive oxygen species generation: Modulation by cytochrome c and NAD(P)+ oxidation-

reduction state. *Biochem J* (2002) 368:545–553. doi:10.1042/BJ20021121

355. Stremming J, Jansson T, Powell TL, Rozance PJ, Brown LD. Reduced Na+K+-ATPase activity may reduce amino acid uptake in intrauterine growth restricted fetal sheep muscle despite unchanged ex vivo amino acid transporter activity. *J Physiol* (2020) doi:10.1113/JP278933

356. Regnault TRH, De Vrijer B, Galan HL, Wilkening RB, Battaglia FC, Meschia G. Umbilical uptakes and transplacental concentration ratios of amino acids in severe fetal growth restriction. *Pediatr Res* (2013) 73:602–611. doi:10.1038/pr.2013.30

357. Jones AK, Brown LD, Rozance PJ, Serkova NJ, Hay WW, Friedman JE, Wesolowski SR. Differential effects of intrauterine growth restriction and a hypersinsulinemic-isoglycemic clamp on metabolic pathways and insulin action in the fetal liver. *Am J Physiol Regul Integr Comp Physiol* (2019) doi:10.1152/ajpregu.00359.2018

358. Sparks JW, Hay WW, Meschia G, Battaglia FC. Partition of maternal nutrients to the placenta and fetus in the sheep. *Eur J Obstet Gynecol Reprod Biol* (1983) 14:331–340. doi:10.1016/0028-2243(83)90009-6

359. Thorn SR, Rozance PJ, Brown LD, Hay WW. The intrauterine growth restriction phenotype: Fetal adaptations and potential implications for later life insulin resistance and diabetes. *Semin Reprod Med* (2011) 29:225–236. doi:10.1055/s-0031-1275516

360. Limesand SW, Rozance PJ, Zerbe GO, Hutton JC, Hay WW. Attenuated insulin release and storage in fetal sheep pancreatic islets with intrauterine growth restriction. *Endocrinology* (2006) 147:1488–1497. doi:10.1210/en.2005-0900

361. Farrag HM, Nawrath LM, Healey JE, Dorcus EJ, Rapoza RE, Oh W, Cowett RM. Persistent glucose production and greater peripheral sensitivity to insulin in the neonate vs. the adult. *Am J Physiol - Endocrinol Metab* (1997) doi:10.1152/ajpendo.1997.272.1.e86

362. Marconi AM, Battaglia FC, Meschia G, Sparks JW. A comparison of amino acid arteriovenous differences across the liver and placenta of the fetal lamb. *Am J Physiol - Endocrinol Metab* (1989) 257: doi:10.1152/ajpendo.1989.257.6.e909

363. Teng C, Battaglia FC, Meschia G, Narkewicz MR, Wilkening RB. Fetal hepatic and umbilical uptakes of glucogenic substrates during a glucagon-somatostatin infusion. *Am J Physiol - Endocrinol Metab* (2002) 282: doi:10.1152/ajpendo.00248.2001

364. Sharma A, Oonthonpan L, Sheldon RD, Rauckhorst AJ, Zhu Z, Tompkins SC, Cho K, Grzesik WJ, Gray LR, Scerbo DA, et al. Impaired skeletal muscle mitochondrial pyruvate uptake rewires glucose metabolism to drive whole-body leanness. *Elife* (2019) 8: doi:10.7554/eLife.45873

365. Jansson T, Scholtbach V, Powell TL. Placental transport of leucine and lysine is reduced in intrauterine growth restriction. *Pediatr Res* (1998) doi:10.1203/00006450-199810000-00011

366. Anderson AH, Fennessey P V., Meschia G, Wilkening RB, Battaglia FC. Placental transport of threonine and its utilization in the normal and growth-restricted fetus. *Am J Physiol - Endocrinol Metab* (1997) doi:10.1152/ajpendo.1997.272.5.e892

367. Ross JC, Fennessey P V., Wilkening RB, Battaglia FC, Meschia G. Placental transport and fetal utilization of leucine in a model of fetal growth retardation. *Am*

J Physiol - Endocrinol Metab (1996) 270:E491–E503. doi:10.1152/ajpendo.1996.270.3.e491

368. Paolini CL, Marconi AM, Ronzoni S, Di Noio M, Fennessey P V., Pardi G, Battaglia FC. Placental transport of leucine, phenylalanine, glycine, and proline in intrauterine growth-restricted pregnancies. *J Clin Endocrinol Metab* (2001) doi:10.1210/jcem.86.11.8036

369. Long B, Yin C, Fan Q, Yan G, Wang Z, Li X, Chen C, Yang X, Liu L, Zheng Z, et al. Global Liver Proteome Analysis Using iTRAQ Reveals AMPK-mTOR-Autophagy Signaling Is Altered by Intrauterine Growth Restriction in Newborn Piglets. *J Proteome Res* (2016) 15:1262–1273. doi:10.1021/acs.jproteome.6b00001

370. De Boo HA, Harding JE. Protein metabolism in preterm infants with particular reference to intrauterine growth restriction. *Arch Dis Child Fetal Neonatal Ed* (2007) 92: doi:10.1136/adc.2006.099697

371. De Boo HA, Van Zijl PL, Lafeber HN, Harding JE. Urea production and arginine metabolism are reduced in the growth restricted ovine foetus. *Animal* (2007) 1:699–707. doi:10.1017/S1751731107710273

372. Visser HKA ed. *Nutrition and Metabolism of the Fetus and Infant*. Dordrecht: Springer Netherlands (1979). doi:10.1007/978-94-009-9318-1

373. Liu C, Lin G, Wang X, Wang T, Wu G, Li D, Wang J. Intrauterine growth restriction alters the hepatic proteome in fetal pigs. *J Nutr Biochem* (2013) doi:10.1016/j.jnutbio.2012.06.016

374. Girard J, Pintado E, Ferre P. Fuel metabolism in the mammalian fetus. *Ann Biol*

Anim Biochim Biophys (1979) 19:181–197. doi:10.1051/rnd:19790206

375. Char VC, Creasy RK. Acetate as a metabolic substrate in the fetal lamb. *Am J Physiol* (1976) 230:357–361. doi:10.1152/ajplegacy.1976.230.2.357

376. Adam PAJ, Felig P. "Carbohydrate, Fat, and Amino Acid Metabolism in the Pregnant Woman and Fetus," in *Principles and Prenatal Growth*, 461–547. doi:10.1007/978-1-4684-0814-0_18

377. Roux JF. Lipid metabolism in the fetal and neonatal rabbit. *Metabolism* (1966) doi:10.1016/0026-0495(66)90178-8

378. Roux JF, Yoshioka T. Lipid metabolism in the fetus during development. *Clin Obstet Gynecol* (1970) doi:10.1097/00003081-197009000-00009

379. Zhu MJ, Ford SP, Means WJ, Hess BW, Nathanielsz PW, Du M. Maternal nutrient restriction affects properties of skeletal muscle in offspring. *J Physiol* (2006) 575:241–250. doi:10.1113/jphysiol.2006.112110

380. Zurlo F, Larson K, Bogardus C, Ravussin E. Skeletal muscle metabolism is a major determinant of resting energy expenditure. *J Clin Invest* (1990) doi:10.1172/JCI114857

381. DeFronzo RA, Jacot E, Jequier E, Maeder E, Wahren J, Felber JP. The effect of insulin on the disposal of intravenous glucose. Results from indirect calorimetry and hepatic and femoral venous catheterization. *Diabetes* (1981) doi:10.2337/diab.30.12.1000

382. Periasamy M, Herrera JL, Reis FCG. Skeletal muscle thermogenesis and its role in whole body energy metabolism. *Diabetes Metab J* (2017) doi:10.4093/dmj.2017.41.5.327

383. Dodds R, Denison HJ, Ntani G, Cooper R, Cooper C, Sayer AA, Baird J. Birth weight and muscle strength: A systematic review and meta-analysis. *J Nutr Heal Aging* (2012) doi:10.1007/s12603-012-0053-9

384. Paalanne NP, Korpelainen RI, Taimela SP, Auvinen JP, Tammelin TH, Hietikko TM, Kaikkonen HS, Kaikkonen KM, Karppinen JI. Muscular fitness in relation to physical activity and television viewing among young adults. *Med Sci Sports Exerc* (2009) doi:10.1249/MSS.0b013e3181a7f3a6

385. SANDLER RB, BURDETT R, ZALESKIEWICZ M, SPROWLS-REPCHECK C, HARWELL M. Muscle strength as an indicator of the habitual level of physical activity. *Med Sci Sport Exerc* (1991) 23:1375???1381. doi:10.1249/00005768-199112000-00009

386. Kaseva N, Wehkalampi K, Strang-Karlsson S, Salonen M, Pesonen AK, Räikkönen K, Tammelin T, Hovi P, Lahti J, Heinonen K, et al. Lower conditioning leisure-time physical activity in young adults born preterm at very low birth weight. *PLoS One* (2012) doi:10.1371/journal.pone.0032430

387. Kajantie E, Strang-Karlsson S, Hovi P, Räikkönen K, Pesonen AK, Heinonen K, Järvenpää AL, Eriksson JG, Andersson S. Adults born at very low birth weight exercise less than their peers born at term. *J Pediatr* (2010) doi:10.1016/j.jpeds.2010.04.002

388. Fernandes FS, Portella AK, Barbieri MA, Bettiol H, Silva AAM, Agranonik M, Silveira PP, Goldani MZ. Risk factors for sedentary behavior in young adults: Similarities in the inequalities. *J Dev Orig Health Dis* (2010) doi:10.1017/S204017441000019X

389. Elhakeem A, Cooper R, Bann D, Kuh D, Hardy R. Birth Weight, School Sports Ability, and Adulthood Leisure-Time Physical Activity. *Med Sci Sports Exerc* (2017) doi:10.1249/MSS.0000000000001077

390. Van Deutekom AW, Chinapaw MJM, Vrijkotte TGM, Gemke RJBJ. The association of birth weight and infant growth with physical fitness at 8-9 years of age - The ABCD study. *Int J Obes* (2015) doi:10.1038/ijo.2014.204

391. Reyes LM, Kirschenman R, Quon A, Morton JS, Shah A, Davidge ST. Aerobic exercise training reduces cardiac function in adult male offspring exposed to prenatal hypoxia. *Am J Physiol - Regul Integr Comp Physiol* (2015) doi:10.1152/ajpregu.00201.2015

392. Kuh D, Hardy R, Butterworth S, Okell L, Wadsworth M, Cooper C, Sayer AA. Developmental origins of midlife grip strength: Findings from a birth cohort study. *Journals Gerontol - Ser A Biol Sci Med Sci* (2006) doi:10.1093/gerona/61.7.702

393. Barker DJP, Hales CN, Fall CHD, Osmond C, Phipps K, Clark PMS. Type 2 (non-insulin-dependent) diabetes mellitus, hypertension and hyperlipidaemia (syndrome X): relation to reduced fetal growth. *Diabetologia* (1993) doi:10.1007/BF00399095

394. De Jesus LC, Pappas A, Shankaran S, Li L, Das A, Bell EF, Stoll BJ, Laptook AR, Walsh MC, Hale EC, et al. Outcomes of Small for Gestational Age Infants Born at <27 Weeks' Gestation. *J Pediatr* (2013) 163:55-60.e3. doi:10.1016/j.jpeds.2012.12.097

395. Brown LD, Hay WW. Impact of placental insufficiency on fetal skeletal muscle growth. *Mol Cell Endocrinol* (2016) 435:69–77. doi:10.1016/j.mce.2016.03.017

396. Yin H, Price F, Rudnicki MA. Satellite cells and the muscle stem cell niche. *Physiol Rev* (2013) doi:10.1152/physrev.00043.2011

397. Rosenblatt JD, Woods RI. Hypertrophy of rat extensor digitorum longus muscle injected with bupivacaine. A sequential histochemical, immunohistochemical, histological and morphometric study. *J Anat* (1992)

398. Wegner J, Albrecht E, Fiedler I, Teuscher F, Papstein HJ, Ender K. Growth- and breed-related changes of muscle fiber characteristics in cattle. *J Anim Sci* (2000) doi:10.2527/2000.7861485x

399. Widdowson EM, Crabb DE, Milner RDG. Cellular development of some human organs before birth. *Arch Dis Child* (1972) doi:10.1136/adc.47.254.652

400. Fahey AJ, Brameld JM, Parr T, Buttery PJ. The effect of maternal undernutrition before muscle differentiation on the muscle fiber development of the newborn lamb. *J Anim Sci* (2005) doi:10.2527/2005.83112564x

401. Costello PM, Rowlerson A, Astaman NA, Anthony FEW, Sayer AA, Cooper C, Hanson MA, Green LR. Peri-implantation and late gestation maternal undernutrition differentially affect fetal sheep skeletal muscle development. *J Physiol* (2008) doi:10.1113/jphysiol.2008.150987

402. Chang EI, Rozance PJ, Wesolowski SR, Nguyen LM, Shaw SC, Sclafani RA, Bjorkman KK, Peter AK, Hay WW, Brown LD. Rates of myogenesis and myofiber numbers are reduced in late gestation IUGR fetal sheep. *J Endocrinol* (2020) doi:10.1530/JOE-19-0273

403. Wagatsuma A, Sakuma K. Mitochondria as a potential regulator of myogenesis. *Sci World J* (2013) doi:10.1155/2013/593267

404. Sin J, Andres AM, Taylo R DJR, Weston T, Hiraumi Y, Stotland A, Kim BJ, Huang C, Doran KS, Gottlieb RA. Mitophagy is required for mitochondrial biogenesis and myogenic differentiation of C2C12 myoblasts. *Autophagy* (2016) 12:369–380. doi:10.1080/15548627.2015.1115172

405. Rochard P, Rodier A, Casas F, Cassar-Malek I, Marchal-Victorion S, Daury L, Wrutniak C, Cabello G. Mitochondrial activity is involved in the regulation of myoblast differentiation through myogenin expression and activity of myogenic factors. *J Biol Chem* (2000) doi:10.1074/jbc.275.4.2733

406. Rochard P, Cassar-Malek I, Marchal S, Wrutniak C, Cabello G. Changes in mitochondrial activity during avian myoblast differentiation: Influence of triiodothyronine or v-erb A expression. *J Cell Physiol* (1996) doi:10.1002/(SICI)1097-4652(199608)168:2<239::AID-JCP2>3.0.CO;2-Q

407. Barbieri E, Battistelli M, Casadei L, Vallorani L, Piccoli G, Guescini M, Gioacchini AM, Polidori E, Zeppa S, Ceccaroli P, et al. Morphofunctional and biochemical approaches for studying mitochondrial changes during myoblasts differentiation. *J Aging Res* (2011) doi:10.4061/2011/845379

408. Porter C, Hurren NM, Cotter M V., Bhattarai N, Reidy PT, Dillon EL, Durham WJ, Tuvdendorj D, Sheffield-Moore M, Volpi E, et al. Mitochondrial respiratory capacity and coupling control decline with age in human skeletal muscle. *Am J Physiol - Endocrinol Metab* (2015) doi:10.1152/ajpendo.00125.2015

409. Zoll J, Sanchez H, N'Guessan B, Ribera F, Lampert E, Bigard X, Serrurier B, Fortin D, Geny B, Veksler V, et al. Physical activity changes the regulation of mitochondrial respiration in human skeletal muscle. *J Physiol* (2002)

doi:10.1113/jphysiol.2002.019661

410. Nicholls DG. Spare respiratory capacity, oxidative stress and excitotoxicity. *Biochem Soc Trans* (2009) doi:10.1042/BST0371385

411. Kunz WS. Different metabolic properties of mitochondrial oxidative phosphorylation in different cell types - Important implications for mitochondrial cytopathies. *Exp Physiol* (2003) doi:10.1113/eph8802512

412. Sriskanthadevan S, Jeyaraju D V., Chung TE, Prabha S, Xu W, Skrtic M, Jhas B, Hurren R, Gronda M, Wang X, et al. AML cells have low spare reserve capacity in their respiratory chain that renders them susceptible to oxidative metabolic stress. *Blood* (2015) doi:10.1182/blood-2014-08-594408

413. Chen J, Henderson GI, Freeman GL. Role of 4-hydroxynonenal in modification of cytochrome c oxidase in ischemia/reperfused rat heart. *J Mol Cell Cardiol* (2001) doi:10.1006/jmcc.2001.1454

414. Ehinger JK, Piel S, Ford R, Karlsson M, Sjövall F, Frostner EÅ, Morota S, Taylor RW, Turnbull DM, Cornell C, et al. Cell-permeable succinate prodrugs bypass mitochondrial complex i deficiency. *Nat Commun* (2016) doi:10.1038/ncomms12317

415. Herst PM, Berridge M V. Cell surface oxygen consumption: A major contributor to cellular oxygen consumption in glycolytic cancer cell lines. *Biochim Biophys Acta - Bioenerg* (2007) doi:10.1016/j.bbabio.2006.11.018

416. Boveris A, Chance B. The mitochondrial generation of hydrogen peroxide. General properties and effect of hyperbaric oxygen. *Biochem J* (1973) doi:10.1042/bj1340707

417. Turrens JF. Mitochondrial formation of reactive oxygen species. *J Physiol* (2003) doi:10.1113/jphysiol.2003.049478

418. Dudkina N V., Kouřil R, Peters K, Braun HP, Boekema EJ. Structure and function of mitochondrial supercomplexes. *Biochim Biophys Acta - Bioenerg* (2010) doi:10.1016/j.bbabio.2009.12.013

419. Gray LR, Tompkins SC, Taylor EB. Regulation of pyruvate metabolism and human disease. *Cell Mol Life Sci* (2014) doi:10.1007/s00018-013-1539-2

420. Bader DA, Hartig SM, Putluri V, Foley C, Hamilton MP, Smith EA, Saha PK, Panigrahi A, Walker C, Zong L, et al. Mitochondrial pyruvate import is a metabolic vulnerability in androgen receptor-driven prostate cancer. *Nat Metab* (2019) doi:10.1038/s42255-018-0002-y

421. DeWaal D, Nogueira V, Terry AR, Patra KC, Jeon SM, Guzman G, Au J, Long CP, Antoniewicz MR, Hay N. Hexokinase-2 depletion inhibits glycolysis and induces oxidative phosphorylation in hepatocellular carcinoma and sensitizes to metformin. *Nat Commun* (2018) doi:10.1038/s41467-017-02733-4

422. Pfleger J, He M, Abdellatif M. Mitochondrial complex II is a source of the reserve respiratory capacity that is regulated by metabolic sensors and promotes cell survival. *Cell Death Dis* (2015) doi:10.1038/cddis.2015.202

423. Zander-Fox DL, Fullston T, McPherson NO, Sandeman L, Kang WX, Good SB, Spillane M, Lane M. Reduction of mitochondrial function by FCCP during mouse cleavage stage embryo culture reduces birth weight and impairs the metabolic health of offspring. *Biol Reprod* (2015) doi:10.1095/biolreprod.114.123489

424. Shelley P, Martin-Gronert MS, Rowlerson A, Poston L, Heales SJR, Hargreaves

IP, McConnell JM, Ozanne SE, Fernandez-Twinn DS. Altered skeletal muscle insulin signaling and mitochondrial complex II-III linked activity in adult offspring of obese mice. *Am J Physiol - Regul Integr Comp Physiol* (2009) doi:10.1152/ajpregu.00146.2009

425. Tarry-Adkins JL, Fernandez-Twinn DS, Chen JH, Hargreaves IP, Neergheen V, Aiken CE, Ozanne SE. Poor maternal nutrition and accelerated postnatal growth induces an accelerated aging phenotype and oxidative stress in skeletal muscle of male rats. *DMM Dis Model Mech* (2016) doi:10.1242/dmm.026591

426. Simmons RA, Suponitsky-Kroyter I, Selak MA. Progressive accumulation of mitochondrial DNA mutations and decline in mitochondrial function lead to β-cell failure. *J Biol Chem* (2005) 280:28785–28791. doi:10.1074/jbc.M505695200

427. Lockwood CJ, Weiner S. Assessment of Fetal Growth. *Clin Perinatol* (1986) 13:3–35. doi:10.1016/S0095-5108(18)30836-4

428. Romo A, Carceller R, Tobajas J. Intrauterine growth retardation (IUGR): Epidemiology and etiology. *Pediatr Endocrinol Rev* (2009)

429. Winterhager E, Gellhaus A. Transplacental nutrient transport mechanisms of intrauterine growth restriction in rodent models and humans. *Front Physiol* (2017) doi:10.3389/fphys.2017.00951

430. Davis TA, Burrin DG, Fiorotto ML, Reeds PJ, Jahoor F. Roles of insulin and amino acids in the regulation of protein synthesis in the neonate. in *Journal of Nutrition* doi:10.1093/jn/128.2.347s

431. Davis TA, Fiorotto ML. Regulation of muscle growth in neonates. *Curr Opin Clin Nutr Metab Care* (2009) 12:78–85. doi:10.1097/MCO.0b013e32831cef9f

432. Hay WW, Brown LD, Rozance PJ, Wesolowski SR, Limesand SW. Challenges in nourishing the intrauterine growth-restricted foetus – Lessons learned from studies in the intrauterine growth-restricted foetal sheep. *Acta Paediatr Int J Paediatr* (2016) 105:881–889. doi:10.1111/apa.13413

433. Economides DL, Nicolaides KH, Gahl WA, Bernardini I, Evans MI. Plasma amino acids in appropriate- and small-for-gestational-age fetuses. *Am J Obstet Gynecol* (1989) doi:10.1016/0002-9378(89)90670-4

434. Hales CN, Barker DJP. The thrifty phenotype hypothesis. *Br Med Bull* (2001) doi:10.1093/bmb/60.1.5

435. Barker DJP. The origins of the developmental origins theory. in *Journal of Internal Medicine*, 412–417. doi:10.1111/j.1365-2796.2007.01809.x

436. Vanderperre B, Bender T, Kunji ERS, Martinou JC. Mitochondrial pyruvate import and its effects on homeostasis. *Curr Opin Cell Biol* (2015) doi:10.1016/j.ceb.2014.10.008

437. Vigueira PA, McCommis KS, Schweitzer GG, Remedi MS, Chambers KT, Fu X, McDonald WG, Cole SL, Colca JR, Kletzien RF, et al. Mitochondrial Pyruvate Carrier 2 Hypomorphism in Mice Leads to Defects in Glucose-Stimulated Insulin Secretion. *Cell Rep* (2014) doi:10.1016/j.celrep.2014.05.017

438. Guvendag Guven ES, Karcaaltincaba D, Kandemir O, Kiykac S, Mentese A. Cord blood oxidative stress markers correlate with umbilical artery pulsatility in fetal growth restriction. *J Matern Neonatal Med* (2013) doi:10.3109/14767058.2012.745497

439. Maisonneuve E, Delvin E, Ouellet A, Morin L, Dubé J, Boucoiran I, Moutquin J-

M, Fouron J-C, Klam S, Levy E, et al. Oxidative conditions prevail in severe IUGR with vascular disease and Doppler anomalies. *J Matern Neonatal Med* (2015) 28:1471–1475. doi:10.3109/14767058.2014.957670

440. Karowicz-Bilínska A, Suzin J, Sieroszewski P. Evaluation of oxidative stress indices during treatment in pregnant women with intrauterine growth retardation. *Med Sci Monit* (2002)

441. Rashid CS, Bansal A, Simmons RA. Oxidative stress, intrauterine growth restriction, and developmental programming of type 2 diabetes. *Physiology* (2018) doi:10.1152/physiol.00023.2018

442. Dan Dunn J, Alvarez LAJ, Zhang X, Soldati T. Reactive oxygen species and mitochondria: A nexus of cellular homeostasis. *Redox Biol* (2015) doi:10.1016/j.redox.2015.09.005

443. Hamanaka RB, Chandel NS. Mitochondrial reactive oxygen species regulate cellular signaling and dictate biological outcomes. *Trends Biochem Sci* (2010) doi:10.1016/j.tibs.2010.04.002

444. Sena LA, Chandel NS. Physiological roles of mitochondrial reactive oxygen species. *Mol Cell* (2012) doi:10.1016/j.molcel.2012.09.025

445. Hernansanz-Agustín P, Ramos E, Navarro E, Parada E, Sánchez-López N, Peláez-Aguado L, Cabrera-García JD, Tello D, Buendia I, Marina A, et al. Mitochondrial complex I deactivation is related to superoxide production in acute hypoxia. *Redox Biol* (2017) doi:10.1016/j.redox.2017.04.025

446. McElroy GS, Chandel NS. Mitochondria control acute and chronic responses to hypoxia. *Exp Cell Res* (2017) doi:10.1016/j.yexcr.2017.03.034

447. Meng L, Yang X, Xie X, Wang M. Mitochondrial NDUFA4L2 protein promotes the vitality of lung cancer cells by repressing oxidative stress. *Thorac Cancer* (2019) doi:10.1111/1759-7714.12984

448. Hochachka PW. Defense strategies against hypoxia and hypothermia. *Science (80-)* (1986) doi:10.1126/science.2417316

449. Hochachka PW, Clark CM, Brown WD, Stanley C, Stone CK, Nickles RJ, Zhu GG, Allen PS, Holden JE. The brain at high altitude: Hypometabolism as a defense against chronic hypoxia? *J Cereb Blood Flow Metab* (1994) doi:10.1038/jcbfm.1994.84

450. Mailloux RJ, Craig Ayre D, Christian SL. Induction of mitochondrial reactive oxygen species production by GSH mediated S-glutathionylation of 2-oxoglutarate dehydrogenase. *Redox Biol* (2016) doi:10.1016/j.redox.2016.02.002

451. Tretter L, Adam-Vizi V. Alpha-ketoglutarate dehydrogenase: A target and generator of oxidative stress. in *Philosophical Transactions of the Royal Society B: Biological Sciences* doi:10.1098/rstb.2005.1764

452. Quinlan CL, Goncalves RLS, Hey-Mogensen M, Yadava N, Bunik VI, Brand MD. The 2-oxoacid dehydrogenase complexes in mitochondria can produce superoxide/hydrogen peroxide at much higher rates than complex I. *J Biol Chem* (2014) doi:10.1074/jbc.M113.545301

453. Wai SG, Rozance PJ, Wesolowski SR, Hay WW, Brown LD. Prolonged amino acid infusion into intrauterine growth-restricted fetal sheep increases leucine oxidation rates. *Am J Physiol - Endocrinol Metab* (2018) doi:10.1152/ajpendo.00128.2018

454. Monné M, Vozza A, Lasorsa FM, Porcelli V, Palmieri F. Mitochondrial carriers for aspartate, glutamate and other amino acids: A review. *Int J Mol Sci* (2019) doi:10.3390/ijms20184456

455. Barker DJP. The Developmental Origins of Adult Disease. *J Am Coll Nutr* (2004) 23:588S-595S. doi:10.1080/07315724.2004.10719428

456. Zhu M-J, Ford SP, Nathanielsz PW, Du M. Effect of Maternal Nutrient Restriction in Sheep on the Development of Fetal Skeletal Muscle1. *Biol Reprod* (2004) 71:1968–1973. doi:10.1095/biolreprod.104.034561